

CRYSTAL GROWTH OF ZnO BAR USING  
JOULE HEATING

HARLAI YEE

BACHELOR OF APPLIED SCIENCES (HONS.)  
MATERIAL TECHNOLOGY  
UNIVERSITI MALAYSIA PAHANG

# UNIVERSITI MALAYSIA PAHANG

## DECLARATION OF THESIS AND COPYRIGHT

Author's full name : HarLai Yee

Date of birth : 04August 1993

Title : Crystal Growth of ZnO Bar Using Joule Heating

Academic Session : Semester I 2016/2017

I declare that this thesis is classified as:

☐

**CONFIDENTIAL** (Contains confidential information under the Official Secret Act 1972)

☐

**RESTRICTED**(Contains restricted information as specified by the organization where research was done)

☒

**OPEN ACCESS** I agree that my thesis to be published as online open access (Full text)

I acknowledge that Universiti Malaysia Pahang reserve the right as follows:

1. The Thesis is the Property of Universiti Malaysia Pahang
2. The Library of Universiti Malaysia Pahang has the right to make copies for the purpose of research only.
3. The Library has the right to make copies of the thesis for academic exchange.

Certified By:

\_\_\_\_\_  
(Student's Signature)

Har Lai Yee  
930804-08-5224  
Date: 25<sup>th</sup> December 2016

\_\_\_\_\_  
(Supervisor's Signature)

Asoc. Prof. Dr. AgusGeterEdySutjipto  
A6821043  
Date: 25<sup>th</sup> December 2016

# CRYSTAL GROWTH OF ZnO BAR USING JOULE HEATING

HAR LAI YEE

Thesis submitted in fulfillment of the requirements  
for the award of the degree of  
Bachelor of Applied Sciences (Honors) Material Technology

Faculty of Industrial Sciences & Technology  
UNIVERSITI MALAYSIA PAHANG

December 2016

## **SUPERVISORS' DECLARATION**

I hereby declare that I have checked the thesis and in my opinion, this thesis is adequate in terms of scope and quality for the award of the degree of Bachelor of Applied Sciences (Honors)Material Technology.

Signature

Name of Supervisor : Asoc. Prof. Dr. AgusGeterEdySutjipto

Position : Associate Professor

Date : 25<sup>th</sup> December 2016

## **STUDENT'S DECLARATION**

I hereby declare that the work in this thesis is my own except for quotations and summaries which have been duly acknowledged. The thesis has not been accepted for any degree and is not concurrently submitted for award of other degree.

Signature :  
Name : Har Lai Yee  
ID Number : SC13014  
Date : 25<sup>th</sup> December 2016

## ACKNOWLEDGEMENTS

First and foremost, I wished to thank Asoc. Prof. Dr. Agus Geter Edy Sutjipto, my supervisor, who willing to sacrifice his time for providing suggestion and solution to complete the work. I truly appreciated the guidance and opinion you gave for this research.

Besides that, I wished to express my appreciation to Shahrul Razi bin Meskon, student of International Islamic University Malaysia, for giving me ideas and some solution regarding on method to synthesis the sample and some tips to conduct joule heating process.

In addition, I would to thank Dr. Saifful Kamaluddin bin Muzakir, for providing solution to operate UV-Vis spectrometer and Photoluminescence spectrometer.

Moreover, I would also extend my appreciation to several laboratory assistant who helped me along the research. They explained the method to operate equipment and provide suggestion to complete the research.

I extended special thanks to several others who have helped me along the way. This includes Yit Pei Shian, Leong Pei Mun, Poh Yi Fei and Lam Kah Hoe. They always taught me on laboratory work and mentally support me.

Furthermore, I would like to express my appreciation to my sponsor at the Faculty Industrial Sciences & Technology in University Malaysia Pahang. The faculty allocated each student RM 1000.00 to purchase the materials needed in the experiment.

Last but not least, I would like to thanks my parents and my sisters for their mentally and financially support to me. They always comforted and encouraged me when I was frustrated.

## ABSTRACT

Crystal growth is important for understanding physiochemical mechanisms for zinc oxide (ZnO). ZnO exists in different crystal structures under specific condition and each of the crystal growth consists of different characteristics. The major problem for growing the ZnO crystal was to conduct electricity through the wide band gap semiconductor. As a solution, joule heating method was adopted to conduct electricity in this research. Joule heating method provided a stable and continuous current and high applied voltage throughout the circuit. New form of zinc oxide crystals was wished to be observed through this research. The three main objectives of this research were to grow various forms of ZnO crystals, master in conducting joule heating technique and characterize the samples through topography characterization, absorbance characterization, emission spectrum characterization and X-Ray Diffraction characterization. Scanning Electron Microscopy (SEM), Ultraviolet-Visible (UV-Vis) Spectroscopy, Photoluminescence Spectroscopy and X-Ray Diffractometer (XRD) were used for the characterization respectively. SEM showed the most of the crystals grew by each sample in the rock like shape and hexagonal shape. UV-Vis showed the wavelength of all samples was located around 380 nm. Therefore, the calculated excitonic energy was around 3.20 eV which was nearly matched with theoretical band gap 3.37 eV. The XRD results showed most of the crystals grew on the plane (1 0 1). The crystals grew were in rock like shape. This was proved by the plane (1 0 1) had the highest intensity in all the samples. As a conclusion, the optimum current for crystals grew was 3.0 A and the crystals were mostly grew in the plane (1 0 1). The easiest grew crystals were in rock and hexagonal shape.

## ABSTRAK

Pertumbuhan kristal adalah penting untuk memahami mekanisme physiochemical untuk zink oksida (ZnO). ZnO wujud dalam struktur kristal yang berbeza di bawah keadaan tertentu dan setiap daripada pertumbuhan kristal terdiri daripada ciri-ciri yang berbeza. Masalah utama yang dihadapi dalam pertumbuhan kristal ZnO adalah untuk mengalirkan elektrik melalui semikonduktor berjalur lebar. Kaedah penyelesaian kes ini adalah dengan penggunaan pemanasan joule dalam pengaliran elektrik dalam kajian ini. Kaedah pemanasan Joule membiarkan pangaliran voltan yang tinggi dan arus elektrikal yang stabil dan berterusan sepanjang litar. Masalah yang dihadapi dalam kajian ini adalah pertumbuhan kristal zink oksida yang baharu. Tiga objektif utama kajian ini adalah untuk mempertingkatkan pelbagai bentuk kristal ZnO, memperoleh kecekapan dalam menjalankan teknik pemanasan joule dan mengetahui ciri-ciri sampel melalui pencirian topografi, pencirian kuantiti cahaya yang diserap, pencirian pelepasan spektrum dan pencirian X-Ray Sinar. Scanning Electron Microscopy (SEM), Ultraviolet-Visible (UV-Vis) Spektroskopi, Photoluminescence Spektroskopi dan X-Ray Diffractometer (XRD) telah digunakan untuk pencirian masing-masing. SEM menunjukkan kebanyakan kristal bertumbuh dalam bentuk batu-batan dan berbentuk heksagon. Keputusan yang ditunjukkan oleh UV-Vis ialah gelombang setiap sampel adalah sepanjang 380 nm. Oleh itu, tenaga excitonic adalah sekitar 3.20 eV yang hampir dipadankan dengan teori 3.37 eV. Keputusan XRD menunjukkan kebanyakan kristal adalah dalam permukaan (1 0 1). Kristal bertumbuh dalam bentuk batu-batan. Ini telah dibuktikan permukaan (1 0 1) mempunyai intensiti yang tertinggi dalam semua sampel. Kesimpulannya, optimum arus untuk pertumbuhan kristal ZnO adalah 3.0 A dan kebanyakan kristal bertumbuh dalam permukaan (1 0 1). Kristal paling mudah bertumbuh dalam bentuk batu-batan dan bentuk heksagon.



## TABLE OF CONTENTS

	Page
<b>DECLARATION OF THESIS AND COPYRIGHT</b>	
<b>SUPERVISORS' DECLARATION</b>	ii
<b>STUDENT'S DECLARATION</b>	iii
<b>ACKNOWLEDGEMENTS</b>	iv
<b>ABSTRACT</b>	v
<b>ABSTRAK</b>	vi
<b>TABLE OF CONTENTS</b>	vii
<b>LIST OF TABLES</b>	ix
<b>LIST OF FIGURES</b>	x
<b>LIST OF SYMBOLS</b>	xii
<b>LIST OF ABBREVIATIONS</b>	xiii
 <b>CHAPTER 1 INTRODUCTION</b>	
 1.1 Background of Study	1
1.2 Problem Statement	2
1.3 Objective of Research	2
1.4 Scope of Study	3
 <b>CHAPTER 2 LITERATURE REVIEW</b>	
 2.1 Introduction	4
2.2 Background of Zinc Oxide	5
2.3 Growth of Zinc Oxide Crystal	9
2.4 Joule Heating	11
2.5 Characterization	
2.5.1 Scanning Electron Microscopy (SEM)	13
2.5.2 Ultraviolet-Visible Spectroscopy (UV-Vis Spectroscopy)	14
2.5.3 Photoluminescence Spectroscopy (PL Spectroscopy)	15
2.5.4 X-Ray Diffractometer	16
2.6 Application	18

## **CHAPTER 3 MATERIALS AND METHODS**

3.1	Introduction	19
3.2	Material and Equipment	
3.2.1	Materials	19
3.2.2	Equipment	20
3.3	Methodology	20
3.3.1	Preparation of ZnO Powder	21
3.3.2	Preparation of ZnO bar for Sintering	22
3.3.3	Process of Sintering	25
3.3.4	Structural Characterization as Baseline	26
3.3.5	Joule Heating Process	26
3.3.6	Energy Absorption and Energy Emission Characterization	29
3.3.7	Topography Characterization	30
3.3.8	Structural Characterization	31

## **CHAPTER 4 RESULT AND DISCUSSION**

4.1	Introduction	32
4.2	Characterization of ZnO Ceramic Bar	
4.2.1	Analysis Compact Results	32
4.2.2	Analysis Sintering Results	34
4.2.3	X-Ray Diffraction Analysis	39
4.3	Characterization of Joule Heating Result	
4.3.1	Analysis of Joule Heating Results	40
4.2.1	Topography Analysis	46
4.2.2	Analysis Results of UV-Vis Spectroscopy	65
4.2.3	Analysis Results of Photoluminescence Spectroscopy	67
4.2.3	X-Ray Diffraction Analysis	69

## **CHAPTER 5 CONCLUSIONS AND RECOMMENDATION**

5.1	Conclusions	79
5.2	Recommendations	79

<b>REFERENCES</b>	80
-------------------	----

## LIST OF TABLES

<b>Table No.</b>	<b>Title</b>	<b>Page</b>
4.1	The dimension and weigh of fabricated ZnO compacts.	34
4.2	The value of volume and density of ZnO compacts.	34
4.3	The dimension and weigh of ZnO bar after sintered.	36
4.4	The value of volume and density of ZnO bar after sintered.	36
4.5	Percentage of relative density and percentage of linear shrinkage of ZnO bar.	37
4.6	The dimension and weigh of small pieces of ZnO bar.	38
4.7	The value of volume, density and percentage of relative density of ZnO bar after sintered.	39
4.8	(h k l) plane, d-spacing and crystalline size of sintered ZnO bar.	40
4.9	Comparison of samples in joule heating process.	45
4.10	Comparison of first excitonic peak of six samples.	67
4.11	Excitonic energy of samples.	67
4.12	Result of photoluminescence spectrum of all samples.	70
4.13	(h k l) plane, d-spacing and crystalline size of SZ3 (2.0 Ton, 2.5 A).	71
4.14	(h k l) plane, d-spacing and crystalline size of SZ4 (2.0 Ton, 3.0 A).	73
4.15	(h k l) plane, d-spacing and crystalline size of SZ2 (2.0 Ton, 3.5 A).	74
4.16	(h k l) plane, d-spacing and crystalline size of SZ15 (3.0 Ton, 2.5 A).	76
4.17	(h k l) plane, d-spacing and crystalline size of SZ12 (3.0 Ton, 3.0 A)	77
4.18	(h k l) plane, d-spacing and crystalline size of SZ13 (3.0 Ton, 3.5 A).	79
4.19	(h k l) plane, d-spacing and crystalline size of SZ14 (3.0 Ton, 3.5 A, with Cu).	80

## LIST OF FIGURE

<b>Table No.</b>	<b>Title</b>	<b>Page</b>
2.1	Hexagonal wurtzite structure of ZnO	6
2.2	Energy band diagram of ZnO which showed the splitting of valence band into three subbands (A, B and C).	7
2.3	French process.	8
2.4	The calculated band structure of ZnO using HSE hybrid function.	8
2.5	Crystal growth of ZnO bars.	10
2.6	Surface of Zn wire before and after heat by electric current.	11
2.7	Temperature distribution in a joule heating circuit.	11
2.8	Joule heating circuit in this research.	13
2.9	Basic working principles of SEM.	14
2.10	Electronic, rotational and vibrational electronic levels.	15
2.11	Photoluminescence spectrum of ZnO thin film.	16
2.12	XRD pattern of ZnO nanoparticles.	18
3.1	Research methodology adopted in this research.	20
3.2	Grinding process	21
3.3	Grinding process for mixture of ZnO with ethanol.	22
3.4	Compaction die for shaping ZnO bar.	22
3.5	Single-punch hydraulic uniaxial compactor.	23
3.6	Vernier caliper for measuring dimension of ZnO compact bar.	24
3.7	Flow chart of preparation of ZnO bar for sintering process.	24
3.8	Box metallurgical furnace.	25
3.9	X-ray Diffractometer, Miniflex II, Rigaku, Japan.	26
3.10	Schematic of joule heating equipment	27
3.11	Laser thermometer.	28
3.12	Flow chart of joule heating process.	28

3.13	Joule heating process	29
3.14	Crystal growth of ZnO bar using joule heating method	29
3.15	UV-Vis spectrometer.	30
3.16	Photoluminescence spectrometer.	30
3.17	Scanning Electron Microscopy with model FEI	31
4.1	Pellet which experienced cracks and inhomogeneous powder flow.	33
4.2	Physical defect experienced by sintered bar	35
4.3	X-Ray Diffractogram of sintered ZnO bar.	40
4.4	Crystal grew on SZ3 ZnO bar.	46,47
4.5	Crystal grew on cross sectional part of SZ4 ZnO bar.	48,49
4.6	Crystal grew on surface of SZ4 ZnO bar.	49-51
4.7	Crystal grew on surface of SZ2 ZnO bar.	52-54
4.8	Crystal grew on surface of SZ15 ZnO bar.	55-57
4.9	Crystal grew on surface of SZ12 ZnO bar.	58-60
4.10	Crystal grew on surface of SZ13 ZnO bar.	61,62
4.11	Crystal grew on surface of SZ14 ZnO bar.	63-65
4.12	The result of UV-Vis spectrometer.	65-67
4.13	Photoluminescence spectrum of all samples.	68,69
4.14	X-Ray Diffractogram of SZ3 (2.0 Ton, 2.5 A).	71
4.15	X-Ray Diffractogram of SZ4 (2.0 Ton, 3.0 A).	72
4.16	X-Ray Diffractogram of SZ2 (2.0 Ton, 3.5 A).	74
4.17	X-Ray Diffractogram of SZ15 (3.0 Ton, 2.5 A).	75
4.18	X-Ray Diffractogram of SZ12 (3.0 Ton, 3.0 A).	77
4.19	X-Ray Diffractogram of SZ13 (3.0 Ton, 3.5 A).	78
4.20	X-Ray Diffractogram of SZ14 (3.0 Ton, 3.5 A, with Cu).	80
4.21	Combination of XRD results of all samples.	81

## LIST OF SYMBOLS

Å	Angstrom ( $10^{-10}$ )
a.u.	Arbitrary unit
A	Current
°C	Degree celcius
$\rho$	Density
eV	Energy
L	Length
$m$	Mass
%	Percentage
T	Thickness
$\lambda$	Wavelength
W	Width
V	Voltage
V	Volume

## LIST OF ABBREVIATIONS

Cu	Copper
CIGS	Copper Indium Gallium Selenide
H. O. M. O.	Highest occupied molecular orbital
L. U. M. O.	Lowest unoccupied molecular orbital
MOVPE	Metal-organic vapor-phase epitaxy
MBE	Molecular beam epitaxy
PL	Photoluminescence
PLD	Pulsed-laser deposition
SEM	Scanning Electron Microscopy
UV-Vis	Ultraviolet-visible
XRD	X-ray Diffraction
ZnO	Zinc oxide

## **CHAPTER 1**

### **INTRODUCTION**

#### **1.1 BACKGROUND OF STUDY**

Zinc oxide is widely applied in many fields due to its physical and chemical properties. In medicine field, ZnO used for skin treatment purposes such as minor burned and diaper rash. It mixed with stearic acid for vulcanization of rubber to produce tires and shoe soles. Besides that, ZnO is applied in solar cell technology. It is fabricated as first layer of Copper Indium Gallium Selenide (CIGS) as a buffer layer to increase the efficiency of the solar cell. It also been applied in nanotechnology devices such as nanowires. Crystal growth of ZnO had gained attention different type of ZnO crystal which carried its own characteristics and thus benefit in manufacturing the devices. Fabrication of each of the product depends on characteristics of ZnO crystal. The more the type of crystal growth discover, the more beneficial it brought to consumers.

In recent years, nanocrystals of ZnO are being further studied in application of optoelectronic devices. Characteristics of ZnO crystal grew such as size, phases, piezoelectricity and others brings an effect in the application. Thus a lot of research had been done to determine the growth of ZnO crystals. Many methods were being studied to grow ZnO crystals which included sputtering (K. K. Kim, etc, all., 2000), thermal evaporation (B. D. Yao, etc, all., 2002), metal-organic vapor-phase epitaxy (MOVPE) (W. I. Park, etc, all., 2002), molecular beam epitaxy( MBE) (M. Kawasaki, etc, all., 1998) and pulsed-laser deposition (PLD) (M. Kawakami, etc, all., 2003). However, electric current heating method was adopted in this research. This main reason for heating ZnO bar by using electric current is to achieve one of the objectives to grow



various forms of ZnO crystals. The method of electric current heating is more encourage the growth of various form of crystals.

## **1.2 PROBLEM STATEMENT**

Zinc Oxide (ZnO) exists in different crystal structure under specific condition. All type of crystal growth consists of different characteristics. Crystal growth is important for understanding physiochemical mechanisms for zinc oxide. One of the major problems for growing the zinc oxide crystal is to provide high power to conduct electricity. Thus, joule heating method has been selected to conduct electricity in the research. Joule heating method provides a stable and continuous current and high applied voltage throughout the circuit. New form of crystal growth of zinc oxide is wished to be observed through this research.

## **1.3 OBJECTIVE OF RESEARCH**

There were several objectives set as target to be investigated in this research. It aimed to achieve the following objectives:

- i. To grow various forms of zinc oxide crystals possibly the new ones by applying an optimum current density in the heating of zinc oxide ceramic bars (joule heating).
- ii. To master in joule heating process.
- iii. To characterize samples using X-ray Diffraction, Scanning Electron Microscopy, Ultraviolet-visible Spectroscopy and Photoluminescence Spectroscopy and analyze and identify various crystal growth.

## 1.4 SCOPE OF STUDY

The scopes of study of the research were:

- i. For synthesis the zinc oxide bar for joule heating process.

ZnO is a semiconductor material with wide bandgap and thus it needed large amount of current density to excite electrons and conduct electricity. Thin and small pellet bars of zinc oxide were synthesized to reduce the current density needed for exciting electrons. In this research, ZnO was grinding until fined particles with mortar and pestle to form rectangular pellet bar with different pressure.

- ii. To master in conducting joule heating process.

Joule heating process provided high density current flow through the circuit. Circuit set up was important to make sure the current flow through the circuit. High resistivity connecting wires were chosen to avoid the connecting wire from burning off. ZnO bars were hold with crocodile clip at both end tip to increase the surface for crystal growth. ZnO bars must be hold tight enough to avoid leakage of current density from the circuit.

- iii. To characterize samples using X-ray Diffraction (XRD), Scanning Electron Microscopy (SEM), Ultraviolet-visible Spectroscopy and Photoluminescence Spectroscopy.

Results of characterization were analyzed to discover the crystal growth of ZnO. XRD was to check the composition of ZnO whereas SEM was to check the topography of crystal growth. Ultraviolet-visible Spectroscopy and Photoluminescence Spectroscopy were used to check the emission intensity of crystal.

## **CHAPTER 2**

### **LITERATURE REVIEW**

#### **2.1 INTRODUCTION**

Zinc Oxide (ZnO) is aII–VI compound semiconductor with wide band gap and exciton binding energy at room temperature. It is nontoxic chemical and low in selling price. ZnO had gained attention from research since various form of nanostructure can be grown. Thus, it played an important role in technologies and industries. It is applied as optoelectronic devices in Light emitting diodes (A. Tsukazaki, etc, all. 2005), Optical wave guide (P.Yu, etc, all. 1998), transparent thin film transistor (B. J. Norris, etc, all. 2003) and Solar cell (E.Fortunato, etc, all. 2004). Besides that, ZnO in nanoscale has been applied to harvest energy in nanogenerator (Z. L. Wang & J. Song. 2006).

In order to discover more crystals of ZnO, this research was done to grow the ZnO crystals by using joule heating technique. The electric current heating method was discovered and developed by Nezaki et al to grow ZnO crystals. This method is carried out by heating the ZnO ceramic bar with electric current and results in the growth of ZnO crystal. The main benefit of this technique is different form of crystals includes hexagonal prisms, double hollow prisms, whiskers, tetrapods and etcetera are obtained. Form of crystals growth are influenced by others factors such as the electric current adopted through the circuit and the growth atmosphere. ZnO growth crystal gave a strong UV emission. The characteristics of crystals growth are analyzed to widen the application of ZnO.

In this chapter, background of zinc oxide, the raw material used in this research was discussed in this chapter. These were followed by background of crystal growth of

zinc oxide and joule heating method. Furthermore, background of Ultra-visible Spectrometer, Photoluminescence Spectrometer and X-ray Diffractometer will be discussed.

## 2.2 BACKGROUND OF ZINC OXIDE

Zinc oxide is an inorganic compound with chemical formula ZnO. It is water insoluble compound but it is soluble in both acid and alkali. ZnO usually exists in white powder form. ZnO has a high melting point (1975 °C) and boiling point (2360 °C). Thermal conductivity of ZnO is 37 W/mK at room temperature. (Xufei Wu, et al., 2015) Due to its thermochromic characteristics in crystalline, color changes from white to yellow when heated and returns to white when cooled down.

Zinc oxide is a group II–VI binary compound semiconductor. Crystalline structure of ZnO is normally in hexagonal wurtzite structure at room temperature as shown in Figure 2.1. In ZnO compound, each of the cation ion ( $\text{Zn}^{2+}$ ) is surrounded at a tetrahedron by four anion ions ( $\text{O}^{2-}$ ), and vice-versa (O. Dulub, et al., 2002). Lattice spacing of hexagonal wurtzite structure is  $a = b = 3.25 \text{ \AA}$  and  $c = 5.206 \text{ \AA}$  (O. Dulub, et al., 2002). There are polar and non-polar faces in the ZnO structure. Zn terminated face  $[0001]$  and O terminated face  $[000\bar{1}]$  were polar faces whereas  $[11\bar{2}0]$  and  $[\bar{1}0\bar{1}0]$  with the same number of zinc and oxygen atom. The basal plane is the plane perpendicular to the c-axis. Therefore, there is polar symmetry along the hexagonal axis. These properties have increased the piezoelectricity in ZnO and play an important role in ZnO crystal growth. Zinc oxide usually exists in white powder form and it is an inorganic compound. It is water insoluble compound but soluble in both acid and alkali solvent. ZnO has the properties of covalent bonding in nature with  $\text{sp}^3$  hybridization. However, the ZnO structure also has strong ionic character which gives rise in band gap beyond from covalent bonding. As a result, ZnO behaves like covalent and ionic compound.

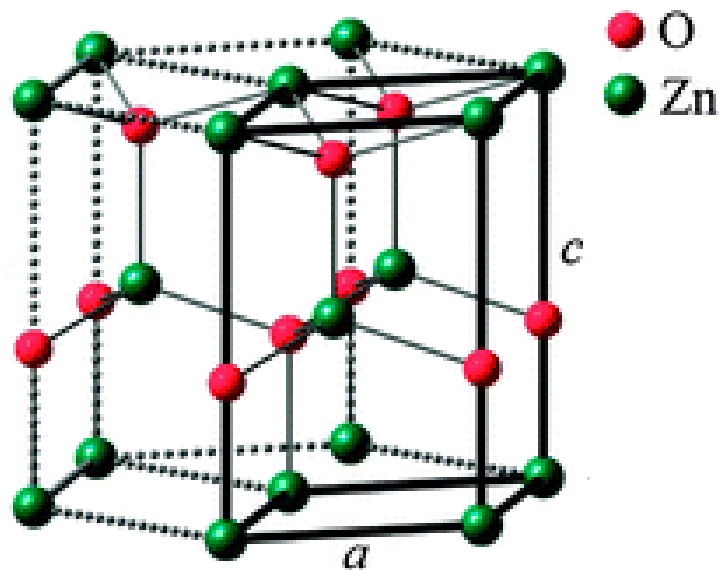


Figure 2.1. Hexagonal wurtzite structure of ZnO.

There are some defects and impurities in ZnO in nature. ZnO can be easily obtained in nature as zincite and usually contains manganese and other impurities that give to a red and yellow color. Pure zinc oxide is obtained in synthetics. ZnO crystals has native point defect which influenced its optical and electrical properties. The optical emission properties of ZnO are affected by electronic states in the band gap and it is generated by native point defect. Thus, the grown ZnO crystals is found in n-type. Theoretically proved that both zinc interstitial,  $Zn_i$  and oxygen vacancy,  $V$  has very high formation energies in n-type ZnO and they are deep level donors (A. F. Kohan, etc, all. 2000). Group III element includes aluminum (Al), gallium (Ga) and indium (In) are donor impurities to ZnO which able substitute Zn with concentration larger than  $10^{20} \text{cm}^{-3}$ . Van de Wall properties in ZnO brought the hydrogen ( $H_2$ ) is a main background donor when exposed to  $H_2$  during growing process. (A. M. Gsies, etc, all. 2014).

The electronic band diagram for hexagonal wurtzite structure of ZnO is shown in Figure 2.2 (B K. Meyer, etc, all. 2004). The diagram shows that both edge maxima of the valence band and edge minima of the conduction band happens at  $k = 0$  and this

proves that ZnO is a direct band gap semiconductor. Some research proved that the valence band of ZnO splits into three subbands which are A, B and C. This is caused by the happened of spin-orbit interaction and crystal-field splitting in ZnO structure (B K. Meyer, etc, all. 2004). ZnO had an energy band gap of 3.4376 eV at  $T = 4.2\text{ K}$ .

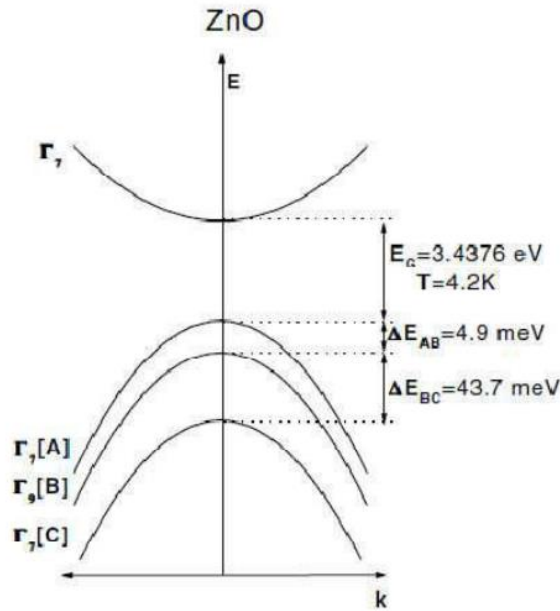


Figure 2.2. Energy band diagram of ZnO which showed the splitting of valence band into three subbands (A, B and C).

Source: Reproduced from (B K. Meyer, etc, all. 2004)

ZnO appears as earth rust naturally as zincite. However, ZnO with high degree of purity (>99%) is produced synthetically. The purity of ZnO highly depends on consumers' needs. For example, special high grade (SHG) of zinc with 99.99% purity is adopted in pharmaceutical whereas ordinary high grade (HG) zinc (around 99.95% purity) is used to form the ZnO used in rubber industries. ZnO is produced through indirect process or normally well known as French process as shown in Figure 2.3 (Amir Moezzi, etc, all. 2007). French process produces maximum 1.245 tons of ZnO when one ton of zinc is used as raw material in theory. However, experimental showed that around 1.2 tons of ZnO was produced when SHG of zinc was used as raw material. The amount of product of ZnO decreases as the purity of raw material getting lower (Amir Moezzi, etc, all. 2007).



*Figure 2.3.*French process.

Source: Reproduced from (Amir Moezzi, etc, all. 2007)

ZnO poses a direct and wide band gap and wide band gap which located around UV spectra region as shown in Figure 2.4 (Thomas D G., 1960). It has a band gap of 3.37 eV and a large free exciton binding energy (60 meV) (Reynolds D. C., etc, all., 1999) and this allow excitonic emission processes at room temperature (Bagnall D. M., etc, all., 1997). ZnOis applied in optoelectronic application in blue and UV regions of the spectrum due to these characteristics.

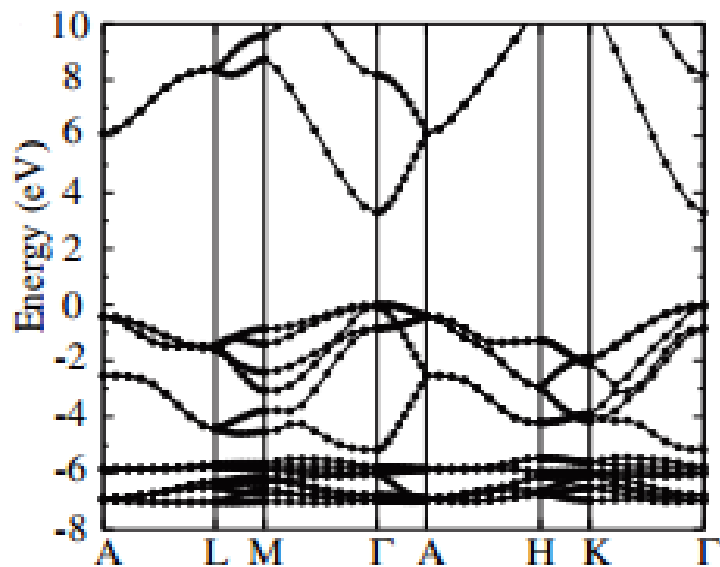


*Figure 2.4.*The calculated band structure of ZnO using HSE hybrid function.

Source: Reproduced from (Thomas D G., 1960)

## 2.3 GROWTH OF ZINC OXIDE CRYSTAL

The outstanding progress of catalyst and thin film growth of ZnO in recent years had increased the application of ZnO in optoelectronic field. Polycrystalline form of ZnO is mainly adopted in current market. High degree of purity and single crystal in the form either crystal or thin film were a must for advanced application. A lot of researches were done about catalyst and thin film to determine the structural characteristics of ZnO. This enhanced the improvement of usage of ZnO in nanotechnology. ZnO crystal can be formed by using different methods included sputtering (K. K. Kim, etc, all., 2000), thermal evaporation (B. D. Yao, etc, all., 2002), metal-organic vapor-phase epitaxy (MOVPE) (W. I. Park, etc, all., 2002), molecular beam epitaxy (MBE) (M. Kawasaki, etc, all., 1998) and pulsed-laser deposition (PLD) (M. Kawakami, etc, all., 2003).

The structural characteristics determined by surface stability of crystal. This influences the equilibrium morphology in the usage to design different micro/nanostructure. Crystals surface characteristics are taking into consideration in fabrication of ZnO micro/nanotube. The three fast growth directions in hexagonal ZnO are along  $[0001]$ ,  $[10\bar{1}0]$  and  $[2\bar{1}\bar{1}0]$ . The  $[0001]$  direction poses a highest growth rate and results in owning the highest surface energy. Therefore,  $[0001]$  direction is the most active crystal surface (W. J. Li, etc, all., 1999). Liquid based technique is used to form ZnO nanotubes (Y. Sun, etc, all., 2005). The hexagonal ZnO rods are formed and the  $[0001]$  phase is dissolved in acidic or alkali solvent. As a result, ZnO crystal with tubular structures is obtained. On the the side, vapor phase method is adopted to obtain hexagonal ZnO. Zinc is deposited into liquid droplet and the less stable side of ZnO nanoparticles are oxidized and formed ZnO shells. The inside Zn at  $[0001]$  phase is sublimated at the same time and thus the hollow ZnO tubes were formed. This occurred based on the intrinsic structure properties. Most of the fabricated ZnO tube-like structure is entangled, irregular and rough surface due to the uncontrollability on crystal intrinsic structure. The imperfection of crystal formed affectes the application as optical resonators.



ZnO consists of three basic types of fast growth direction. The structure will experience vast changes when growth rates along the direction are changes. This morphology can be done under specific condition. The topography of crystal growth is observed under Scanning Electron Microscopy. The phase of crystal is characterized by using X-ray Diffractometer. Ultraviolet-visible Spectroscopy and Photoluminescence Spectroscopy are used to determine the absorbance and emission of light.

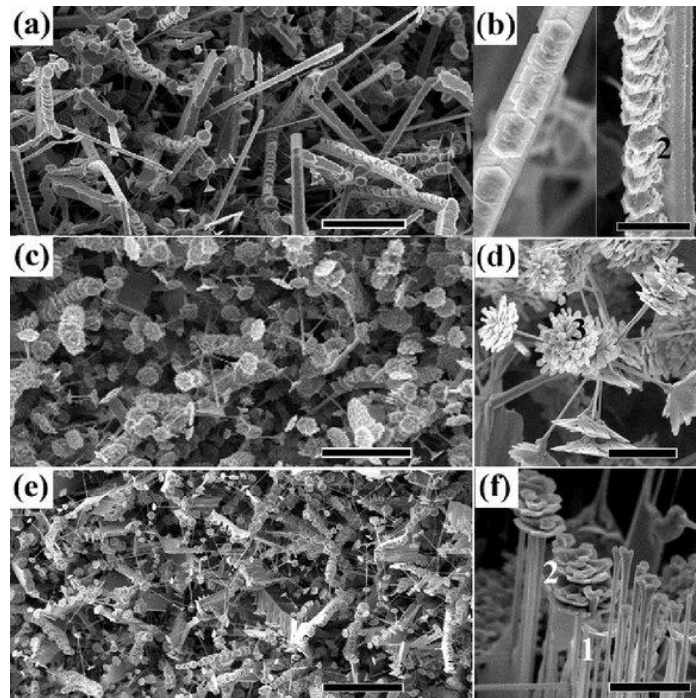


*Figure 2.5.*Crystal growth of ZnO bars. (a), (c) and (e) shows morphology of crystal growth from low temperature to high temperature, whereas (b), (d) and (f) shows the enlarge image of (a), (c) and (e) respectively

Source: Reproduced from (G. K. Mani & J.B.B. Rayappan. 2014).

A research about growth of ZnO crystals with ultra emission by electric current heating method with Zn wire was carried out. The shape of crystals grew under the effect of oxygen concentration in the atmosphere was examined. Direct current (D.C.) power supply was connected to Zn wire with 99.99% purity which put inside a glass tube. The flow rates of argon (Ar) and oxygen (O<sub>2</sub>) were controlled to control the oxygen concentration in the glass tube. The crystals grew as shown in Figure 2.6. The current applied was 8.5 A to 9.2 A and voltage applied was 0.8 V through the circuit. Figure 2.6 (a) showed Zn wire before joule heating whereas Figure 2.6 (b) showed Zn

wire heat under oxygen. Zn wire was heated under argon with 20% of oxygen and the result was shown in Figure 2.6 (c) and Figure 2.6 (d) showed Zn wire heated under argon atmosphere (Haruo Yamasaki, etc, all., 2004.).

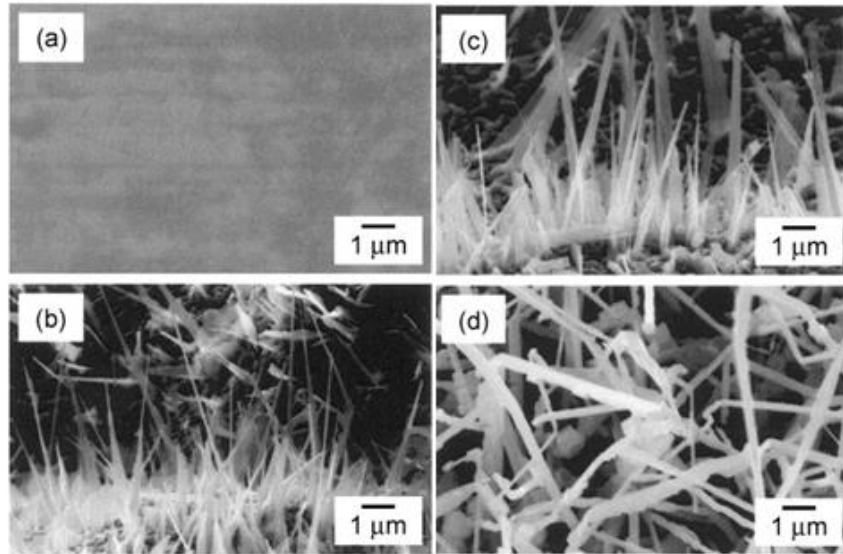


*Figure 2.6.*Surface of Zn wire before and after heat by electric current.

Source: Reproduced from (Haruo Yamasaki, etc, all., 2004.).

## 2.4 JOULE HEATING

Joule heating also called as ohmic or resistive heating. Joule heating is defined as the process where the energy of an electric current is converted into heat as it flows through a resistance. Electrical energy is converted to heat when the electric current flows through a material through resistive loss in the material. The conduction electrons transfer energy to conductor's atoms through collisions and results in heat is generated.

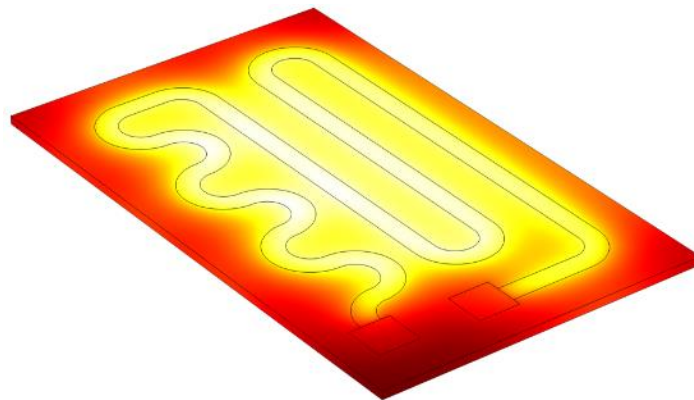


*Figure 2.7.*Temperature distribution in a joule heating circuit.

Crystal growth by using electric current heating method was developed by Nezaki and etc. ZnO crystals grew on the ZnO bar when heated by electric current. This method brought benefit various forms of crystal would be formed which included whiskers, hexagonal prisms, tetrapods and double-hollow prisms. The crystals grew varying with the electric current applied and condition of growth atmosphere. Besides that, ZnO crystals emitted a strong ultraviolet spectrum after experience electric current heating (D. Nezaki, etc, all., 2002.).

A research was carried out to study the effect of substrate temperature on ZnO nanowire growth by electric current heating method. The ZnO bar was heated for 10 mins by using electric current method. The DC power supply applied a direct current of  $50 \text{ Acm}^{-2}$  through the ZnO bar. The ZnO bar was heated at around  $1000^\circ\text{C}$ . The results showed hexagonal shape crystal prefer to grow along (0 0 2) orientation. At temperature  $800^\circ\text{C}$ , nanowire grew and this was proved by SEM. The length of nanowire grew was in the range of 4 to  $20 \mu\text{m}$  whereas the diameter of nanowire was 20 to 100 nm (R.Sivakumar, etc, all., 2012.).

Another research was study to investigate the selective area growth of ZnO crystals by electric current heating. The sample was heated by an electric current of  $50 \text{ Acm}^{-2}$  and the temperature is around  $1000^\circ\text{C}$ . The crystal grew formed nanowhiskers slowly. The nanowhiskers grew with diameter of 70 to 300 nm. The length of the nanowhiskers was in the range of 1 to  $20 \mu\text{m}$ . The most interesting nanowhisiker obtained from this research was a novel zigzag shape. The one dimension nanowhiskers were more benefits in manufacturing optoelectronic circuits (Dai Nezaki, etc, all., 2004.).

This research adopted joule heating method to heat the ZnO for growth of various forms of crystals. The joule heating circuit for the research was shown in Figure 2.8.

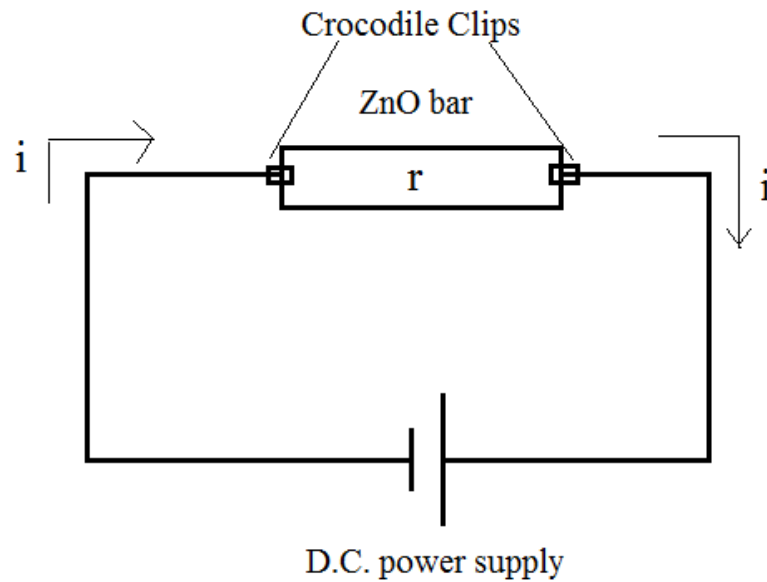


Figure 2.8. Joule heating circuit in this research.

## 2.5 CHARACTERIZATION

### 2.5.1 Scanning Electron Microscopy (SEM)

The main working concept of Scanning Electron Microscopy (SEM) is based on the wave nature of rapidly moving electrons. Electrons accelerate to 10,000 keV with a wavelength of 0.012 nm. Wavelength of visible light is from 380 nm to 780 nm. Optical microscope is limited by diffraction of light to about 1000 diameters magnification. SEM has overcome the resolution limitation of optical microscope as the magnification of SEM might be up to 1,000,000 diameters.

SEM generates beam of electrons in a vacuum. The electromagnetic condense lenses collimates the beam and the beam is then focused by an objectives lens. Lastly, the beam scans through the surface of samples by electromagnetic deflection coils. The collected secondary electrons which are released by sample correspond to primary image. After that, scintillation material produces flash light to detect secondary electrons. An image which is nearly similar to image seen though an optical microscope is obtained by relates and compares the sample scan position with the resulting signal.

Secondary mode is available in SEM. The image is produced by inelastic collision with incident electron beam. Besides that, energy adopted in secondary mode is around 50 eV which is lower than primary mode. It is mainly used for shape and topographic identification of nanostructures.

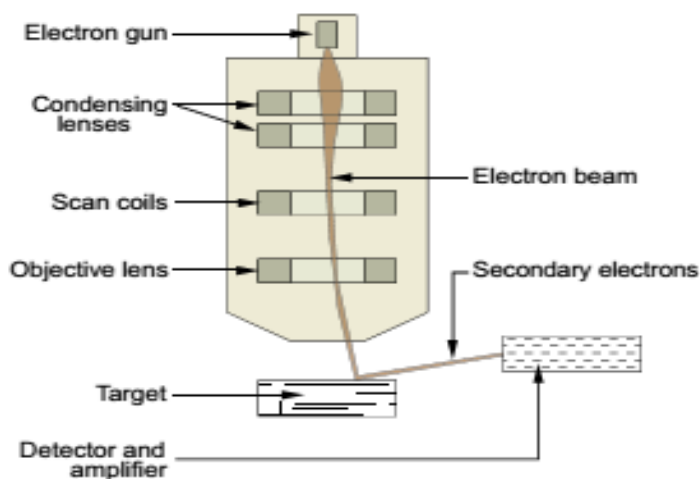


Figure 2.9. Basic working principles of SEM.

### 2.5.2 Ultraviolet-Visible (UV-Vis) Spectroscopy

A lot of molecules absorb visible or ultraviolet light. The wavelength of visible light is from 380 nm to 780 nm. On the other sides, the ultraviolet light has a wavelength range from 100 nm until 380 nm. The absorbance increases as the attenuation of the beam increases. According to Beer's law, absorbance,  $A$  is directly proportional to the concentration of the absorbing species and the path length as shown in Equation 2. 1.

$$A = \epsilon bc \quad (2.1)$$

where  $\epsilon$  is constant of proportionality, called absorptivity, in  $L \text{ mol}^{-1} \text{ cm}^{-1}$ ,  $b$  is the path length and  $c$  is the concentration of absorbing species.

The excitation of the outer electrons is the absorption of either ultra-visible or visible radiation. The electronic transition is divided into three types as shown in the following:

1. Transitions involving charge-transfer electrons.
2. Transitions involving  $\pi, \sigma$  and  $n$  electrons.
3. Transitions involving  $d$  and  $f$  electrons.

Atom or molecules absorbs energy and excited from highest occupied molecular orbital (H. O. M. O.) to lowest unoccupied molecular orbital (L. U. M. O.). The atoms in a molecule rotate and vibrate results in producing discrete energy levels. It is located on top of electronic level. The wavelength obtained from first excitonic peak is used to calculate the threshold of energy, E for electron to be excited from H. O. M. O. to L. U. M. O. as shown in Equation 2.2.

$$E = \frac{hc}{\lambda} \quad (2.2)$$

where h is plank constant, c is constant of light and  $\lambda$  is the wavelength of first excitonic peak.

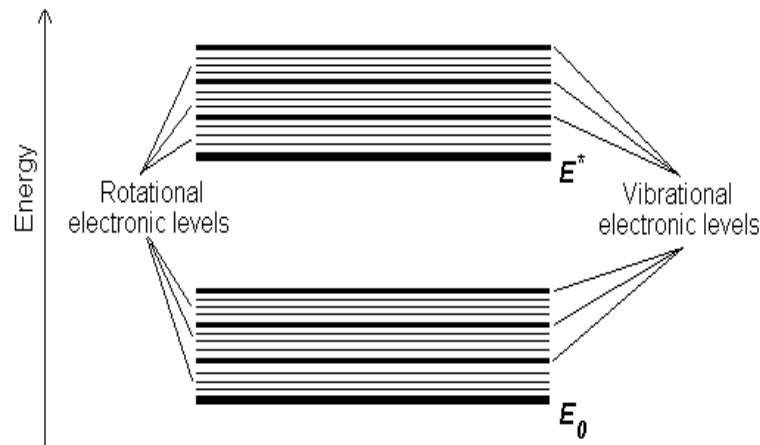


Figure 2.10. Electronic, rotational and vibrational electronic levels.

### 2.5.3 Photoluminescence Spectroscopy

Photoluminescence spectrometer is a device for examine the electronic structure of materials. Light is subjected to the sample. Photo-excitation process occurred when the light is absorbed and passed the remaining energy into the sample. Luminescence or emission of light is dissipated by sample. The luminescence in the photo-excitation phenomenon is called as photoluminescence.

The process of photo-excitation results in electrons to be excited to excited states. The excess energy is released when the electron return from excited states to equilibrium states. This may leads to process of radiative or emission of light. The energy of emitted light is the difference in energy levels between two electrons states

that participated in transition between excited and equilibrium states. The contribution of radiative process is the amount of light emitted (RuquanYe& Andrew R. Barron., 2011.).

ZnO exhibit two luminescence bands include short wavelength and long wavelength band. The absorption edge of crystal contributes to short wavelength band whereas long wavelength of band is the maximum of crystal. The long wavelength band normally falls into the range of green spectral with wavelength of 510 nm. The short wavelength band is corresponds to emission peak at 380 nm.

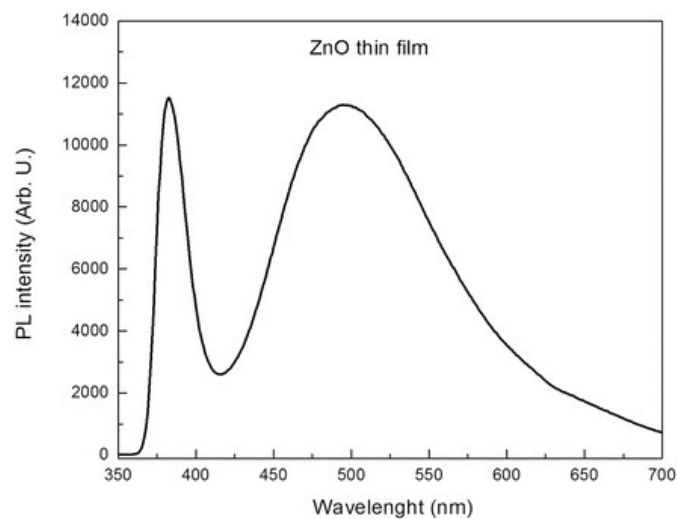


*Figure 2.11.*Photoluminescence spectrum of ZnO thin film.

Source: Reproduced from (Ruquan Ye & Andrew R. Barron., 2011)

#### **2.5.4 X-Ray Diffractometer (XRD)**

X-ray crystallography is a method where the diffraction of X-rays produced passes through the closely spaced lattice of atom. It is recorded and analyzed to reveal the characteristics of the lattice. It helps in study of material and molecular structure of a substance.

There were some equations related to the X-ray diffraction. According Scherrer's equation, crystalline size of a crystal was calculated by using the Equation 2.3 (P. Bindu&Sabu Thomas., 2014.)(P. J. M., etc, all., 2001).

$$T = \frac{0.9\lambda}{\beta \cos\theta} \quad (2.3)$$

where T is the average crystalline size in nm,  $\lambda$  is the wavelength of x-ray,  $\beta$  is the full width at half maximum of diffraction peak in radian and  $\theta$  is the diffraction angle.

Besides that, the peaks of scattered intensity were observed when X-rays were scattered from a crystal lattice. Bragg's law was adopted in calculated the details about the crystal structure. Thus, the d-spacing of the crystal could be found (Thornton & Andrew, 1993).

$$n\lambda = 2d\sin\theta \quad (2.4)$$

where n is the number of order and d is the lattice spacing.

The lattice parameter for tetragonal crystal structure was calculated with Equation 2.5.

$$\frac{1}{d^2} = \frac{h^2+k^2}{a^2} + \frac{1}{c^2} \quad (2.5)$$

where h, k and l were the Miller index belong to each peaks, a and c were the lattice parameter.

The wavelength of X-Ray was  $1.5406 \times 10^{-10}$  .

The X-Ray Diffraction pattern of pure ZnO nanoparticles was shown in Figure 2.12. All diffraction peaks corresponded to the characteristics of ZnO. The peaks with the corresponding phases were  $31.82^\circ$  (100),  $35.54^\circ$  (002),  $36.42^\circ$  (101),  $47.46^\circ$  (102),  $56.74^\circ$  (110),  $62.96^\circ$  (103),  $66.06^\circ$  (200),  $68.42^\circ$  (112),  $69.06^\circ$  (201) and  $78.82^\circ$  (202). Lattice parameters a and c were 0.315 nm and 0.529 nm respectively. According Scherrer equation, The crystalline size of ZnO nanoparticles was 10.00nm. Impurities was absent in this condition (Harish Kumar &Renu Rani., 2013.).



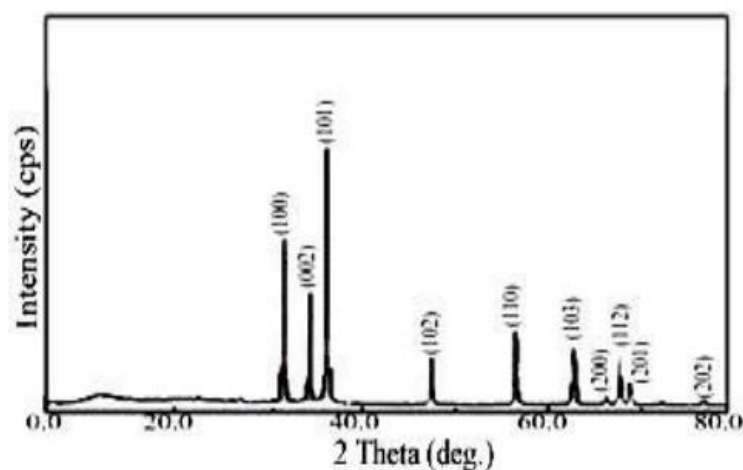


*Figure 2.12.* XRD pattern of ZnO nanoparticles.

Source: Reproduced from (Harish Kumar & Renu Rani., 2013)

## 2.6 APPLICATION

Crystal growth of ZnO widely applied in fabrication on devices. ZnO platelets, thin films and clusters consisted of Zn nano crystal and ZnO nanowires are applied in optical pump laser. This is because direct and wide band gap of ZnO. As mentioned above, ZnO has band gap of 3.37 eV at room temperature which responds to blue or UV region. It is applied in optoelectronic devices such as light- emitting diodes, photodetectors and laser diodes (Jagadish C & Pearton S J., 2006). ZnO also been fabricated into optical resonator with low dimensional structure and regular geometric configuration (A. Manekkathodi, etc, all., 2013). Large single crystal results in high quality of thin film and thus lowered the concentration of extended defects (Maeda K., etc, all., 2005). The application of strong non-linear resistance of polycrystalline ZnO into devices still under debate. Non-linear resistance has brought grain boundaries. The microscope mechanisms are in research progress.

## **CHAPTER 3**

### **MATERIALS AND METHODOLOGY**

#### **3.1 INTRODUCTION**

The materials and equipments used and methodology adopted in the research were listed and explained in this chapter. This research consisted of three stages which were synthesis of zinc oxide (ZnO) bars, conduct joule heating process and characterize the ZnO pellet bars. ZnO powder with 99.00% purity was grinded to form pellet bar and sintered at furnace. The joule heating process was conduct by introduced direct current density to the ZnO bar. After the process of joule heating, each of the zinc oxide bars was characterized by using Scanning Electron Microscopy (SEM), Ultraviolet-visible Spectroscopy, Photoluminescence Spectroscopy and X-ray Diffraction (XRD). Figure 3.1 illustrated the research methodology that adopted in this research.

#### **3.2 MATERIAL AND EQUIPMENT**

##### **3.2.1 Materials**

Materials used in this research were zinc oxide powder (ZnO) with 99.00% purity, copper powder (Cu) and ethanol.

### 3.2.2 Equipment

Equipment needed in this research were mortar and pestle, rectangular crucible, chattraway, spatula, five 200 ml vials, 200 ml beaker, vernier caliper, petri dish, rectangular die, digital weighing machine, single punch uniaxial hydraulic compactor, digital vernier caliper, laser thermometer, direct current (DC) power supply, crocodile clips, connecting wires, Bunsen burner, lighter and microscope slide.

### 3.3 METHODOLOGY

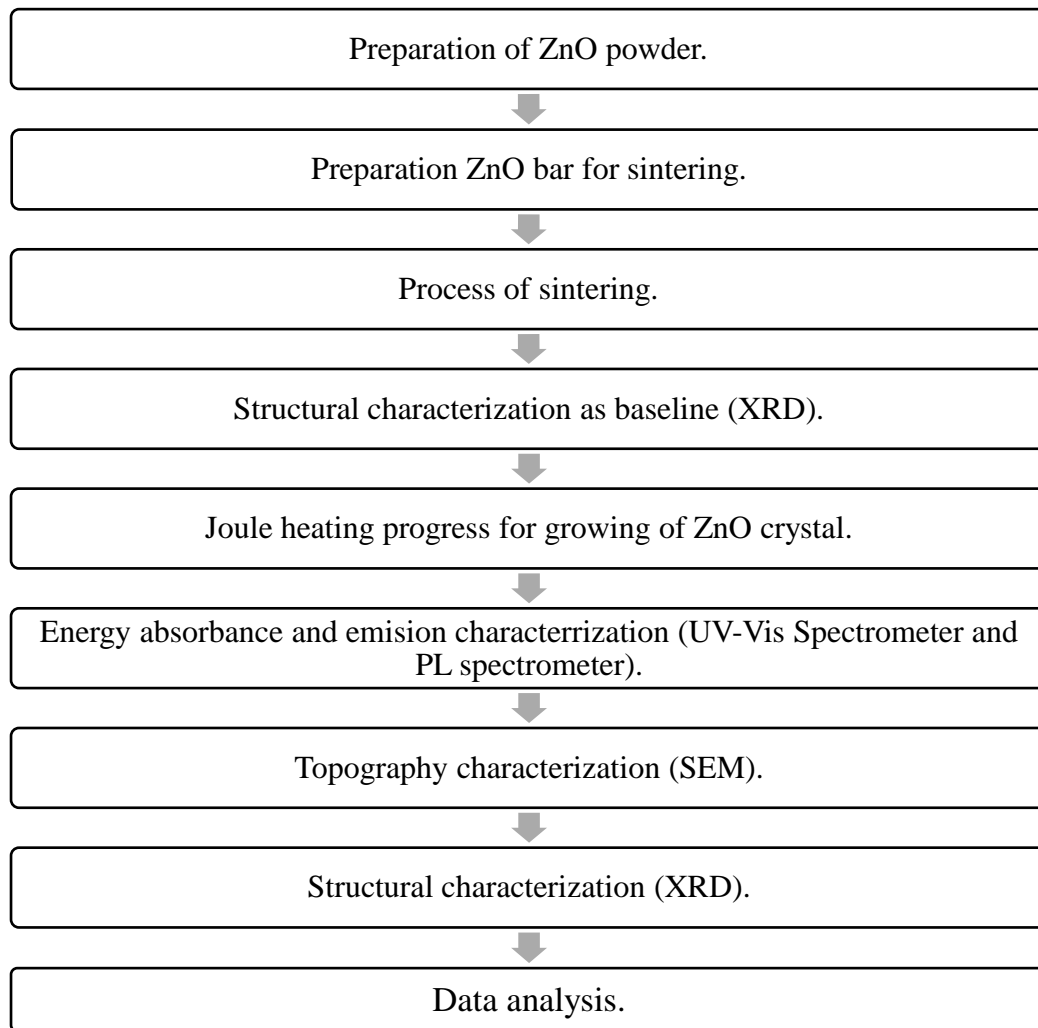


*Figure 3.1.*Research methodology adopted in this research.

### 3.3.1 Preparation of ZnO Powder

10 grams of ZnO powder with 99.00% purity was measured using digital weighing machine. The weighted ZnO powder was grinded manually with mortar and pestle for 6 hours at room temperature to achieve fine particles. The grinding process was shown in Figure 3.2 below.



*Figure 3.2.*Grinding process.

Ball mill were used to reduce the powder size into finer particles in usual case. However, ball mill were not suitable in this research since ZnO powder will be contaminated. The impaction between grinding ball (made from copper) with the inner wall of mechanical mill produced attritional heat which possibly leads to the happened of contamination. The color of ZnO powder had changed after grinded using ball mill. Thus, grinding with ball mill technique was not adopted in the research.

ZnO ceramic powder bar with average dimension of 13.00mm x 2.50mm x 1.00mm each were formed by adopting powder metallurgy methods. It contained three basic steps which were powder grinding, die compaction and sintering. Firstly, half of the amount of 30ml ethanol was added into ZnO powder gently. The mixture was grinded on hotplate manually and heated with temperature around 70.0°C. Another half of the amount ethanol was added slowly into the mixture during grinding process. Grinding process was end once the mixture was dry. The additional of ethanol was to ensure the pellet formed won't crack easily. The process was shown in Figure 3.3.



*Figure 3.3.*Grinding process for mixture of ZnO with ethanol.

### **3.3.2 Preparation of ZnO Bar for Sintering**

The compaction die used for shaping was a base-ended design with cavity dimension of 14.95mm x 30mm x 40mm as shown in Figure 3.4. The round shape compaction die was not adopted in this research since the pellet formed faced the challenged in cut into a fixed dimension bar. This gave effect on result analysis. The die was cleaned with ethanol before compaction. No lubrication should be added in the compaction die to prevent contamination of the sample. Binder was not added into ZnO powder in this research as it would reduce the resulting sintered density.

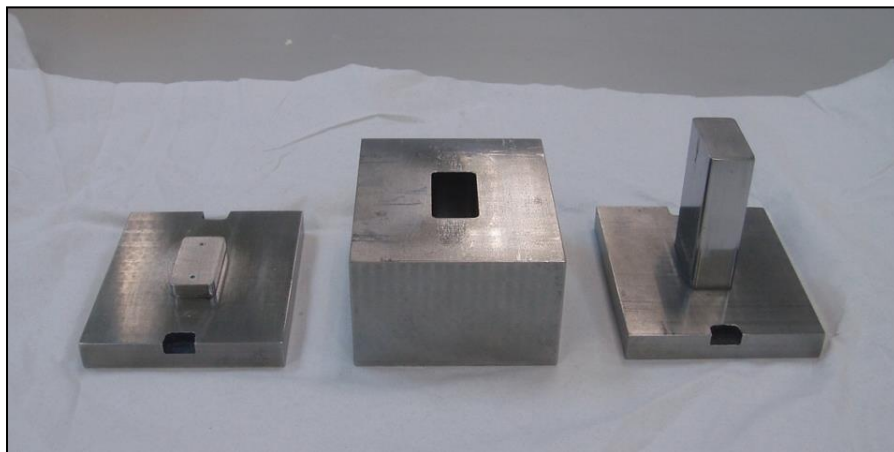


*Figure 3.4.*Compaction die for shaping ZnO bar.

Amount of ZnO powder used in formation of each bar was 1.5g. This amount of ZnO powder was adopted since it resulted in compaction height around 1.15mm and was expected to reduce to 1.00mm after sintered. The amount of ZnO powder was measured with digital weighing machine.

A small amount of zinc stearate was added on the surface of the compaction die to avoid ZnO powder stick on the surface of compaction die. 1.5g of ZnO powder was gently poured into the compaction cavity. Chattaway used to ensure the height of ZnO powder bar was same. Single-punch hydraulic uniaxial compactor was adopted for compaction of ZnO bar as shown in Figure 3.5. ZnO compact bars were compacted at different compaction pressure which includes 2 Ton and 3 Ton. There were three ZnO compact bars for each compaction pressure category. The unsatisfied formed ZnO compact bars with uneven surfaces, unacceptable fracture surfaces or many apparent cracks were demolished and reginded into finely divided particles using mortar and pestle.



*Figure 3.5.*Single-punch hydraulic uniaxial compactor.

Dimension of fabricated ZnO compact bar was measured carefully and scrupulously with a digital vernier caliper as shown in Figure 3.6. Vernier caliper must avoid contacted with ZnO compact bar body tightly as it would result in fracture or deformation. ZnO compact bars weight was measured.



Figure 3.6. Vernier caliper for measuring dimension of ZnO compact bar.

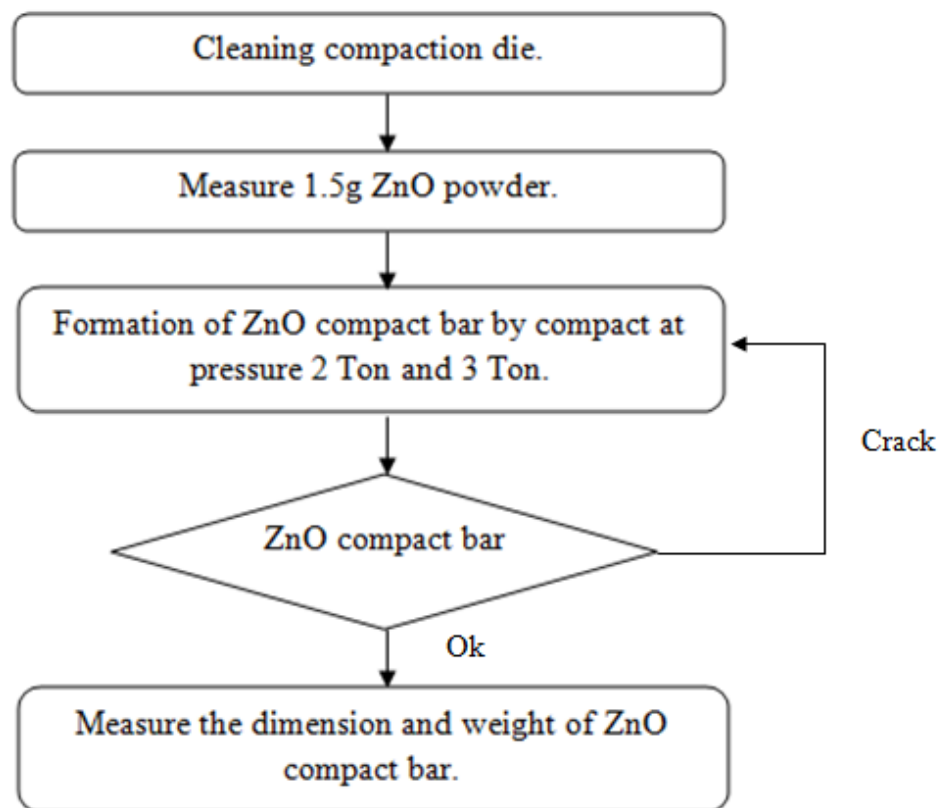


Figure 3.7. Flow chart of preparation of ZnO bar for sintering process.

### 3.3.3 Process of Sintering

Final step of powder metallurgy method was the sintering process. The ZnO compact bars were sintered in a box metallurgical furnace as shown in Figure 3.9. The reason for box metallurgy furnace was chosen because it was convenience for the ZnO compact bars in handling into or out of the furnace. The ZnO compact bars were placed inside crucible boats before handling into the box metallurgy furnace. The ZnO compact bars were sintered at 1100°C to prevent formation of large grain size. The sintered rate was 16.5°C/min to avoid grain growth rates increase rapidly. The sintering process took 3 hours to ensure a complete densification of ZnO bars through high isolation of pores at grain edges and high neck growth.



*Figure 3.8.*Box metallurgical furnace.

The ZnO bars were left inside the box metallurgy furnace 24 hours after sintering process for cooling purpose. Cooling purpose lowered the possibility of cracking from occurring and decreased the internal stress resulted from sintering process on ZnO bars. Dimension and weight of ZnO bars after cooling process was measured. Density of ZnO bars before and after sintered were calculated and compared to determine the percent relative density of each sintered compact.



### 3.3.4 Structural Characteristics as Baseline

The X-ray diffractometer model adopted in this research was XRD, Miniflex II, Rigaku, Japan as shown in Figure 3.11. X-ray diffraction is a nondestructive test technique. The X-ray diffraction was carried by the calcined nanowires for determination of crystalline size of sample with its orientation, phase analysis and chain orientation. The sample was cut and placed on top of a holder finally placed inside the X-ray Diffractometer. Data was taken for  $2\theta$  range of 3 to 80 degrees with a step of 0.02 degree and at the scan rate of  $1.0^\circ/\text{min}$ .



*Figure 3.9.* X-ray Diffractometer, Miniflex II, Rigaku, Japan.

### 3.3.5 Joule Heating Process

Small piece ZnO bar was adopted for joule heating process to lower the need of current density to heat the ZnO bar. In this research, ZnO bars with dimension 13.00mm x 2.50mm x 1.00mm were adopted. The diamond cutter with a very hard and sharp coated tip was normally used to cut glass slides. The design of diamond cutter result it suitable to cut brittle and low hardness ceramics. Diamond cutter was used to create a groove on the surface of ZnO bar which lead to initial crack site for the propagation of the formed crack to happened. Then, the groove size would become larger when repeated stresses were applied on the surface of ZnO bar. The formed rough edges and surface of cut ZnO bar were flatten and smoothened by rubbing with sand paper. The

dimension of ZnO bar was measured during rubbing process at different time interval to ensure closely reach desired sample dimension. Final ZnO bar dimension were recorded and the weight was measured. The ZnO bar was rubbed with tissue paper to remove the powder on surface.

The set up of equipment for joule heating was shown in the Figure 3.10. Sample was connected to direct current power supply with high current density to speed up the crystal growth rate. Stranded connecting wires with high resistivity were used to connect the power supply with crocodile clips. Normally, single strand wire works better for direct current supply compared to alternating current due to skin effect of alternating current. Skin effect was a phenomenon which caused the current travel through the outer layers of wire and increased with increasing of frequency. Stranded wires not affected by skin effect due to high surface area and low cross sectional area. However, stranded wires were adopted in this research since its characteristics works better for crystal growth on surface area and increase the resistivity. Crocodile clips were used to connect connecting wires with ZnO bar.

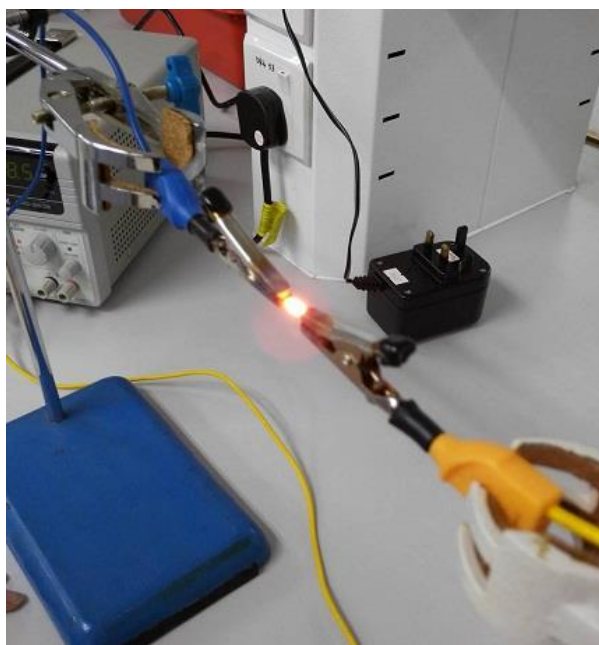


*Figure 3.10.* Schematic of joule heating equipment.

The voltage was set as 15.0V at the beginning of the process. Current was set at different category which were 2.5 A, 3.0 A and 3.5 A for comparison of amount and type of crystal growth. ZnO was a wide band gap semiconductor ceramic. Thus, Bunsen

burner was used to excite the electrons to conduction band at the beginning of the joule process. Bunsen burner was removed once the current passed through the ZnO bar. Temperature of surface of ZnO bar was taken every 5 minutes with laser thermometer as shown in Figure 3.11. Observation such as brightness and growth of crystal was recorded.



Figure 3.11. Laser thermometer.

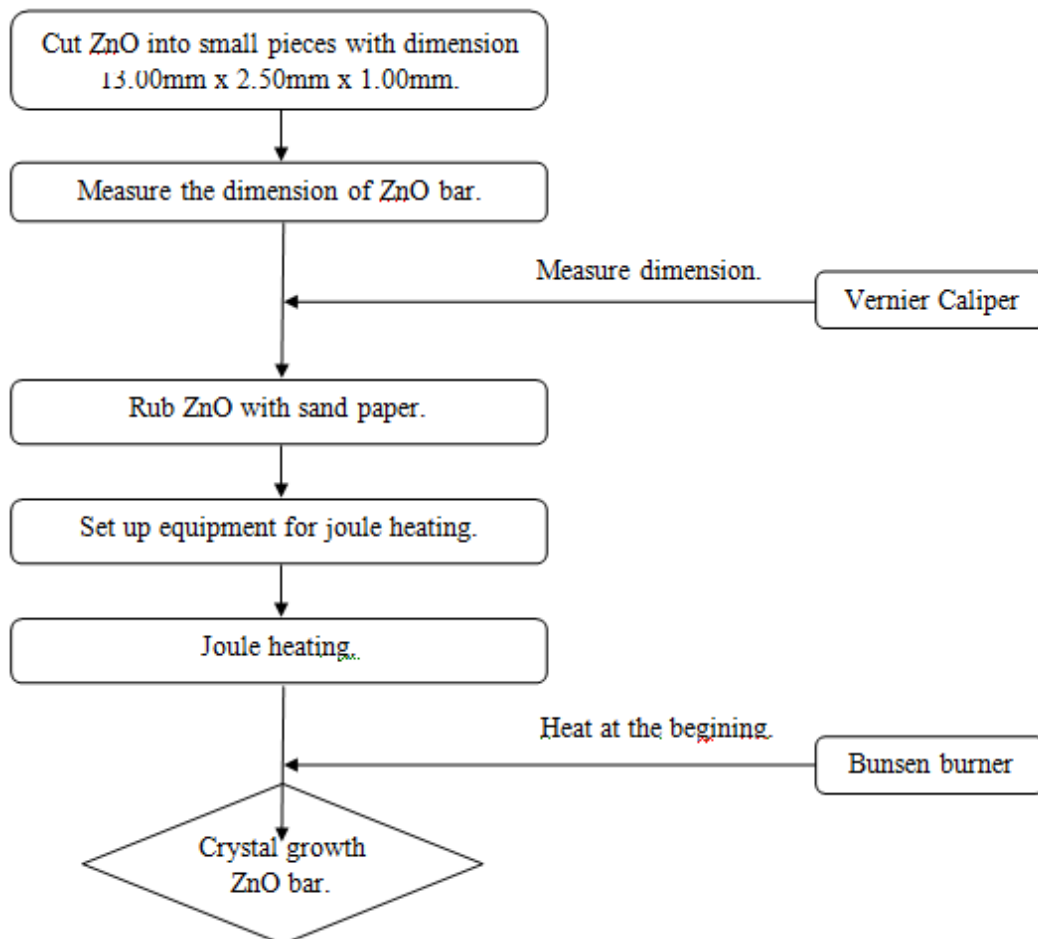
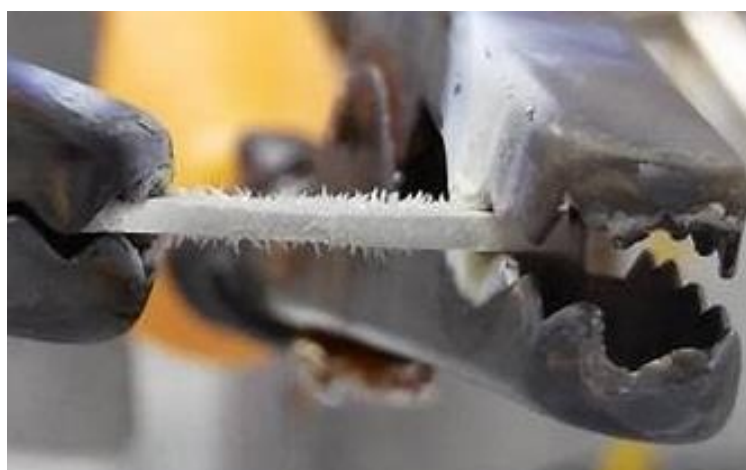


Figure 3.12. Flow chart of joule heating process.



*Figure 3.13.*Joule heating process.



*Figure 3.14.*Crystal growth on ZnO bar using joule heating method.

### **3.3.6 Energy Absorbance and Energy Emission Characterization**

Energy absorbance characterization was carried out by using UV-Vis spectrometer as shown in Figure 3.15. Firstly, microscope glass slide was set as reference and the baseline was measured. The ZnO bar was stick on microscope glass slide by using double side tape. The glass slide was hold with solid compartment holder and placed inside the UV-Vis spectrometer gently. The system was run with range of wavelength set from 200 nm until 1400 nm. The result was saved. The first excitonic peak of the absorbance wavelength was the threshold of wavelength where the electron required to be excited from highest occupied molecular orbital (HOMO) to lowest unoccupied molecular orbital (LUMO).



*Figure 3.15.*UV-Vis spectrometer.

Energy Emission characterization was carried out by using Photoluminescence spectrometer as shown in Figure 3.16. The glass slide of 434 nm was set as reference. The ZnO bar was stick on microscope glass slide by using double side tape. The glass slide was hold and placed inside the Photoluminescence spectrometer gently. The cover of Photoluminescence spectrometer was opened to ensure the light pass through ZnO bar. The system was run with range of wavelength set from 300 nm until 900 nm. The result was saved. The peak of the wavelength was the wavelength released when the excited electron from LUMO recombined hole in HOMO.



*Figure 3.16.*Photoluminescence spectrometer.

### 3.3.7 Topography Characterization

Topography characterization was carried out by using Scanning Electron Microscopy with model FEI as shown in Figure 3.17. Each of the samples was mounted on specimen stub and attached using carbon tape. Surface of the samples were not coated with platinum atom since the samples still have to undergo structural characterization. For each sample, few areas were detected randomly with different magnification.



*Figure 3.17.* Scanning Electron Microscopy with model FEI.

### 3.3.8 Structural Characterization

The crystal growth ZnO bars were undergoes X-ray diffraction characterization to determine the peak of different crystal growth. The X-ray diffraction was carried by the calcined nanowires for determination of crystalline size of sample with its orientation, phase analysis and chain orientation. The crystal growth on surface of ZnO bar was scrapped with laboratory blade into a low background holder. The holder was then put inside the cavity of X-ray Diffractometer for characterization. Data was taken for  $2\theta$  range of 3 to 80 degrees with a step of 0.02 degree and at the scan rate of  $1.0^\circ/\text{min}$ .

## **CHAPTER 4**

### **RESULT AND DISCUSSION**

#### **4.1 INTRODUCTION**

This chapter consisted of the details of the characterization of crystal growth of ZnO. A brief summary of the results were discussed in the next paragraph.

This research found out that the optimum compact pressure and current for crystal grew are 3.0 Ton and 3.0 A respectively. The biggest quantity of crystal grew by this sample. The most common crystal is in hexagonal shape and the conjecture made is it is correspond to the plane (1 0 1). Mostly the excitonic energy was around 3.20 eV which was nearly matched with theoretical band gap 3.37 eV. All the value of peaks was around 410 nm. The XRD results showed most of the crystals grew on the plane (1 0 1). The crystal grew were in rock like shape. This was proved by the plane (1 0 1) had the highest intensity in all the samples.

#### **4.2 CHARACTERIZATION OF ZnO CERAMIC BAR**

##### **4.2.1 Analysis Compaction Results**

This research had proved that fine compacts with no physical cracks were difficult to be obtained as large compaction pressure was applied. The compacts experienced fractures, cracks and inhomogeneous powder flow as shown in Figure 4.1. Besides that, the ZnO compacts also experienced delamination and large density gradients. The ZnO compact had higher probability in experienced cracks at compaction



pressure higher than 3.5 Ton. A lot of tries to find out the suitable pressure in forming fined ZnO compact. As a result, 2.0 Ton and 3.0 Ton were applied as compact pressure in this research. Improper distribution of ZnO powder inside the cavity of the die and ununiform pressure distribution during compaction caused inhomogenous powder flow defect. ZnO powder should be initially dried on a hot plate for about 5 minutes at 50 °C to reduce moisture. This helped to lower the interparticle bonding and made the ZnO powder became homogenous. Thus, it lowered the possibility of appearance of density gradient over ZnO compact and prevented the compact stick on the inner surface of the compact die (Rahaman, M. N., 2003). Formation of crack on compact may occurred when removed fabricated compact from die. A piece of paper was used to transport the fabricated compact from die to petri dish. The process was done carefully.

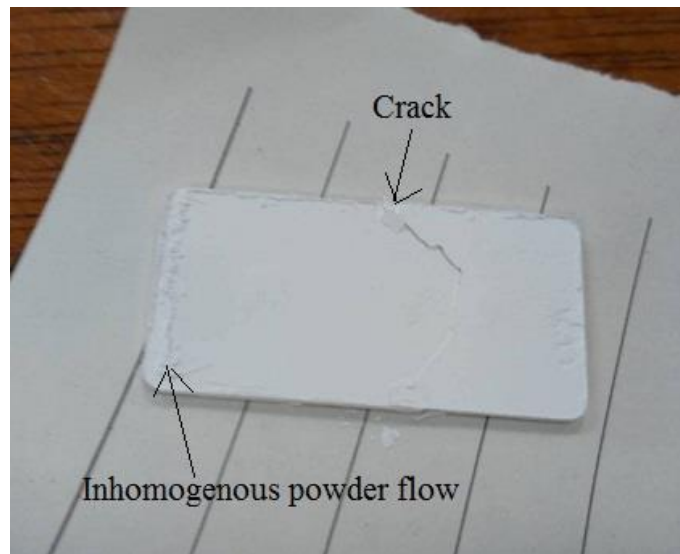


*Figure 4.1.* Pellet which experienced cracks and inhomogeneous powder flow.

The dimension of fabricated ZnO compacted bars were measured and recorded in Table 4.1. The volume of the compact bars was calculated with Equation 4.1 whereas the density of fabricated ZnO compact before sintering process was calculated using the Equation 4.2. The calculated volume and density of ZnO compact bars were calculated in Table 2.

$$V = L \times W \times T \quad (4.1)$$

where volume,  $V$  of the ZnO compact bar was measured in  $\text{mm}^3$ ,  $L$  was the length of ZnO compact bar in mm whereas  $W$  and  $T$  were weigh and thickness of compact bar respectively and measured in mm.



$$\rho = \frac{m}{v} \quad (4.2)$$

where density is  $\rho$  and measured in g/cm<sup>3</sup>, m is the mass of ZnO compact bar and v is the volume of ZnO compact bar.

Table 4.1

*The dimension and weigh of fabricated ZnO compacts.*

<b>Pressure Applied (Ton)</b>	<b>Sample</b>	<b>Length (mm)</b>	<b>Width (mm)</b>	<b>Thickness (mm)</b>	<b>Weight (g)</b>
2.0	S1	30.31	15.20	1.11	1.48
	S2	30.31	15.26	1.12	1.46
	S3 (regrind)	30.31	15.22	1.11	1.44
3.0	S4	30.33	15.30	1.10	1.49
	S5	30.26	15.24	1.12	1.45
	S6 (regrind)	30. 34	15.30	1.11	1.49

Table 4.2

*The value of volume and density of ZnO compacts.*

<b>Sample</b>	<b>Volume (mm<sup>3</sup>)</b>	<b>Density (g/cm<sup>3</sup>)</b>
S1	511.39	2.89
S2	518.03	2.82
S3 (regrind)	512.06	2.81
S4	510.45	2.92
S5	516.50	2.81
S6 (regrind)	515.26	2.89

#### 4.2.2 Analysis Sintering Results

ZnO sintered bars experienced color changed from white to yellow brownish after sintered in box furnace as shown in Figure 4.2. ZnO sintered bar experienced color changing due to its thermochromic characteristic of ZnO. ZnO sintered bar experienced some defects. The bar formed had experienced cracks, fracture, incomplete sintering

effect, black spot and meandering.

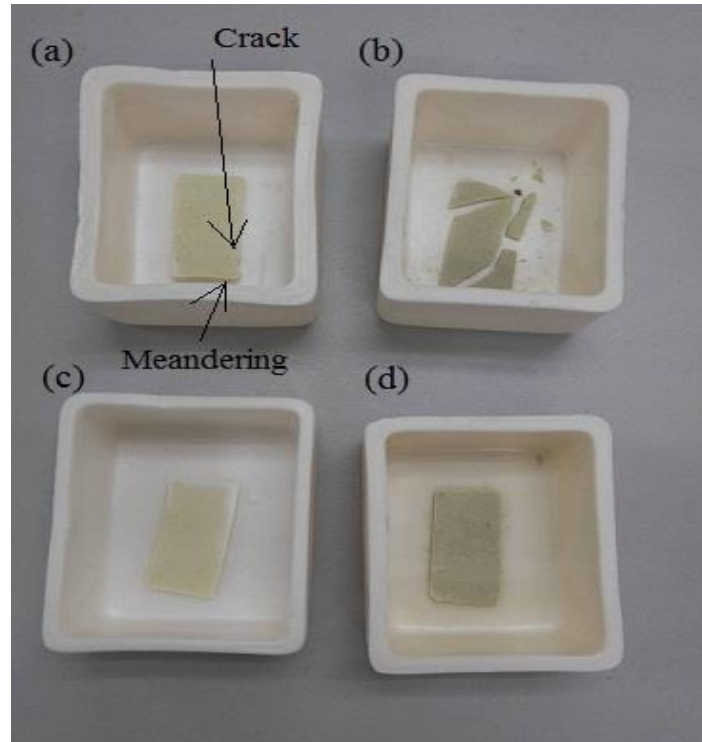


*Figure 4.2.* Physical defect experienced by sintered bar included (a) crack and meandering, (b) fractures, (c) incomplete sintered effects and (d) black spots.

The ZnO bars were transferred to petri dish carefully from crucible boat. The dimensions of ZnO sintered bar were measured and recorded in Table 4.3. The volume and density of ZnO bar after sintering process were calculated using Equation 4.1 and Equation 4.2 respectively and recorded in Table 4.4. Density of ZnO pellet increased after sintered due to the decreasing in weigh and dimension. The dimension of ZnO pellet decreased after sintered since the grain boundaries had decreased. The moisture had evaporated during sintering process.

Table 4.3  
*The dimension and weigh of ZnO bar after sintered.*

<b>Pressure Applied (Ton)</b>	<b>Sample</b>	<b>Length (mm)</b>	<b>Width (mm)</b>	<b>Thickness (mm)</b>	<b>Weight (g)</b>
2.0	S1	25.33	12.60	1.03	1.48
	S2	25.52	12.89	0.93	1.44
	S3 (regrind)	25.11	12.61	1.05	1.43
3.0	S4	25.31	12.66	1.07	1.45
	S5	25.67	12.83	0.91	1.42
	S6 (regrind)	25.23	12.70	0.83	1.46

Table 4.4  
*The value of volume and density of ZnO bar after sintered.*

<b>Sample</b>	<b>Volume (mm<sup>3</sup>)</b>	<b>Density (g/cm<sup>3</sup>)</b>
S1	328.73	4.50
S2	305.93	4.71
S3 (regrind)	332.47	4.30
S4	342.85	4.23
S5	299.70	4.74
S6 (regrind)	265.95	5.49

Percentage of relative density of ZnO bar was determined by comparing density of ZnO sintered bar with theoretical density of ZnO which was 5.606 g/cm<sup>3</sup> (T. Asokan, etc, all., 1987). The percentage of linear shrinkage value of the thickness was compared. The results of percentage of relative density and percentage of linear shrinkage were recorded in Table 4.5.

Table 4.5

*Percentage of relative density and percentage of linear shrinkage of ZnO bar.*

<b>Pressure Applied (Ton)</b>	<b>Sample</b>	<b>Percentage of relative density (%)</b>	<b>Percentage of linear shrinkage (%)</b>
2.0	S1	80.27	7.21
	S2	84.02	16.96
	S3 (regind)	76.70	5.41
3.0	S4	75.45	2.73
	S5	84.55	18.75
	S6 (regrind)	97.93	25.23

Table 4.5 showed that the samples with 3.0 applied pressure experienced larger percentage of linear shrinkage compare to samples with 2.0 applied pressure. This might be due to bigger amount of air molecular between the grains had been removed when larger compact pressure was applied.

Sample 6 had a highest density and very closed to the theoretical value. The result in Table 4.5 showed that it had the highest percentage of relative density. It should be the most idea sample but the sample experienced fracture as shown in Figure 4.2 (b). Therefore, the uniform dimension of small pieces of ZnO bar cannot be obtained from Sample 6. As a result Sample 6 was rejected. The reason for Sample 6 to experience fracture defect might be due to Sample 6 undergoes regrind process. Unsatisfied compact pellet formed was grinded and formed Sample 6.

Sample 2 (2.0 Ton) and Sample 5 (3.0 Ton) were selected to proceed with joule heating process. Sample 2 and Sample 5 had quite high percentage of relative density and experienced the less physical defects among the others. Both of Sample 2 and Sample 5 were cut into small pieces using glass cutter. The value of dimension and weigh were measured and recorded in Table 4.6.

Table 4.6  
*The dimension and weigh of small pieces of ZnO bar.*

<b>Pressure Applied (Ton)</b>	<b>Sample</b>	<b>Length (mm)</b>	<b>Width (mm)</b>	<b>Thickness (mm)</b>	<b>Weigh (g)</b>
2.0	SZ1	12.81	2.64	0.88	0.128
	SZ2	12.84	2.41	0.85	0.141
	SZ3	12.96	2.34	0.82	0.129
	SZ4	12.86	2.41	0.80	0.131
	SZ5	12.92	2.57	0.90	0.130
	SZ6	12.84	2.71	0.95	0.158
	SZ7	12.87	2.54	0.84	0.137
	SZ8	12.81	3.16	0.91	0.174
	SZ9	12.82	3.33	0.99	0.183
3.0	SZ10	12.81	2.18	0.93	0.118
	SZ11	12.85	2.86	0.88	0.145
	SZ12	12.82	2.62	0.86	0.146
	SZ13	12.80	2.96	0.84	0.165
	SZ14	12.79	3.21	0.87	0.167
	SZ15	12.84	2.64	0.91	0.149
	SZ16	12.76	2.42	0.95	0.132

All the samples failed in getting the exact dimension of 13.00 mm x 2.50 mm x 1.00 mm due to the tip of the diamond cutter was not sharp enough and the force was not evenly applied. It might be improved by replaced with a new glass cutter and practiced more in cutting skills. Samples with nearly same dimension would be used to proceed with joule heating process to reduce the effect caused by dimension difference in characterization. Therefore, samples SZ2, SZ3, SZ4, SZ12, SZ13 and SZ15 were choosed to conduct joule heating process. The density and percentage of relative density of each sample were calculated.

Table 4.7

*The value of volume, density and percentage of relative density of ZnO bar after sintered.*

Pressure Applied (Ton)	Current (A)	Sample	Volume (cm <sup>3</sup> )	Density (g/cm <sup>3</sup> )	Percentage of relative density (%)
2.0	2.50	SZ3	0.0249	5.1807	92.41
	3.00	SZ4	0.0248	5.2823	94.23
	3.50	SZ2	0.0263	5.3612	95.63
3.0	2.50	SZ15	0.0308	4.8377	86.29
	3.00	SZ12	0.0289	5.0519	90.12
	3.50	SZ13	0.0318	5.1887	92.56
	3.50	SZ14	0.0357	4.6779	83.44

#### 4.2.3 X-Ray Diffraction Analysis

Sintered ZnO was undergoes X-Ray Diffraction characterization as a baseline to compare with the sample grew of crystal. The sample was cut into the dimension of area 1.00 cm x 1.00 cm. Characterization result was shown in Figure 4.3. The known diffraction peaks were positioned at  $2\theta = 34.8300^\circ$ ,  $36.6210^\circ$ ,  $47.8910^\circ$ ,  $56.8988^\circ$  and  $63.2040^\circ$ . All characteristics peaks could be indexed to the (0 0 2), (1 0 1), (1 0 2), (1 1 0) and (1 0 3) respective angle. The d-spacing of sintered ZnO bar was  $d_{002} = 8.7015 \text{ \AA}$ ,  $d_{101} = 8.8783 \text{ \AA}$ ,  $d_{102} = 9.8514 \text{ \AA}$ ,  $d_{110} = 10.4922 \text{ \AA}$  and  $d_{103} = 10.9614 \text{ \AA}$ . The observed value was nearly match with the reference of a standard pure ZnO nanoparticles (Harish Kumar & Renu Rani., 2013.). The intensity peaks were 4384 cps, 8132 cps, 3296 cps, 3420 cps and 3550 cps corresponded to respective angle.

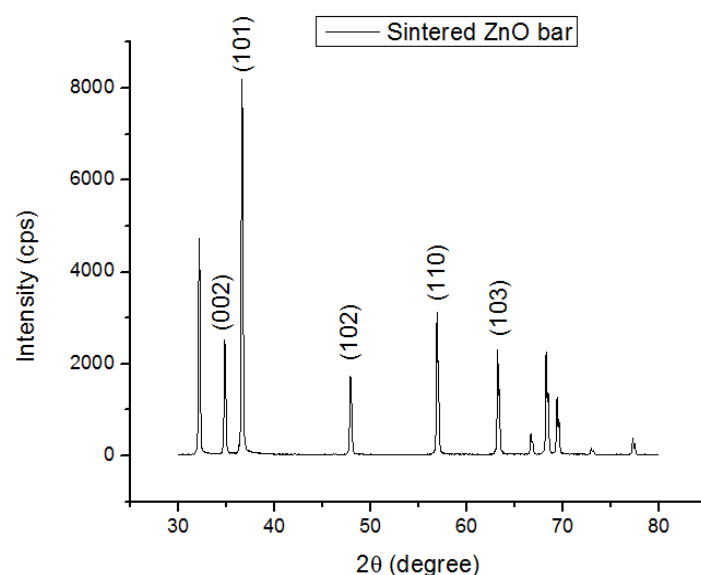


Figure 4.3.X-Ray Diffractogram of sintered ZnO bar.

Table 4.8

(*h k l*) plane, *d*-spacing and crystalline size of sintered ZnO bar.

<b>h</b>	<b>k</b>	<b>l</b>	<b>2θ</b> <b>(degree)</b>	<b>β (degree)</b>	<b>d-spacing</b> <b>(Å)</b>	<b>Crystalline size</b> <b>(Å)</b>	<b>Intensity</b> <b>(cps)</b>
0	0	2	34.8300	0.1670	2.5737	8.7015	4384
1	0	1	36.6210	0.1645	2.4518	8.8783	8132
1	0	2	47.8910	0.1540	1.8979	9.8514	3296
1	0	3	63.2040	0.1510	1.4700	10.9614	3420
1	1	0	56.8988	0.1503	1.6169	10.4922	3550

### 4.3 CHARACTERIZATION OF JOULE HEATING RESULT

#### 4.3.1 Analysis of Joule Heating Result

At the beginning of the research, different range of current and voltage were applied to obtain the optimum value. It was first try with 10.0 V and 2.00 A, there was no change on surface of ZnO bar. Thus, the current was increase to 3.00 A for another test. The ZnO bar experienced color changing from yellowish become bright orange.

However, the process took very long period to finish. Therefore, the voltage increased to 15.0 V and the current was set as 3.00 A, the crystal grow vigorously and the brightness of the ZnO bar increased. The current was increased to 5.00 A and the voltage was remained at 15.0 V for the third test. There was fire spark and the process end within 20 minutes and no significant growth of crystal on the surface of ZnO bar. The current through the circuit was too high and affected the growth of crystal. Therefore, the current applied was lowered down to 4.00 A and the changes of the surface of ZnO was observed. Significant crystal growth on surface and the ZnO bar broke down into two parts before process end. The crystal growth on the broken part was in huge amount and more firm as compare to the crystal on the surface. However, 4.00 A was not adopted in the research since the sample with 2 Ton applied pressure failed to withstand the high current as the process will end within 13 minutes. As a result, the optimum voltage in this research was 15.0 V whereas the optimum range of current applied was 2.50 A, 3.00 A and 3.50 A.

Sample, SZ3 (2.0 Ton) with cross sectional area  $0.3033 \text{ cm}^2$  was used to carry out joule heating process with voltage 15.0 V and 2.50 A. The current density threshold of SZ3 was  $8.2427 \text{ A/cm}^2$ . The output current and voltage throughout the circuit were 0.01 A and 15.0 V respectively once the power supply turned on since the electrons were not being excited. After ten minutes the process started, the ZnO bar remained unchanged. Bunsen burner was used to heat the ceramic bar as an agent to excite electron from valence band to conduction band. The heating process took 3.01 minutes until the current pass through the circuit became stable and maximum. The current through the circuit was 2.48 A and remained stable throughout the process whereas the voltage was keep on changing throughout the process. Current density exceeded the current density threshold now. The ZnO bar experienced color changed and became very bright in the middle of the bar. The voltage was 14.3 V and temperature was  $136.6^\circ\text{C}$ . After 55 minutes, a small amount of crystal was grew on the surface near negative terminal and the brightness increased. The temperature and voltage were  $233.2^\circ\text{C}$  and 13.3 respectively. Crystal grew at the bottom of ZnO bar after 70 minutes and temperature was 183.4 with same voltage. The whole process took 1 hour and 50 minutes. The ZnO bar changed back to yellowish once the process end.



The research was carried on with another sample, SZ4 (2.0 Ton) with cross sectional area  $0.3099 \text{ cm}^2$ . The 3.00 A and 15.0 V were set at the beginning of the experiment. The current density threshold of SZ4 was  $9.6805 \text{ A/cm}^2$ . The output current and voltage throughout the circuit were 0.01 A and 15.0 V respectively once the power supply turned on since the electrons were not being excited. After ten minutes the process started, the ZnO bar remained unchanged. Bunsen burner was heat for 3.05 minutes until the current pass through the circuit became stable and maximum. The stable current 2.98 A remained unchanged through the process whereas the voltage keep on changing. The ZnO bar near the positive terminal very bright and slowly extend to negative terminal. Wool like crystal grew on the surface of ZnO bar. The temperature was  $223.4 \text{ }^\circ\text{C}$  and the voltage was 11.3 V at that moment. There were larger amount of crystal grew near to negative terminal. The brightness of ZnO bar became dimmer after 70 minutes and the temperature dropped to  $176.6 \text{ }^\circ\text{C}$ . The process took 1 hour 29 minutes.

Sample SZ2 was the last sample in 2.0 Ton category. It had a cross sectional area of  $0.3094 \text{ cm}^2$  and the applied current and voltage were set as 3.50 A and 15.0 V respectively. The current density threshold of SZ2 was  $11.3122 \text{ A/cm}^2$ . The output current and voltage throughout the circuit were 0.01 A and 15.0 V respectively once the power supply turned on since the electrons were not being excited. Thus, Bunsen burner was used to heat the ZnO bar for 2.11 minutes until the the current pass through the circuit became stable and maximum. The stable current 3.48 A remained unchanged through the process whereas the voltage keep on changing. ZnO bar gave spark and very bright. The temperature was  $319.0 \text{ }^\circ\text{C}$  at 15<sup>th</sup> minute with 10.1 V. The spark was released on negative terminal and the brightness become dimmer and the crystal grew near negative terminal. The temperature ws  $254.0 \text{ }^\circ\text{C}$  with 9.5 V. Both upper and bottom surface of ZnO bar grew crystal. The process took 1 hour and 47 minutes.

The research was continued with the second category with 3.0 Ton of applied pressure. Sample SZ15 with cross sectional area  $0.3390 \text{ cm}^2$  was carried out joule heating process with 2.50 A and 15.0 V. The current density threshold of SZ15 was  $7.3746 \text{ A/cm}^2$ . The output current and voltage throughout the circuit were 0.01 A and 15.0 V respectively once the power supply turned on since the electrons were not being

excited. Thus, Bunsen burner was used to heat the ZnO bar for 2.28 minutes until the the current pass through the circuit became stable and maximum. The stable current 2.48 A remained unchanged through the process whereas the voltage keep on changing. Wool like crystal grew at the bottom of ZnO bar at 25<sup>th</sup> minute. The voltage and temperature were 12.5 V and 169.4 °C respectively. The crystal grew more as the time passed and mainly focused on the part near to negative terminal. After that, the crystal started to grow at the side and slowly extended to positive terminal. The crystal grew on the surface started and the temperature increased to 227.2 °C and the voltage was around 12.7 V. Brightness of the ZnO bar increased and the crystal grew more vigorously. The voltage was changing non-stop from 13.5 V to 13.8 V before process end. The process took 3 hours and 18 minutes.

Sample SZ12 (3.0 Ton) with cross sectional area 0.3359 cm<sup>2</sup> was proceed with joule heating process with 3.00 A and 15.0 V. The current density threshold of SZ12 was 8.9312 A/cm<sup>2</sup>. The output current and voltage throughout the circuit were 0.01 A and 15.0 V respectively once the power supply turned on since the electrons were not being excited. Thus, Bunsen burner was used to heat the ZnO bar for 1.18 minutes until the the current pass through the circuit became stable and maximum. The stable current 2.98 A remained unchanged through the process whereas the voltage keep on changing. Crystal grew on the surface of ZnO vigorously and the brightness of ZnO bar increased. Temperature was 284.9 °C whereas voltage was 13.4 V. There were more crystal grew near to positive terminal. The process end after 31 minutes and ZnO bar showed very bright before process ended.

Sample SZ13 was the last sample for joule heating in the second category. It consisted a cross sectional area of 0.3789 cm<sup>2</sup>. The current and voltage were set as 3.50 A and 15.0 V respectively at the beginning of the experiment. The current density threshold of SZ13 was 9.2373 A/cm<sup>2</sup>. The output current and voltage throughout the circuit were 0.01 A and 15.0 V respectively once the power supply turned on since the electrons were not being excited. Thus, Bunsen burner was used to heat the ZnO bar for 2.19 minutes until the the current pass through the circuit became stable and maximum. The stable current 3.48 A remained unchanged through the process whereas the voltage keep on changing. The positive terminal of ZnO bar very bright whereas the

negative part was dimmer. Temperature was around 355.6 °C and voltage was 11.9 V. Brightness became dimmer and the crystal grew more vigorously at negative part. The temperature dropped to 271.4 °C. At 20<sup>th</sup> minute, the crystal grew on upper surface of ZnO bar and the part clipped by crocodile clips. The ZnO bar produced spark before process end. It took 32 minutes.

On the other hand, sample SZ14 (3.0 Ton) was used for other purpose. Copper powder was added in the joule heating process as a catalyst agent for ZNO crystal growth. It had a cross sectional area of 0.4106 cm<sup>2</sup> and with a background setting of current and voltage of 3.00 A and 15.0 V respectively. The current was set as 3.0 A since 3.00 A was the optimum current for crystal grew. The current density threshold of SZ14 was 8.5241 A/cm<sup>2</sup>. The output current and voltage throughout the circuit were 0.01 A and 15.0 V respectively once the power supply turned on since the electrons were not being excited. Thus, Bunsen burner was used to heat the ZnO bar for 2.32 minutes until the the current pass through the circuit became stable and maximum. The stable current 3.48 A remained unchanged through the process whereas the voltage keep on changing. ZnO bar grew wool like crystal and very bright. The temperature and voltage was 360.2 °C and 12.8 V respectively. The copper powder was added on the surface and the crystal grow immediately within 2 second. The temperature dropped to 259.2 °C and voltage was 8.4. The brightness of ZnO bar became dimer, the light was trapped by copper powder. The whole process finished within 47 minutes. As compared to the other sample, SZ14 experienced crystal grew once the copper powder added. It speed up the rate of reaction and act as a catalyst agent.

As a summary, samples with higher applied compact pressure (3.0 Ton) ended the process faster as compared to samples with 2.0 Ton applied pressure. Besides that from the range of current applied, it showed that, 3.0 A was the optimum current for joule heating process. Both sample SZ4 and SZ12 were the fastest ended the joule heating process among each categories. Samples SZ4 and SZ12 grew larger amount of crystal on the surface of ZnO bar as compared to other samples. The brightness of ZnO bar was more focus at negative terminal as compare to positive terminal. This was because the current flew from cathode to anode whereas electron flew from anode to

cathode. Therefore, larger amount of crystal grew at negative terminal part. The comparison of samples in joule heating process were shown in Table 4.9.

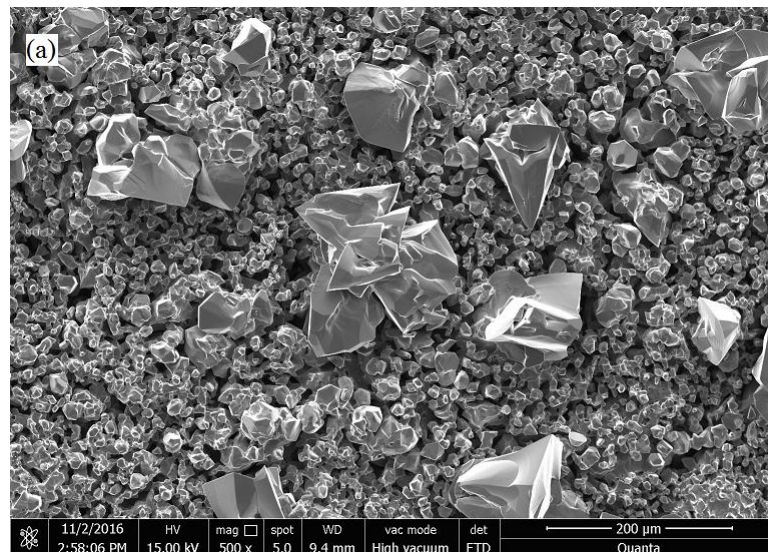
**Table 4.9**  
*Comparison of samples in joule heating process.*

Applied Pressure (Ton)	Sample	Highest Voltage Achieved (V)	Current (A)	Highest Temperature Achieved (°C)	Duration	Observation on crystal grew
<b>2.0 Ton</b>	SZ3	14.3	2.48	233.2	1 hr 50 mins	Crystal grew very slow.
	SZ4	12.2	2.98	292.6	1 hr 29 mins	Large amount of crystal grew. The ZnO bar broke into two parts by the end of the process.
	SZ2	11.1	3.48	388.8	1 hr 47 mins	Crystal grew in both surface of ZnO bar. The ZnO bar broke into two parts by the end of the process.
<b>3.0 Ton</b>	SZ15	13.7	2.48	386.8	3 hrs 18 mins	Crystal grew in low speed.
	SZ12	13.4	2.98	284.9	31 mins	Large amount of crystal grew vigorously.
	SZ13	11.9	3.48	355.6	32 mins	Crystal grew in the early of the process. The ZnO bar broke into two parts by the end of the process.
	SZ14	13.1	2.98	361.4	47 mins	Crystal grew was trapped by copper powder.

### 4.3.2 Topography Analysis

The surface topography of ZnO crystals were examined by using SEM. The samples were not coated with platinum since the samples had to undergo next characterization. Therefore, some of the diagrams were blur and affected by charging effect. The characterization was carried out at high vacuum mode. Grain structure images of the ZnO crystals were examined with different magnifications.

There were three main types of crystals were found on sample SZ3 under SEM. Figure 4.4(a), (b), (c) were three types of crystals found in SZ3 whereas Figure 4.4 (d) was the enlargement of Figure 4.4 (c). A rose crystal like structure was obtained under 500 X magnification in Figure 4.4 (a). In Figure 4.4 (b), it showed rock like crystal and it was observed under 500 X magnification. The most interesting crystal was shown in Figure 4.4 (c) and (d). The crystal grew in inversely needle shape. The beginning part of the crystal was sharp and the end of crystal was hexagonal shape. There was some powder like crystal on the surface of hexagonal crystal. Besides that, there were branches crystal grew at the end of the hexagonal crystallike structure. The sintered density of SZ3 was 5.1807 g/cm<sup>3</sup> whereas the percentage of relative density was 92.41 %.



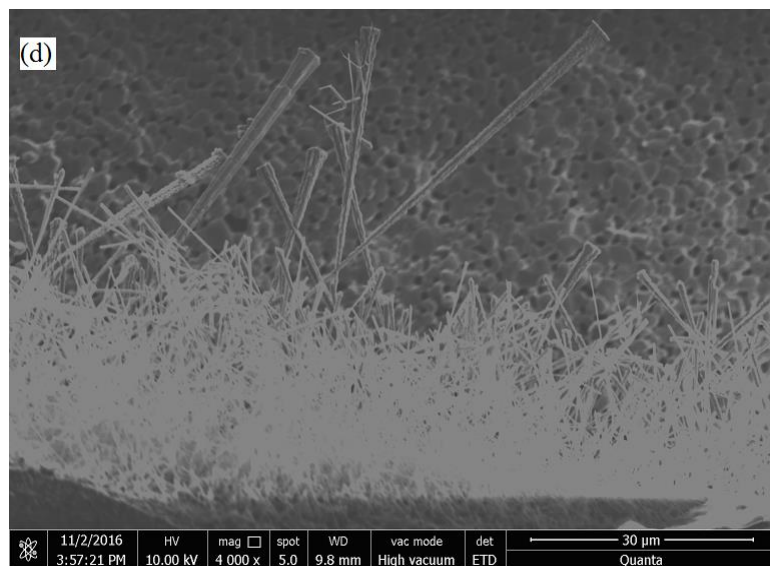
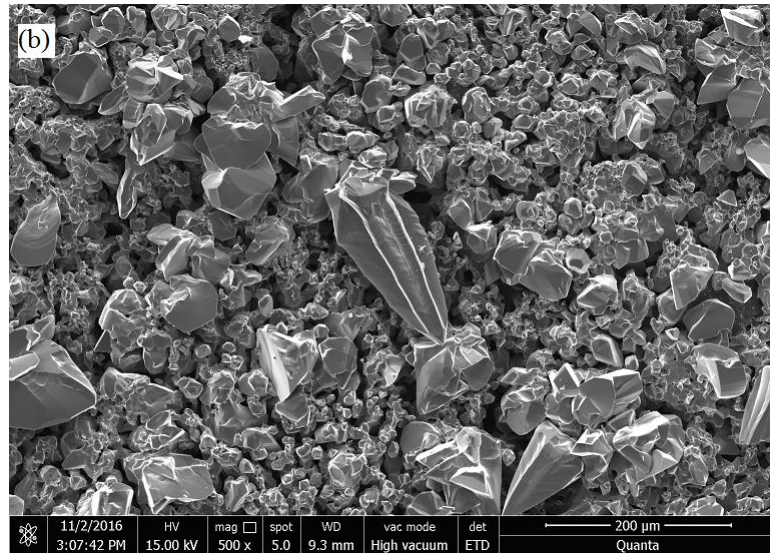
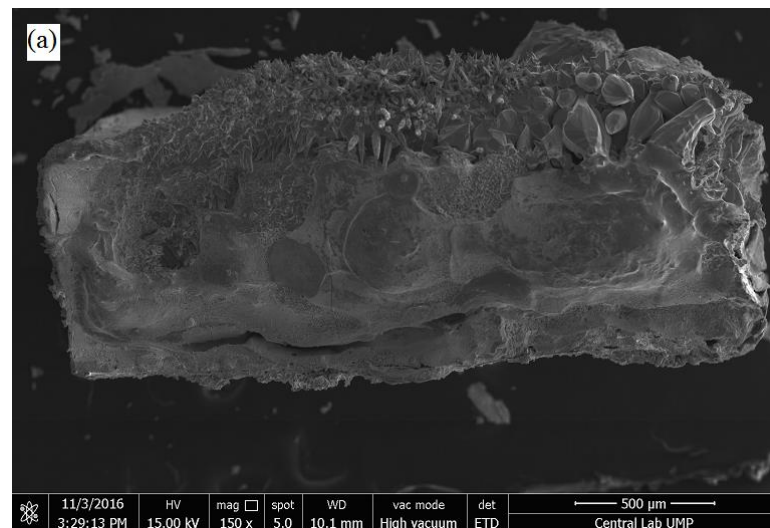


Figure 4.4 (a), (b), (c) and (d). Crystal grew on SZ3 ZnO bar.



Sample SZ4 was broke into two parts in joule heating process. Both broken parts were examined. Figure 4.5 showed two types of crystal on the cross sectional surface of broken part. Figure 4.5 (a) showed the cross section of broken part whereas Figure 4.5 (b) and (c) showed enlargement of crystal on cross sectional surface. The ZnO crystal in Figure 4.5 (b) was hexagonal shape with extended tip in stair case stage which obtained under 1000 X magnification. Figure 4.5 (c) showed the crystal grew from big irregular rock shape crystal to form thin hexagonal shape crystal as shown in Figure 4.5 (b). A conjecture had made on the process of growing of crystal. It grew from Figure 4.5 (c) to formed crystal in Figure 4.5 (b). On the other hand, there were five types of crystal grew on the surface of SZ4. Figure 4.6 (a) showed the overall crystal obtained 1000 X magnification. The overall shape of crystal in Figure 4.6 (b) was in sword shape. However, the crystal was split into different direction and each direction there were two hexagonalcrystallike structure came together. Crystal grew in Figure 4.6 (c) was look alike with crystal in Figure 4.6 (f). The crystal grew in both diagrams were look like coral but the surface of crystal in Figure 4.6 (c) were rough and the surface of crystal in Figure 4.6 (f) were smooth. Besides that, some of the crystal in Figure 4.6 (c) with Dandelion shape tips. In Figure 4.6 (d), the crystal look like needles shape and branches extended from the middle and tips of crystal. The crystal in Figure 4.6 (e) seemed like a cluster of cancer cell in human body. The sintered density of SZ4 was 5.2823 g/cm<sup>3</sup> whereas the percentage of relative density was 94.23 %.



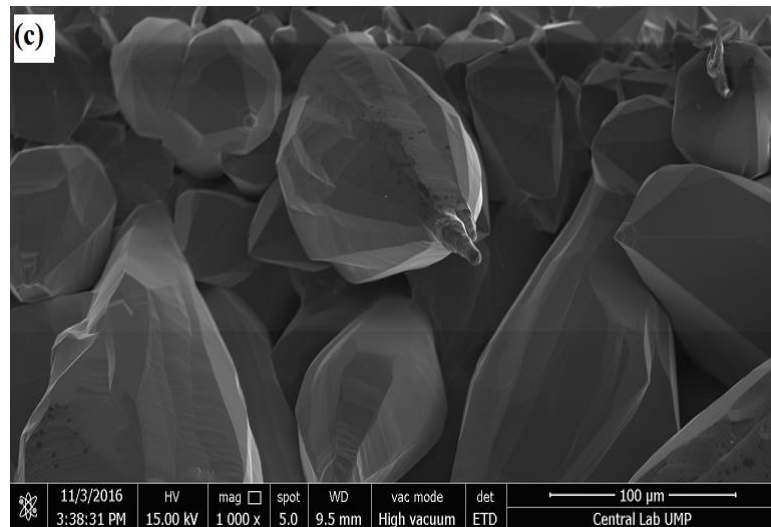
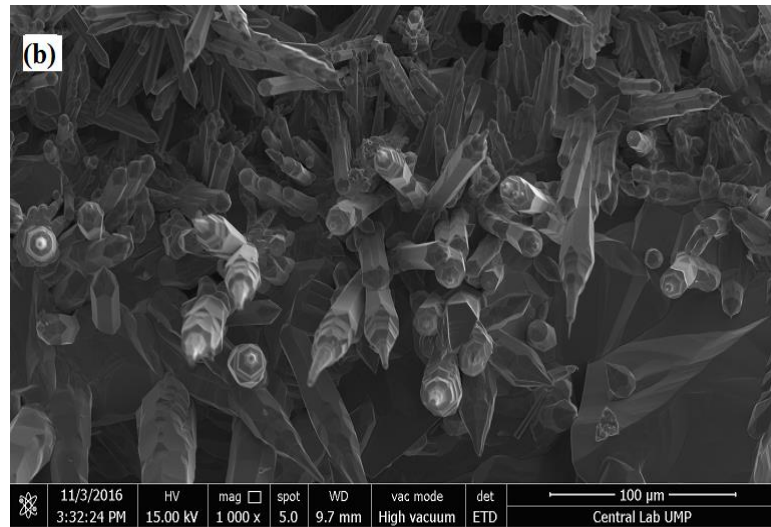
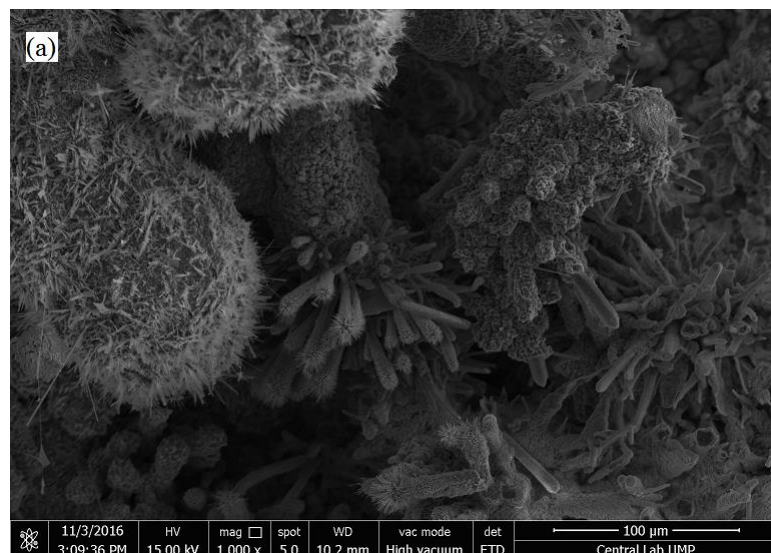
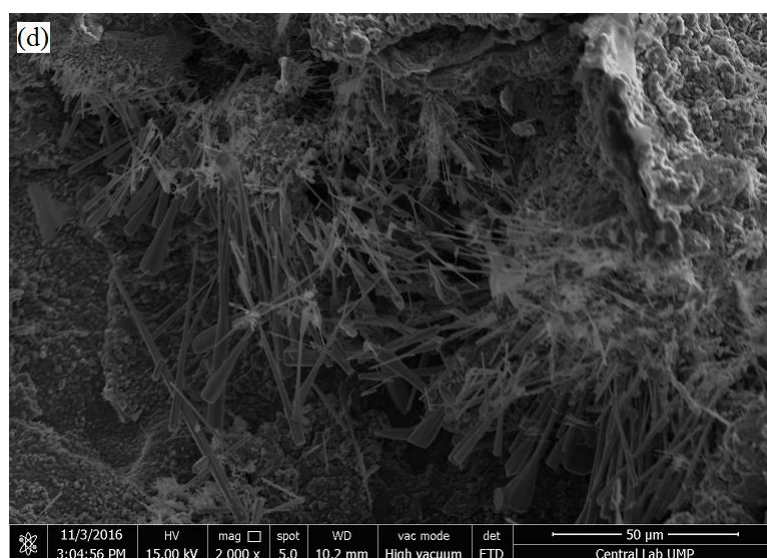
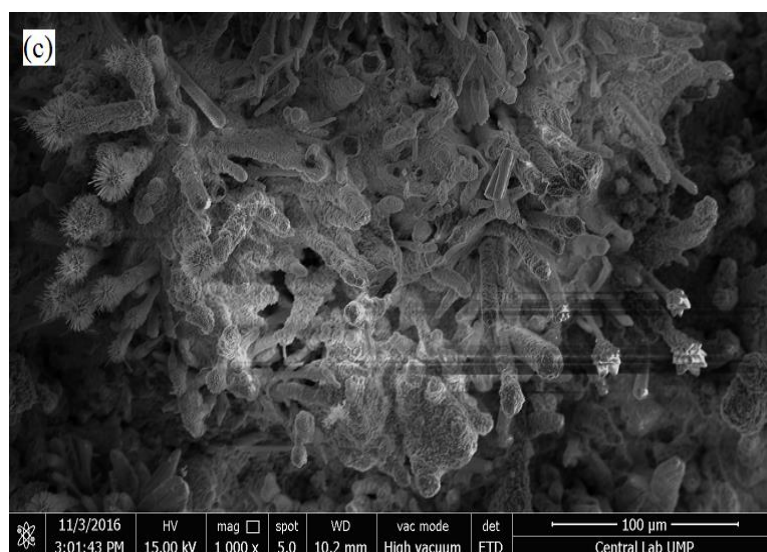
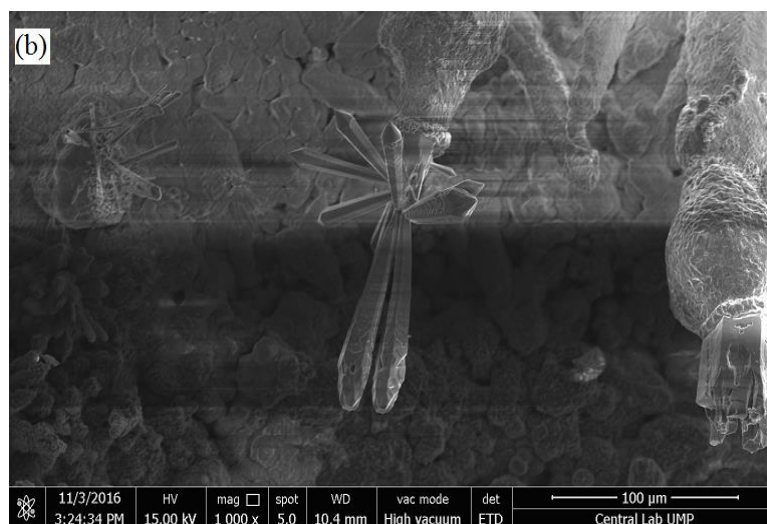


Figure 4.5 (a), (b) and (c). Crystal grew on cross sectional part of SZ4 ZnO bar.







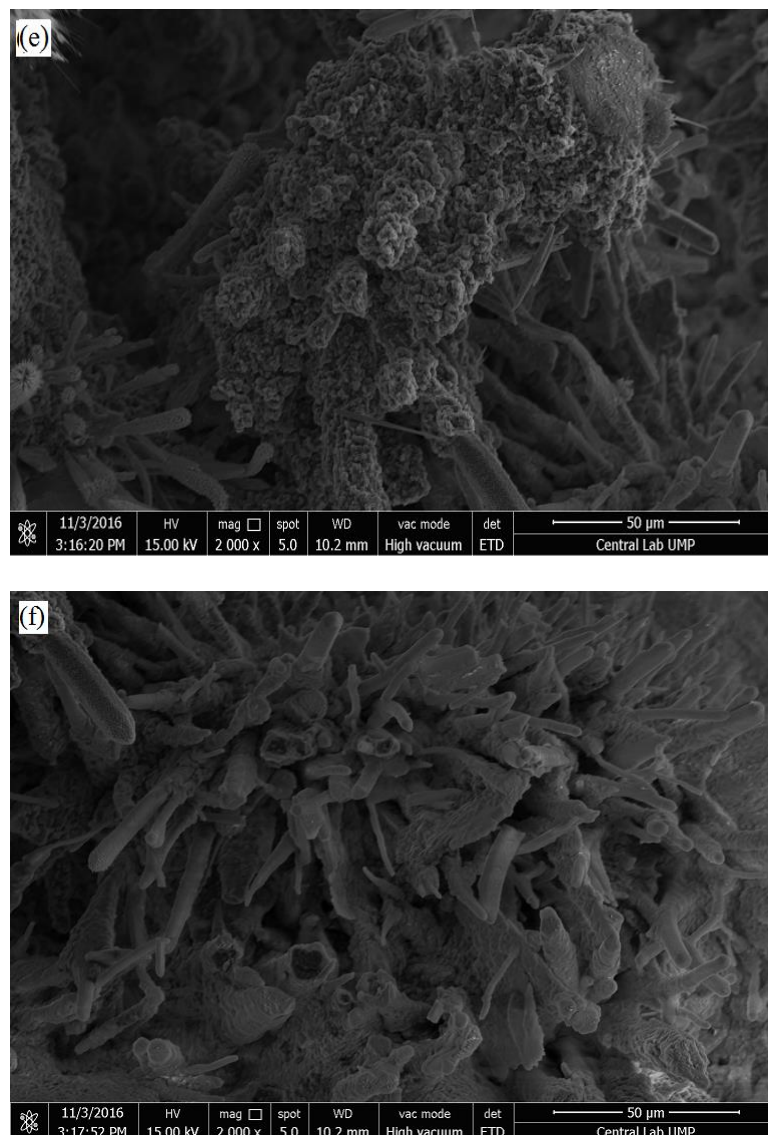
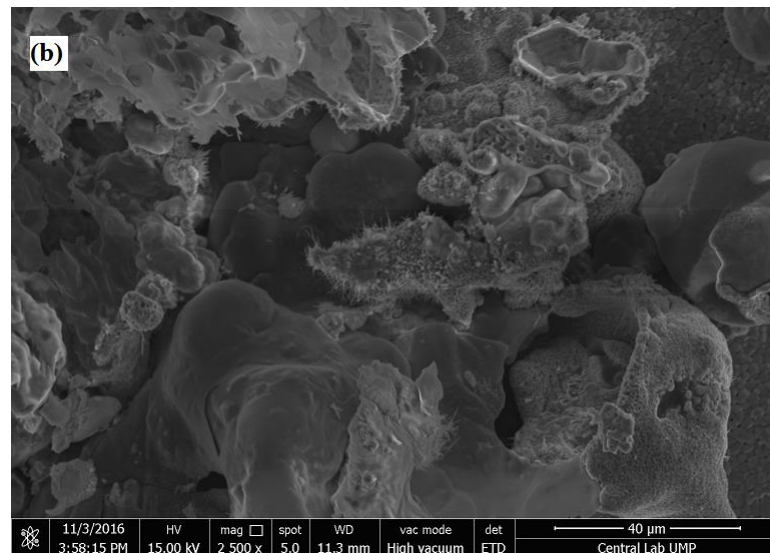
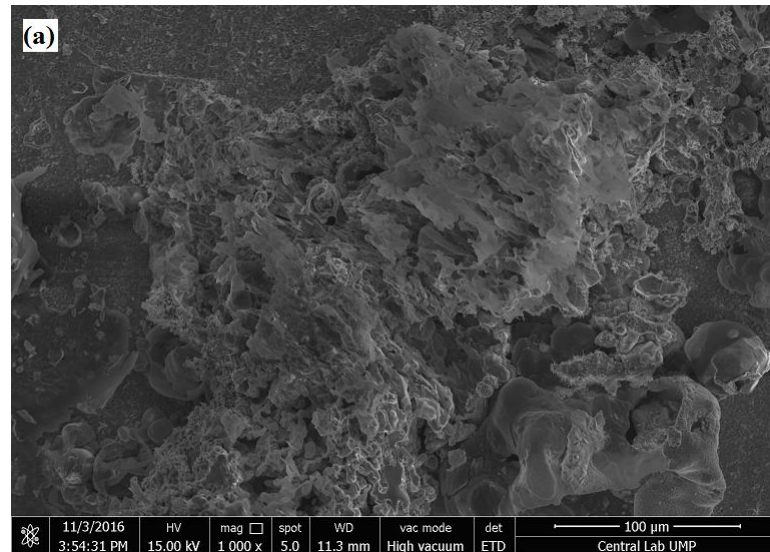


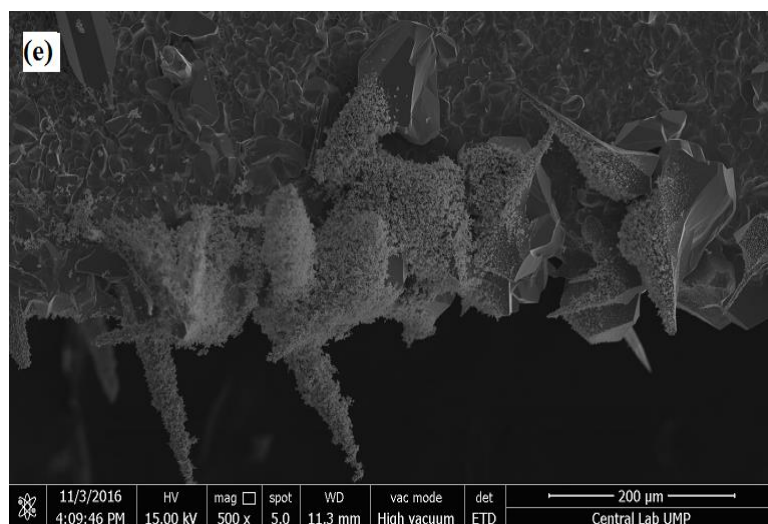
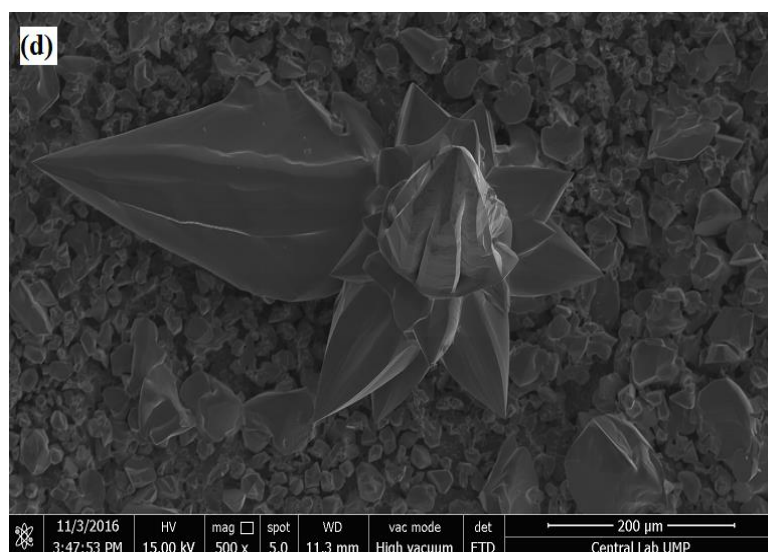
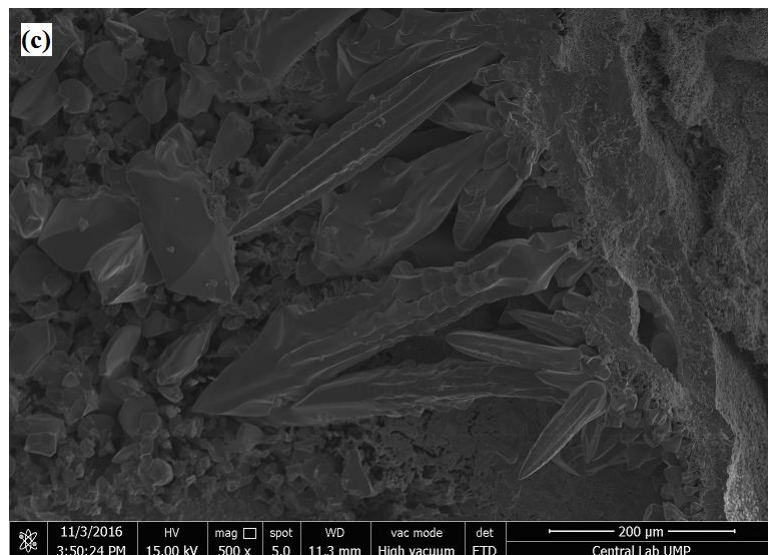
Figure 4.6 (a), (b), (c), (d), (e) and (f). Crystal grew on surface of SZ4 ZnO bar.

Although sample SZ2 was broke into two parts, only the crystal on surface were examined under SEM as the result might became blur since there was a huge difference in height between cross sectional and surface. This was caused by the brightness received by the surface and cross sectional were different. There were five types of crystal were obtained as shown in Figure 4.7 (a), (c), (d), (e) and (f) whereas Figure 4.7 (b) was enlargement of Figure 4.7 (a) and Figure 4.7 (g) and (h) were enlargement of Figure 4.7 (f). Figure 4.7 (a) showed sea weed and coral like crystal. The interesting crystal in Figure 4.7 (c) was in sea weed shape under 500 X magnification. Besides that, a rose shape crystal was obtained under 500 X magnification as shown in Figure 4.7 (d).

Figure 4.7 (e) showed the crystal grew at the edge of ZnO bar under 500 X magnification. The crystal grew had a sharp tip and the surface of the crystal was stick with new born powder like crystal. Furthermore, the crystal grew on Figure 4.7 (f) were in rock and the end of the sting fish shape. Figure 4.7 (g) showed the enlargement of one of the irregular shape of crystal. The surface was stick with powder like new born crystal. Last but not least, the crystal grew in Figure 4.7 (h) was the most interesting crystal in SZ2. There were a lot of new born crystal surrounded the surface of the original crystal (the end part of sting fish). The new born crystal was in irregular shape. The sintered density of SZ2 was 5.3612 g/cm<sup>3</sup> whereas the percentage of relative density was 95.63 %.







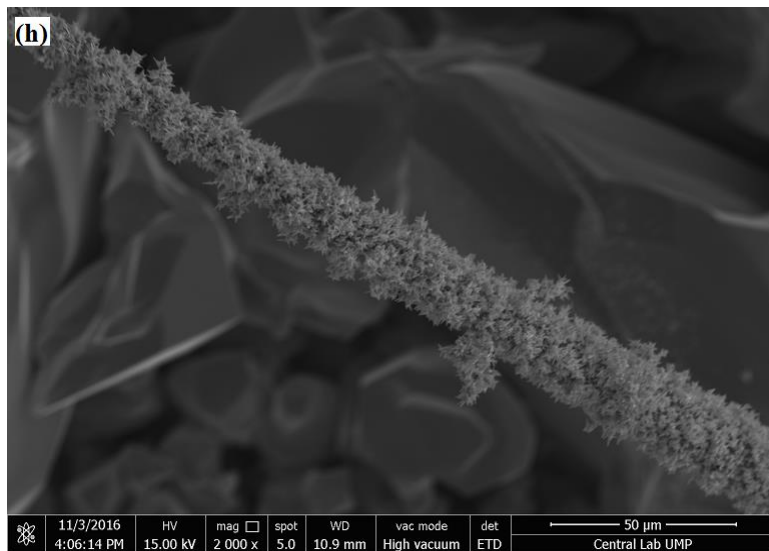
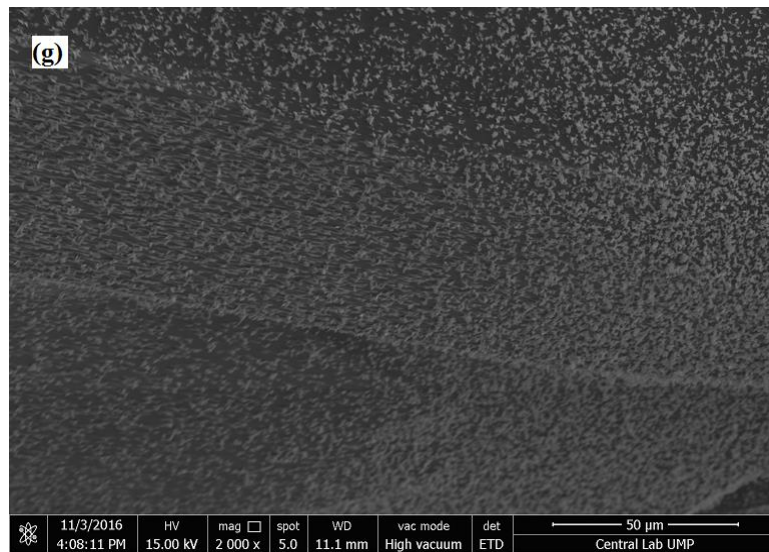
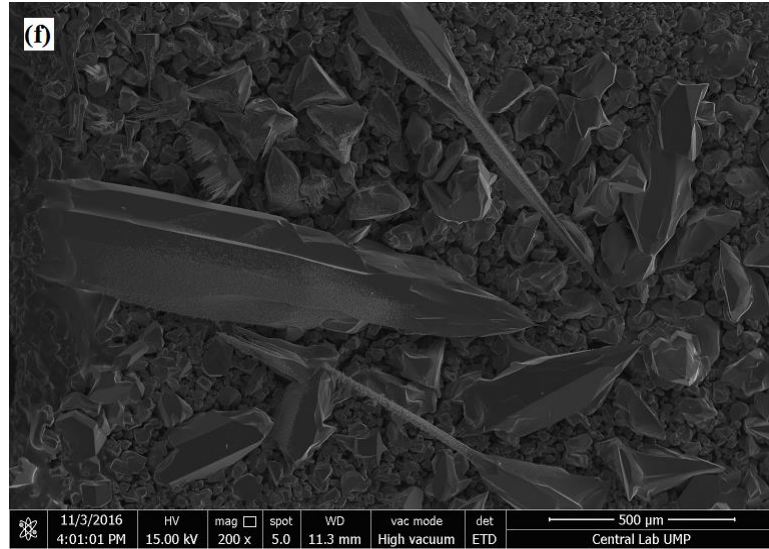
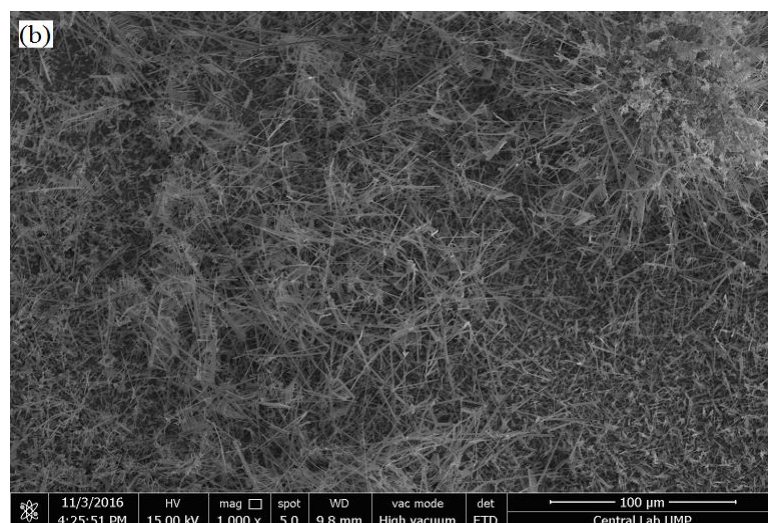
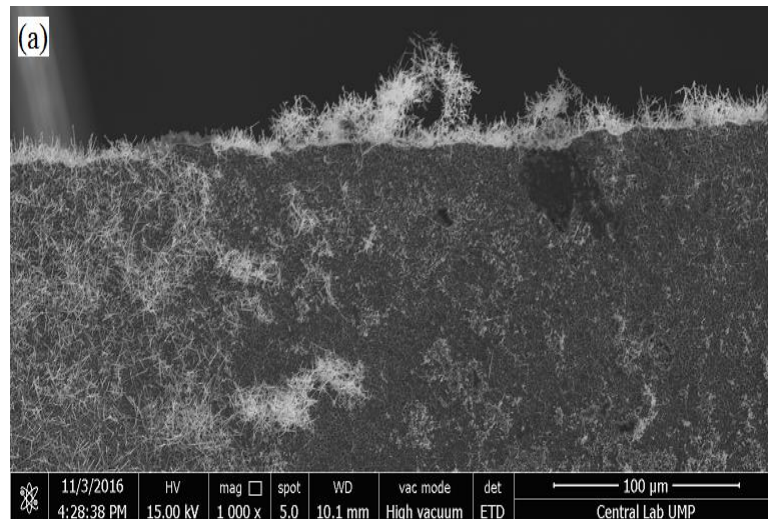
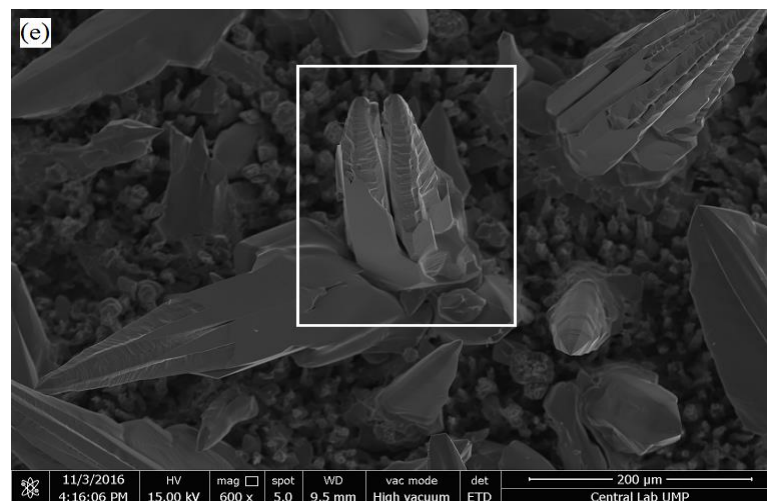
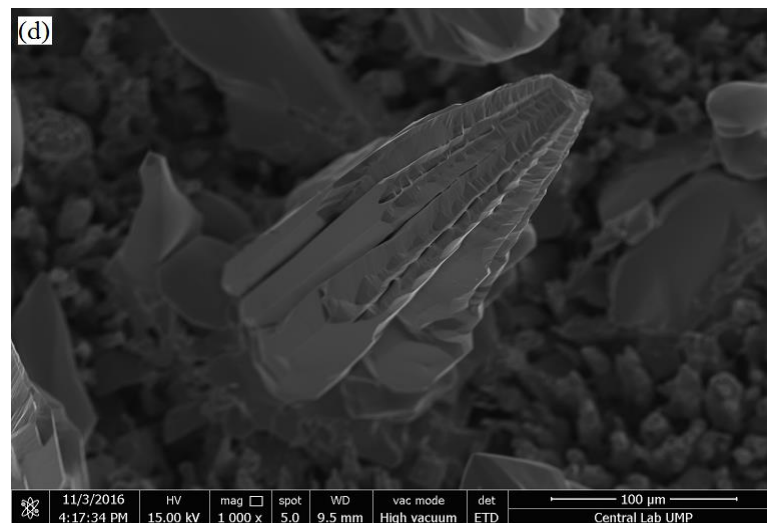
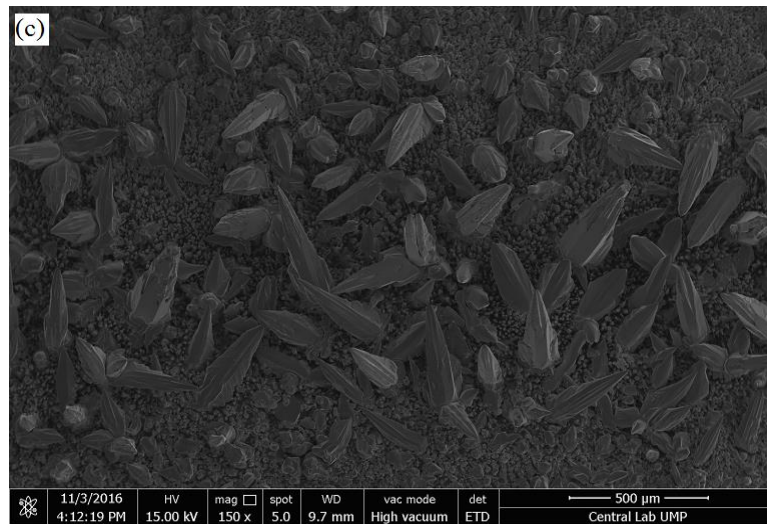


Figure 4.7 (a), (b), (c), (d), (e), (f), (g) and (h). Crystal grew on surface of SZ2 ZnO bar.

Next, sample SZ15 was observed under SEM. There were three main types of crystal grew on the surface of ZnO bar as shown in Figure 4.8 (a), (c) and (f). Figure 4.8 (b) was the enlargement of Figure 4.8(a). Figure 4.8 (d) and (e) showed the process of formation of crystal in Figure 4.8 (c). Mostly crystal grew at the edge and end of the SZ15 were in fibercrystal like structure. Some of the crystal was wreathed by new born powder like crystal. These were obtained under 1000 X magnification. On the other side, rocket crystal like structure grew as shown in Figure 4.8 (f) which observed under 500 X magnification. Besides that, KLCC tower crystal like structure were shown in Figure 4.8 (e) which observed under 600 X magnification. It started with the corn shape crystal in Figure 4.8 (d) under 1000 X magnification. It was the trunk for the branches and some stages on the surface of crystal. The energy gained by crystal increased as the time pass, the trunk crystal started to split into two crystals as shown in Figure 4.8 (e). The sintered density of SZ 15 was 4.8377 g/cm<sup>3</sup> whereas the percentage of relative density was 86.29 %.







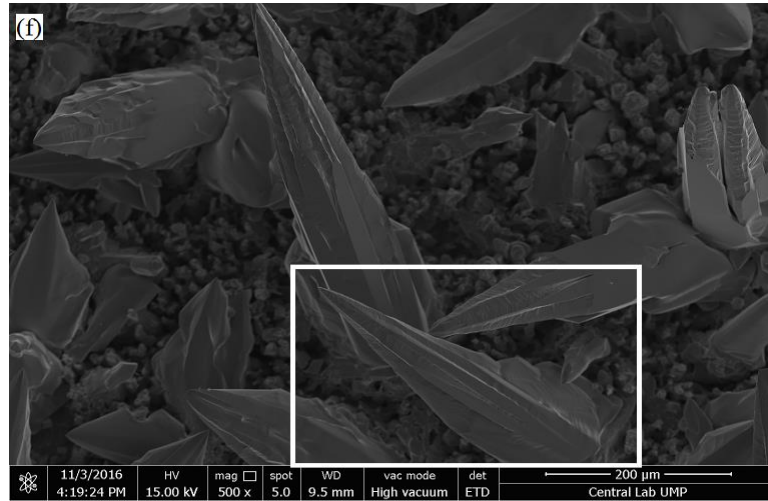
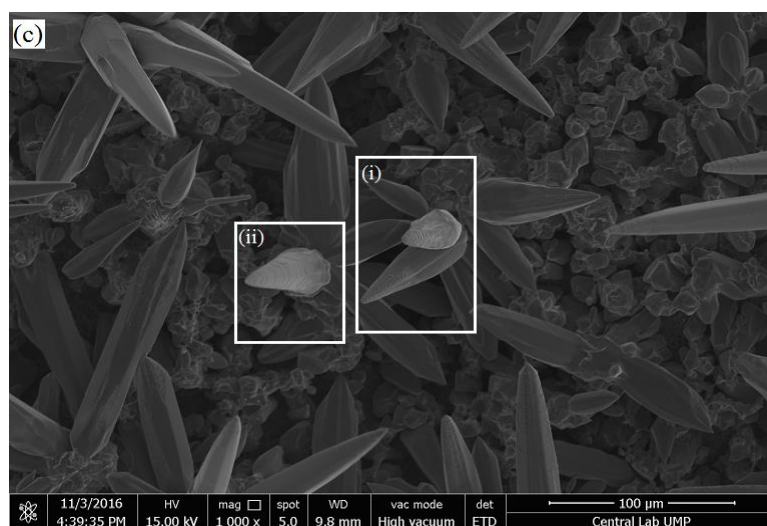
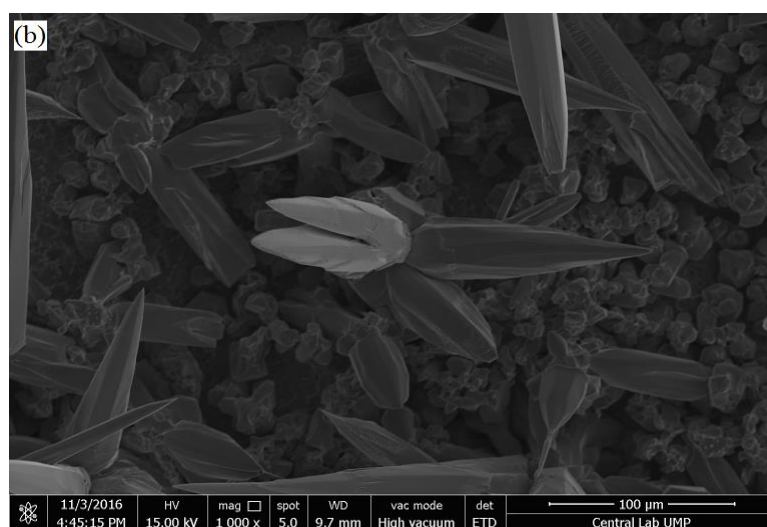
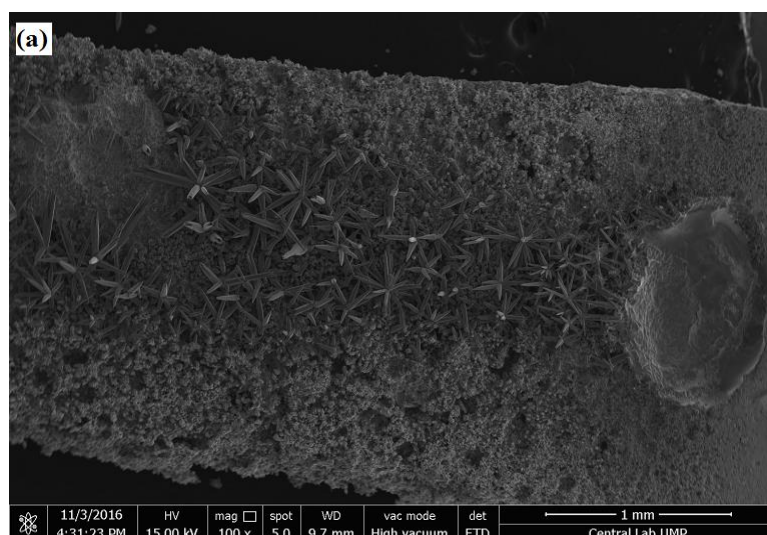
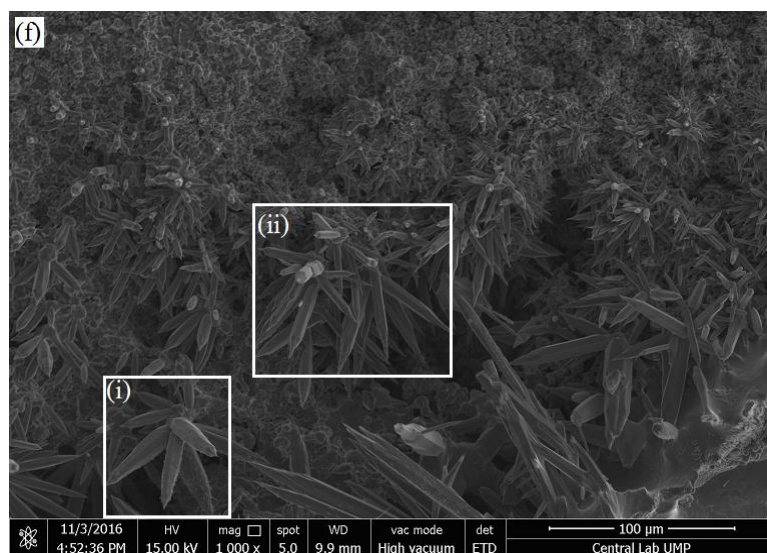
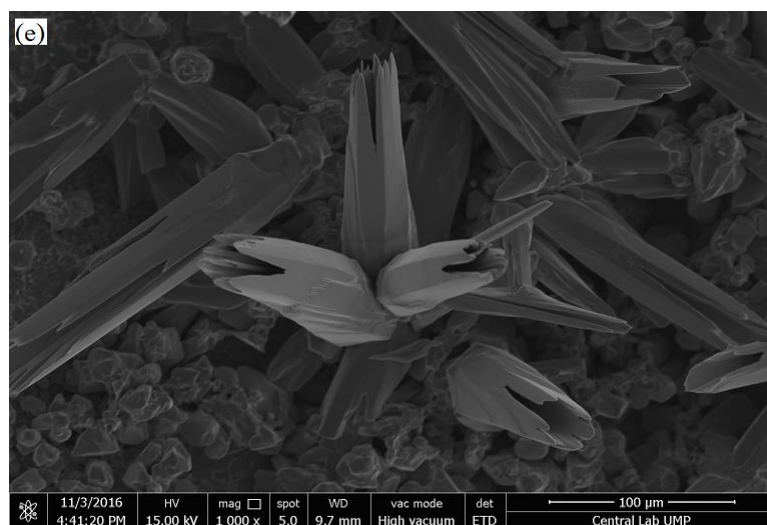
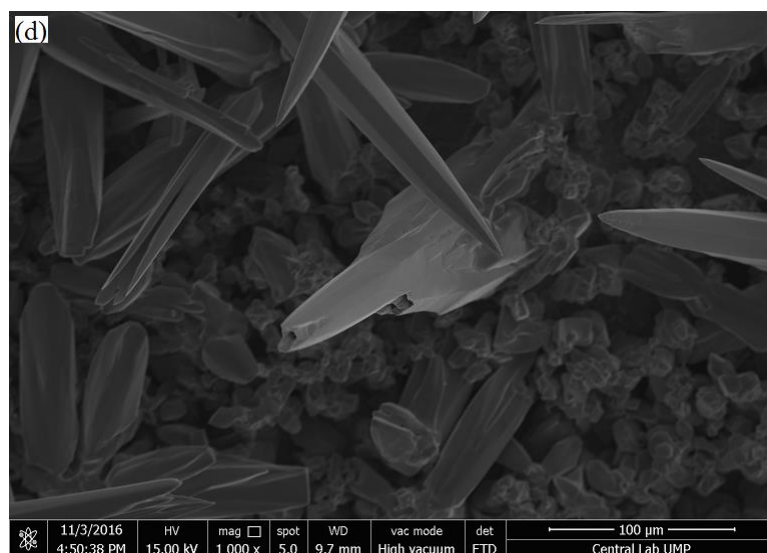


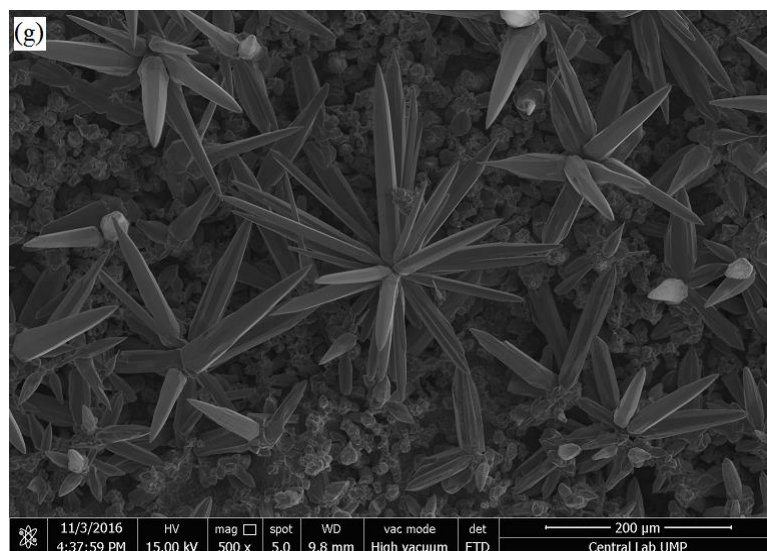
Figure 4.8 (a), (b), (c), (d), (e) and (f). Crystal grew on surface of SZ15 ZnO bar.

There were four main types of crystal grew in SZ12. Figure 4.9 (a) showed the overall crystal grew on SZ12 under magnification of 100 X. The crystal in Figure 4.9 (b) was in the progress to split to two and formed the crystal in Figure 4.9 (c) (i). It was the formation process. The corn like crystal in Figure 4.9 (c) (ii) had the same physical appearance in Figure 4.9 (c) (i). Besides that, there was a rocket like crystal grew in Figure 4.9 (d). The interesting side on this crystal was the internal part of crystal was hollow. As the energy received by crystal increased, it started to split to become three branches of crystal as shown in Figure 4.9 (e). On the other hand, the flower crystal like structure in Figure 4.9 (f) (i) were obtained under magnification 1000 X. The surface of the crystal was wreathed by new born powder like crystal. However, the crystal in Figure 4.9 (f) (ii) was in hexagonal shape and grew stage by stage. The size of the crystal decreased as the crystal extended. Moreover, flower like crystals with smooth surface grew as shown in Figure 4.9 (g). The sintered density of SZ 15 was  $5.0519 \text{ g/cm}^3$  whereas the percentage of relative density was 90.12 %.





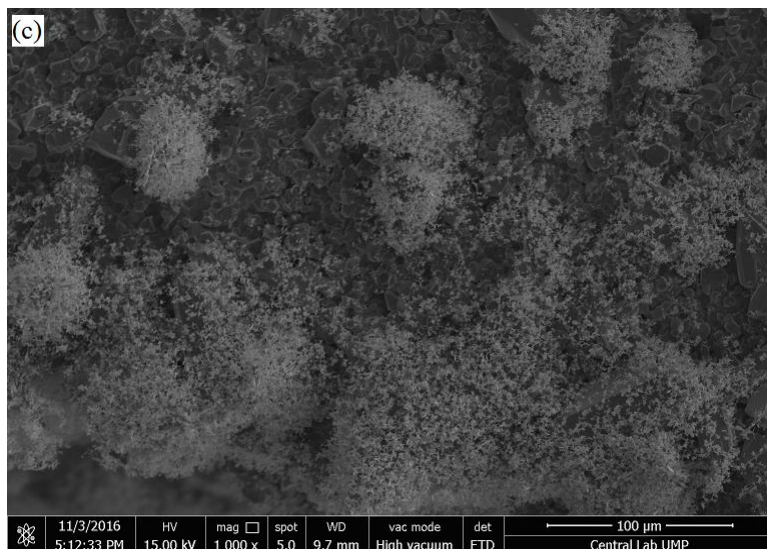
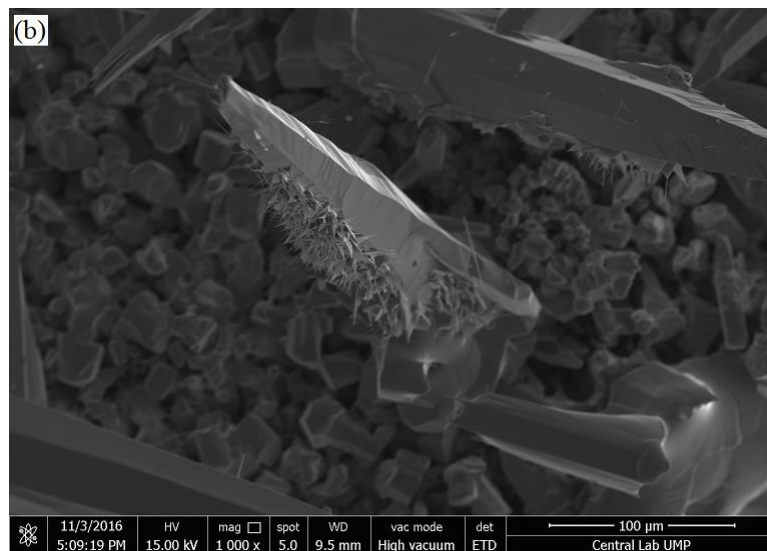
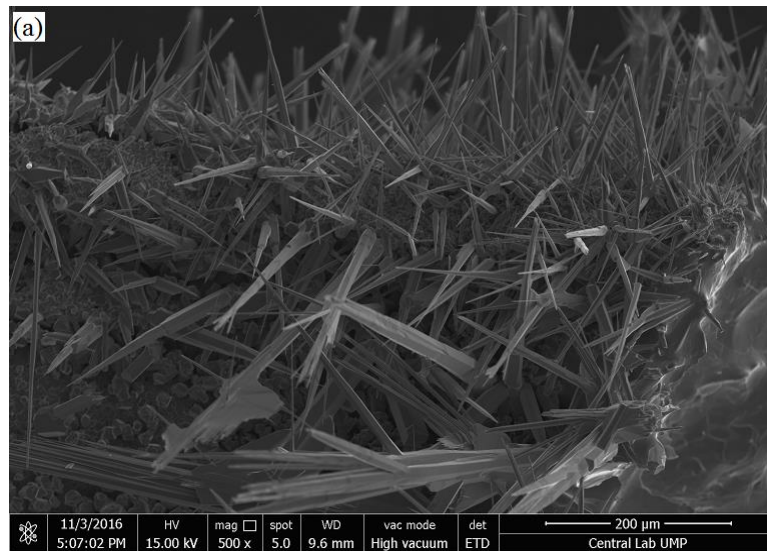




*Figure 4.9(a), (b), (c), (d), (e), (f) and (g).Crystal grew on surface of SZ12 ZnO bar.*

The topography analysis of second category was ended with sample SZ13. There were five main types of crystal found under SEM in SZ13. The crystal grew vigorously as shown in Figure 4.10 (a). The crystals were in hexagonal shape with sharp tip. A crystal with special physical appearance found under magnification of 1000X as shown in Figure 4.10 (b). One side of the crystal was full of new born crystals. Besides that, the crystal grew in Figure 4.10 (c) was like snow. The crystal grew in Figure in 4.10(d) with a hammer like branch. It was observed under 1000 X magnification. Last but not least, there was a crystal grew in heptagonal shape and extended with a sharp tip. This crystal was observed under 5000 X magnification as shown in Figure 4.10 (e).The sintered density of SZ 15 was  $5.1887 \text{ g/cm}^3$  whereas the percentage of relative density was 92.56 %.





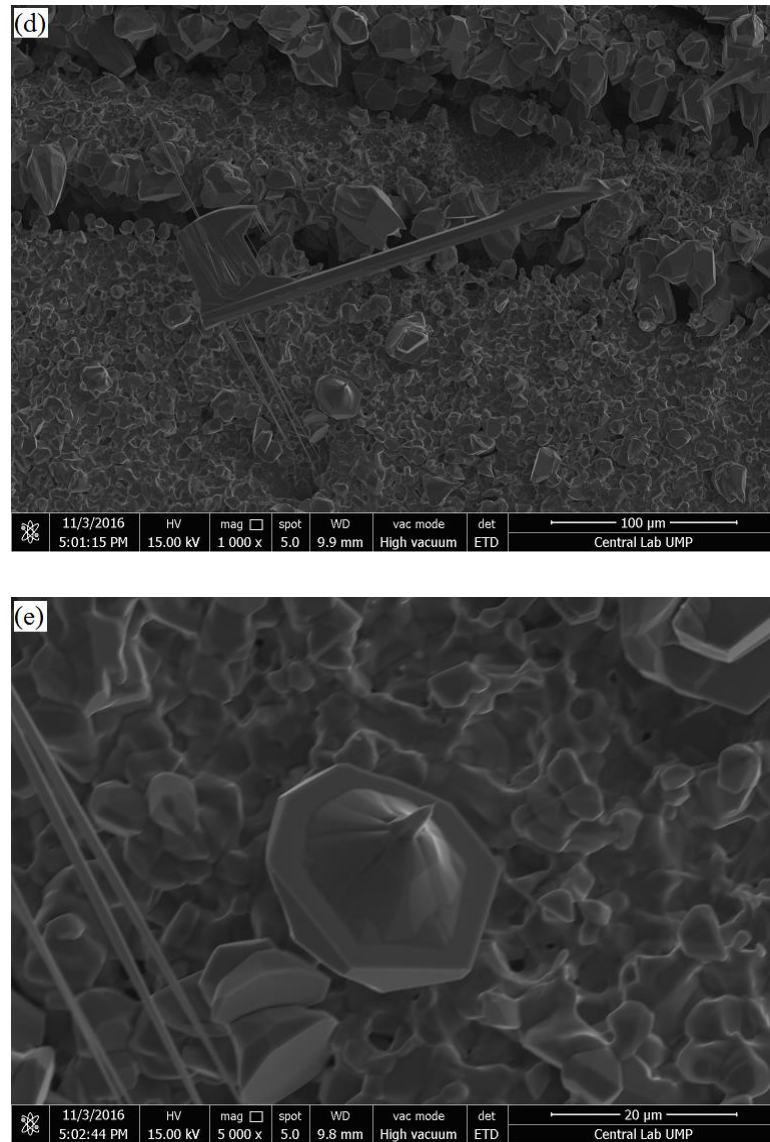
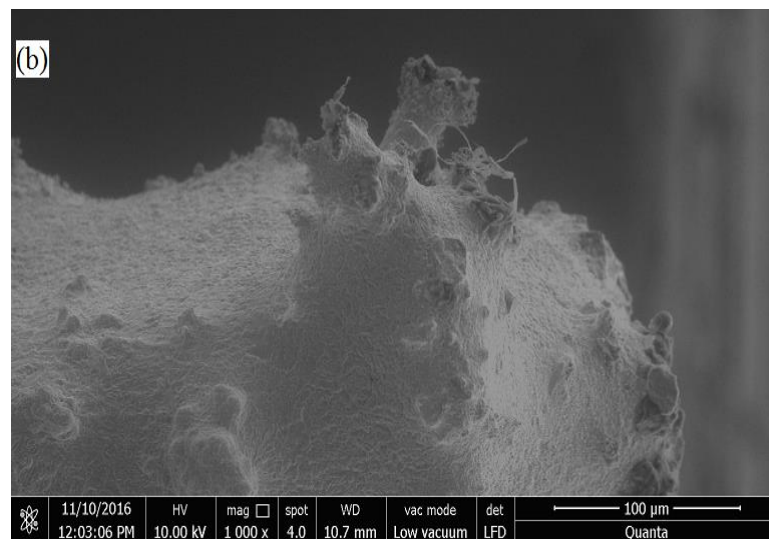
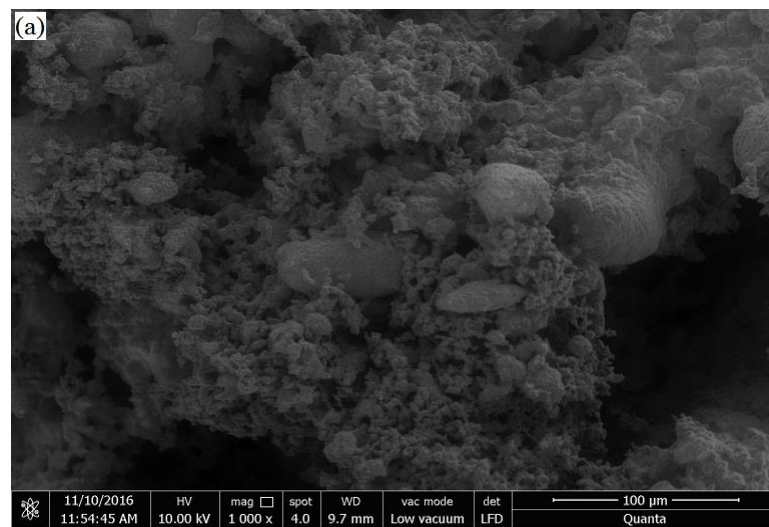
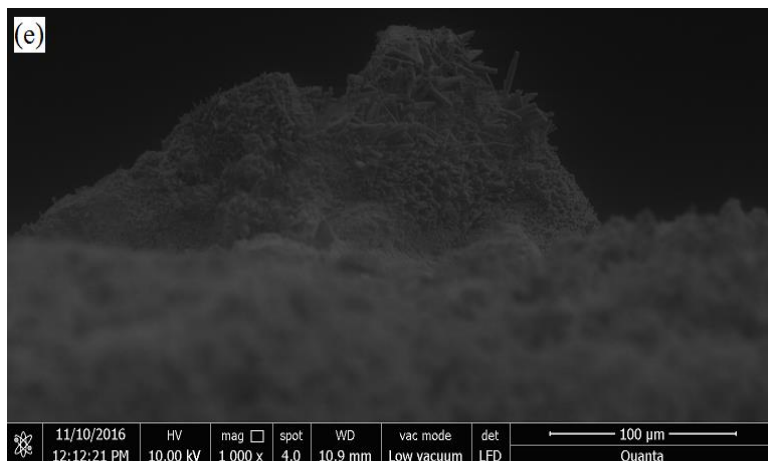
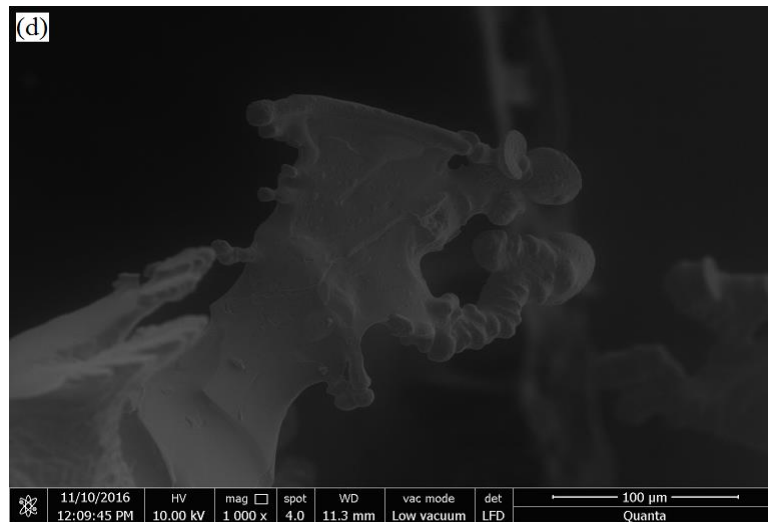
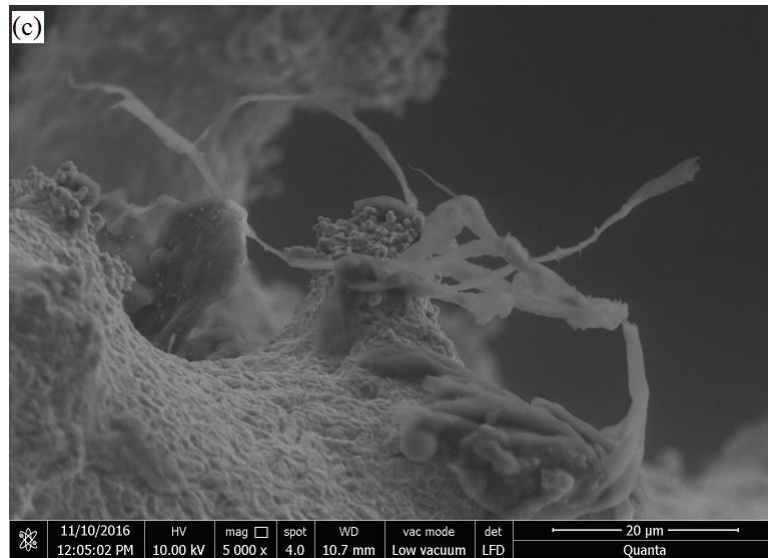


Figure 4.10 (a), (b), (c), (d), (e), (f) and (g). Crystal grew on surface of SZ13 ZnO bar.

On the other side, copper powder was added on the surface sample SZ14 as catalyst agent for crystal grew. SEM captured most of the crystals were covered by layer of copper powder. Figure 4.11 (a), (b), (d) and (e) were four main type of crystals grew in SZ14 whereas Figure 4.11 (c) and (f) were enlargement of Figure 4.11 (b) and (e) respectively. Porous like crystals grew in Figure 4.11 (a) and it was captured with 1000 X magnification. Besides that, thread like crystal was found under 1000 X magnification as shown in Figure 4.11 (b) and (c). Figure 4.11 (d) showed twins like crystal grew. The crystals found on surface of SZ14 were hardly examined since the crystals were covered by thick layer of copper powder. A suggestion had made to

decrease the amount of copper powder on the surface of sample. The copper powder should spray but not placed on the surface of sample. This method might help to form a nearly similar thickness of copper powder on surface of sample. On the other hand, crystal which does not fully covered by copper powder were found at the edge of sample as shown in Figure 4.11 (e). The crystals grew in Figure 4.11 (e) and (f) were in hexagonal shape with sharp tip. The crystals were wreathed by new born powder like crystal. The sintered density of SZ 14 was 4.6779 g/cm<sup>3</sup> whereas the percentage of relative density was 83.44 %.





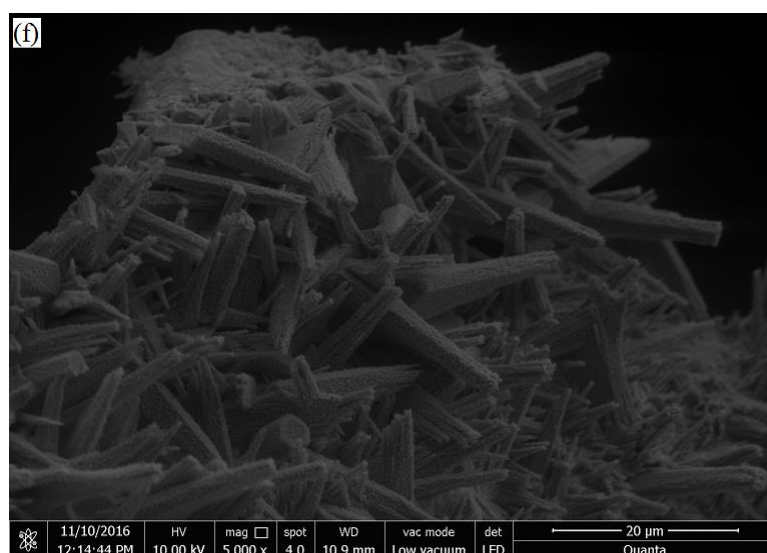
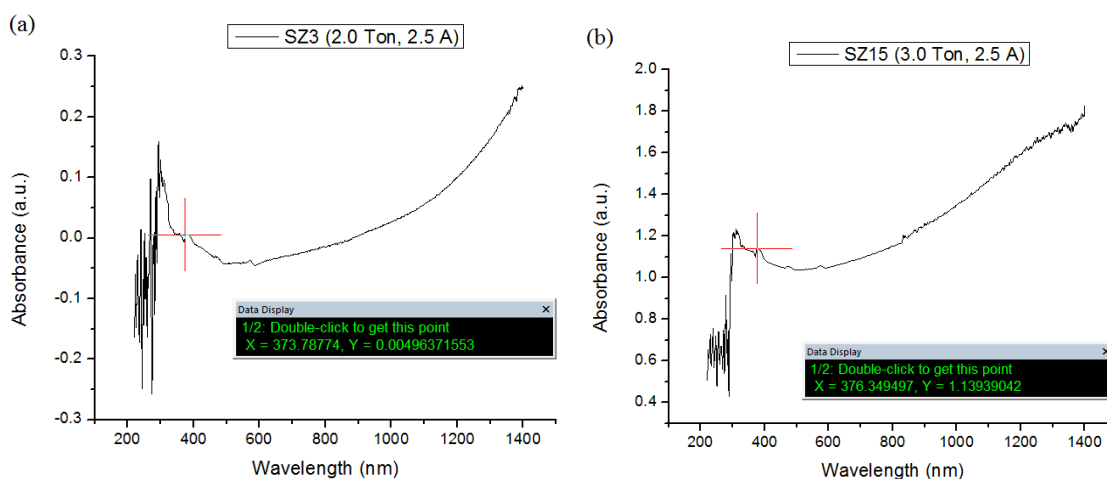


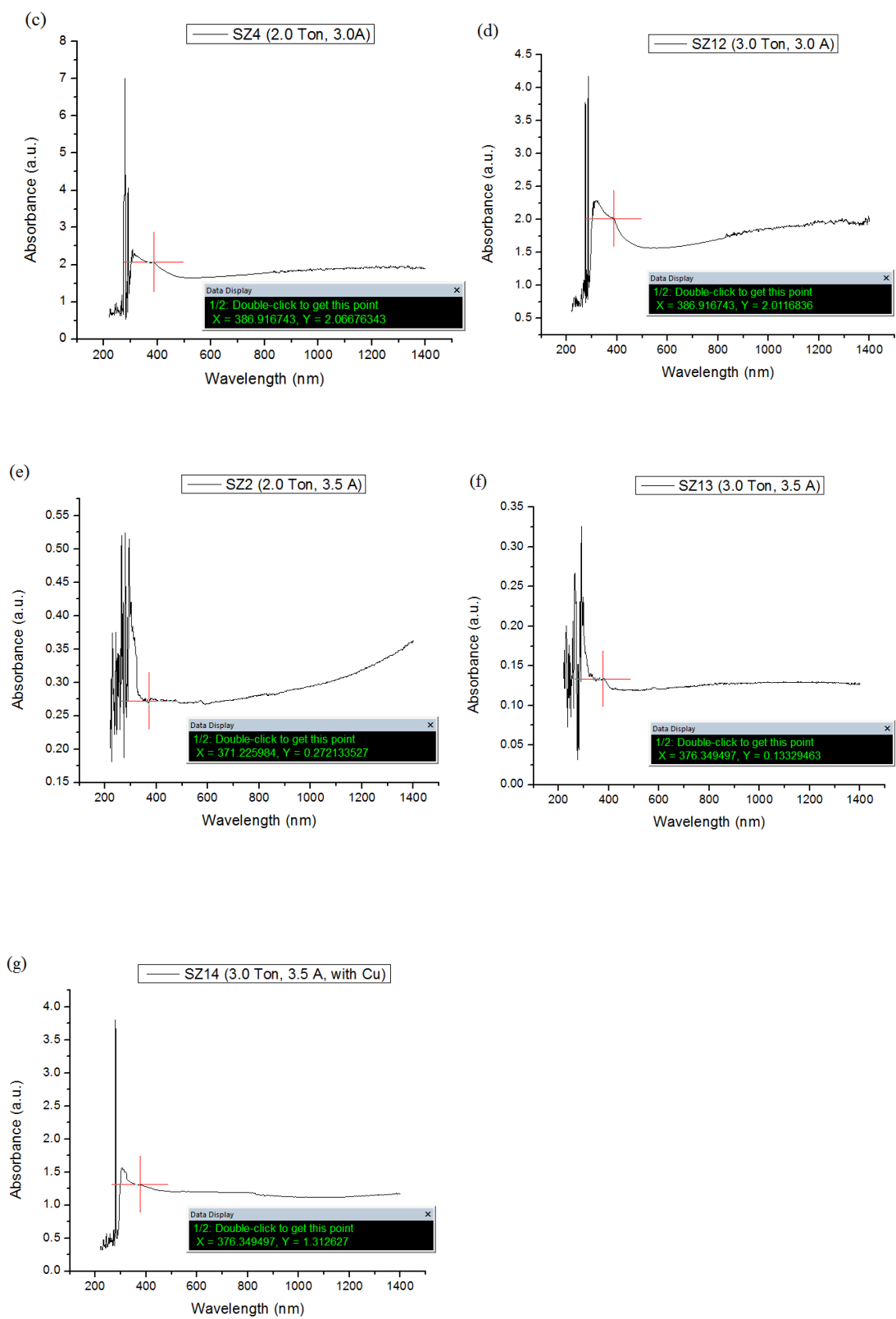
Figure 4.11 (a), (b), (c), (d), (e) and (f). Crystal grew on surface of SZ14 ZnO bar.

### 4.2.3 Analysis Results of UV-Vis Spectroscopy

The characterization results were as shown in Figure 4.12 (a), (b), (c), (d), (e), (f) and (g). Table 4.10 showed the comparison of first excitonic peak of six samples. The threshold of excitonic energy was calculated with Equation 2.2 and the results were recorded in table 4.11. The wavelength of first excitonic peak of each samples were around 380 nm. Mostly the excitonic energy was around 3.20 eV which was nearly match with theoretical band gap 3.37 eV. The samples which undergoes 3.0 Ton compact pressure absorbed the longest wavelength and thus with the lowest excitonic energy.







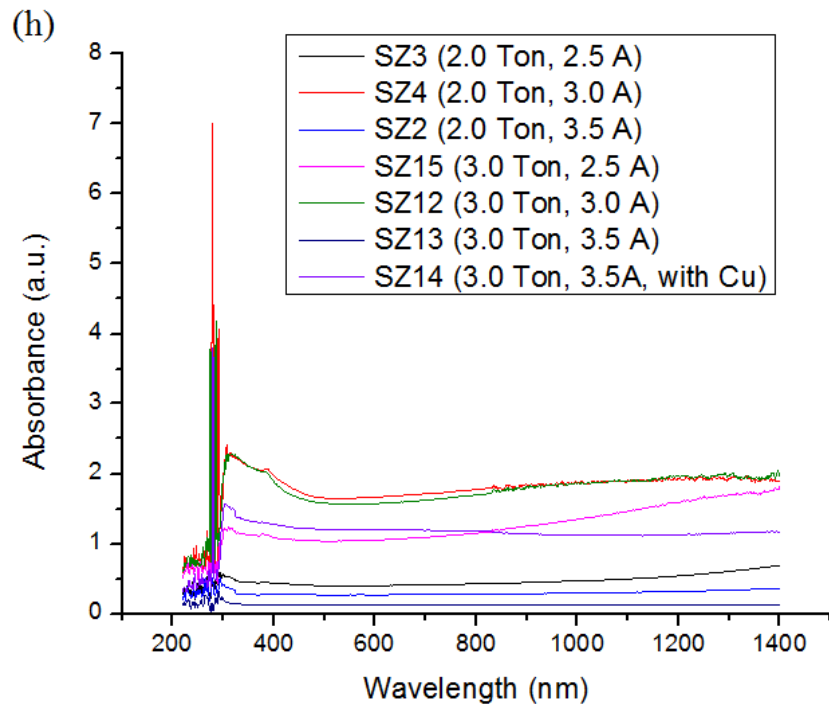


Figure 4.12. The result of UV-Vis spectrometer.

Table 4.10

Comparison of first excitonic peak of six samples.

Current (A)	Absorbance (a.u.)				Wavelength (nm)			
		2.0 Ton		3.0 Ton		2.0 Ton		3.0 Ton
2.5	Z3	0.0050	SZ15	1.1394	Z3	371.7877	SZ15	376.3495
3.0	Z4	2.0667	SZ12	2.0117	Z4	386.9167	SZ12	386.9167
3.5	Z2	0.2721	SZ13	0.1333	Z2	371.2260	SZ13	376.3495

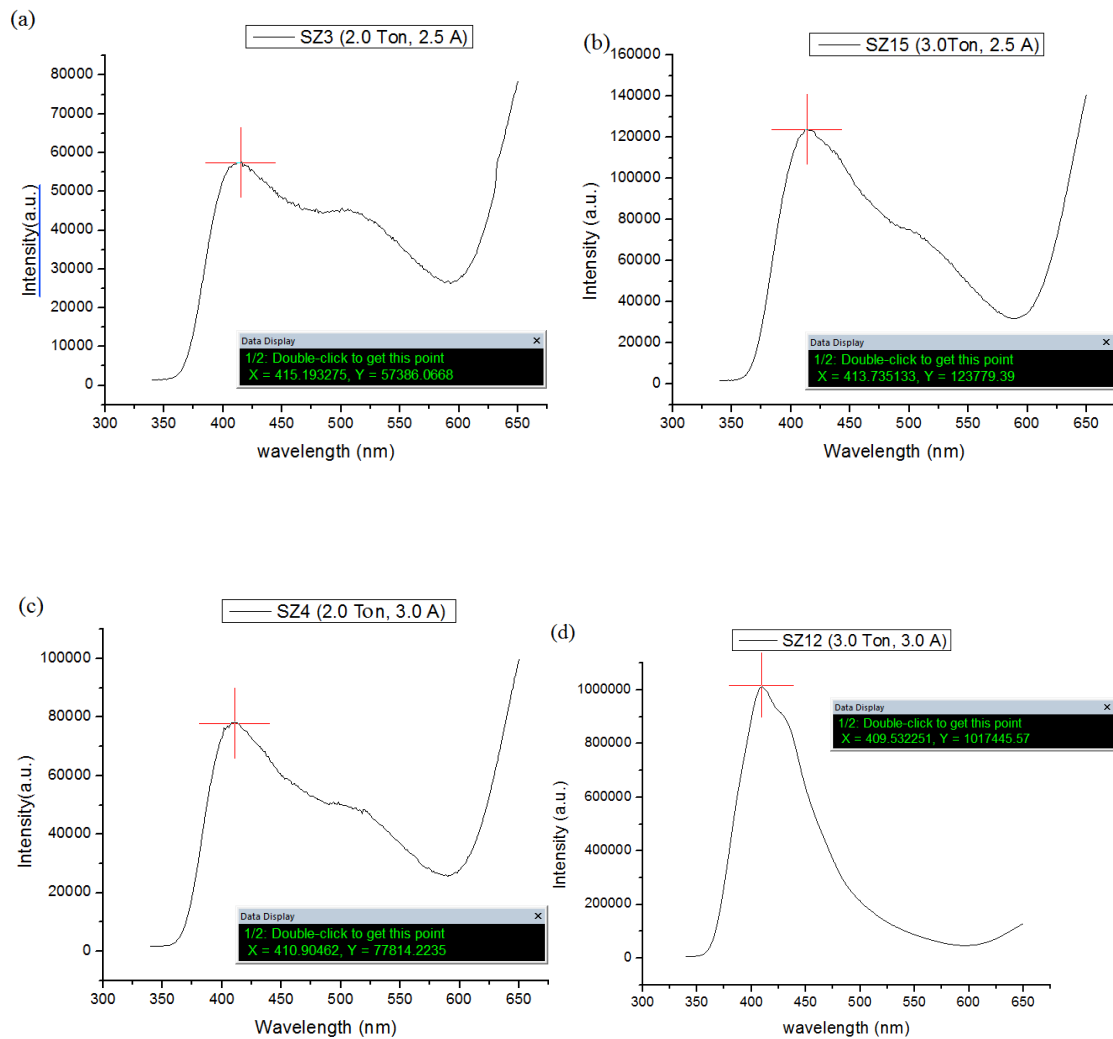
Table 4.11

Excitonic energy of samples.

Sample	Wavelength (nm)	Excitonic Energy (eV)
SZ3	371.7877	3.3371
SZ4	386.9167	3.2066
SZ2	371.2260	3.3422
SZ15	376.3495	3.2967
SZ12	386.9167	3.2066
SZ13	376.3495	3.2967
SZ14	376.3495	3.2967

#### 4.3.4 Analysis Results of Photoluminescence Spectroscopy

The photoluminescence spectrum of each samples were shown in Figure 4.13. All the value of peaks was around 410 nm. The samples were not located in the best position for characterization. This caused the light were not 100% subjected to the samples and thus results in the value of peaks were not precise. Besides that, SZ12 own the highest intensity and the conclusion made was sample which compacted by 3.0 Ton compact pressure and carried out joule heating process with 3.0 A grew the most amount of crystal.



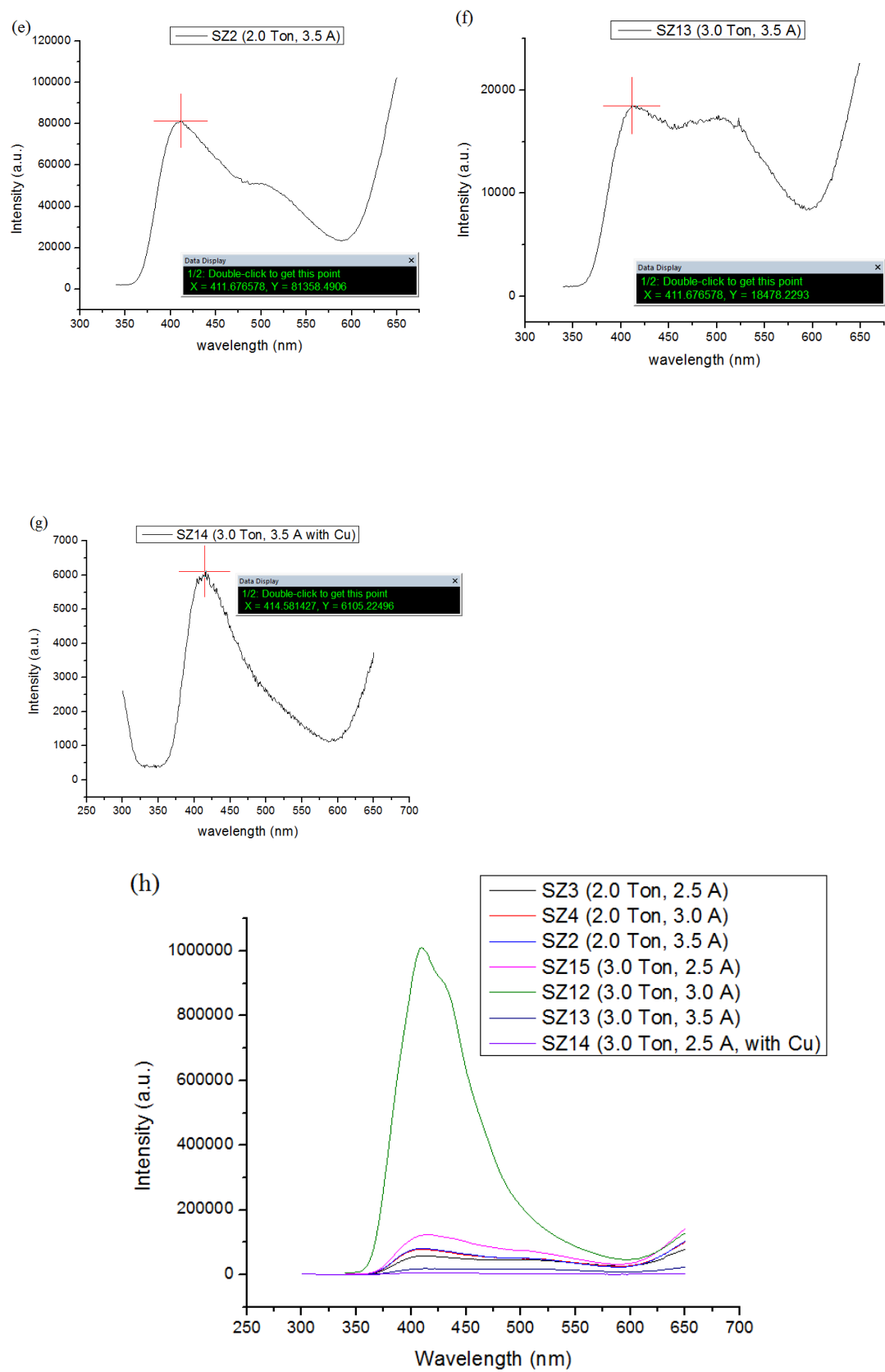


Figure 4.13 (a), (b), (c), (d), (e), (f), (g) and (h). Photoluminescence spectrum of all samples.

Table 4.12

*Result of photoluminescence spectrum of all samples.*

<b>Pressure Applied (Ton)</b>	<b>Sample</b>	<b>Current (A)</b>	<b>Wavelength (nm)</b>	<b>PL counts (intensity)</b>	<b>Emission Energy (eV)</b>
2.0	SZ3	2.5	415.1933	57386.0668	2.9882
	SZ4	3.0	410.9046	77814.2235	3.0194
	SZ2	3.5	411.6766	81358.4906	3.0138
3.0	SZ15	2.5	413.7351	123779.3900	2.9988
	SZ12	3.0	409.5323	1017445.5700	3.0296
	SZ13	3.5	411.6766	18478.2293	3.0138
	SZ14	3.5	414.5814	6105.2250	2.9927

#### 4.3.5 X-Ray Diffraction Analysis

The X-Ray analysis was first start with first category, which was 2.0 Ton applied compact pressure. Figure 4.14 showed the X-Ray Diffraction result of SZ3 (2.5 A). The plane (1 0 1) had the highest intensity, that was 2170 cps, with d-spacing 2.4771 and crystalline structure 14.7360 Å. This peak might be given by rock crystal like structure as shown in Figure 4.4 (b) since mostly rock crystal like structure were grew on surface SZ3.

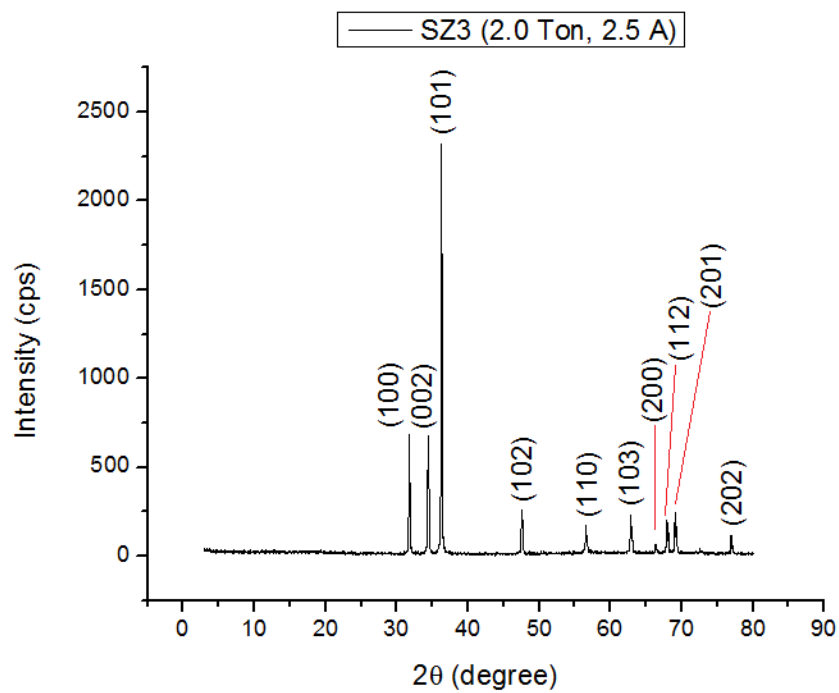


Figure 4.14. X-Ray Diffractogram of SZ3 (2.0 Ton, 2.5 A).

Table 4.13

(*h k l*) plane, *d*-spacing and crystalline size of SZ3 (2.0 Ton, 2.5 A).

<b>h</b>	<b>k</b>	<b>l</b>	<b>2θ</b> (degree)	<b>β</b> (degree)	<b>d-spacing</b> (Å)	<b>Crystalline</b> <b>size (Å)</b>	<b>Intensity</b> (cps)
0	0	2	34.3840	0.1240	2.6060	11.7047	604
1	0	0	31.7310	0.1260	2.8176	11.4401	558
1	0	1	36.2340	0.0990	2.4771	14.7360	2170
1	0	2	47.5230	0.1010	1.9117	14.9996	260
1	0	3	62.8330	0.1560	1.4777	10.4149	199
1	1	0	56.5780	0.1420	1.6253	11.0887	130
1	1	2	67.9220	0.1300	1.3789	12.8592	187
2	0	0	66.3420	0.0900	1.4078	18.4053	43
2	0	1	69.0960	0.1310	1.3583	12.8504	241
2	0	2	76.9560	0.1290	1.2380	13.7298	94

The analysis was continued with SZ4 (3.0 Å) and the X-Ray Diffraction result were shown in Figure 4.15. The plane (1 1 0) had the highest intensity, that was 1014 cps, with d-spacing 1.6259 Å and crystalline structure 16.0657 Å. This peak might be given by crystal grew in Figure 4.6 (a) whereas the hexagonal crystal like stucture grew in Figure 4.5 (b) might contribute to the peak (1 0 1). The plane (1 0 1) had aintensity of 1009 cps, d-spacing 2.4752 Å and crystalline structure 10.6495 Å.

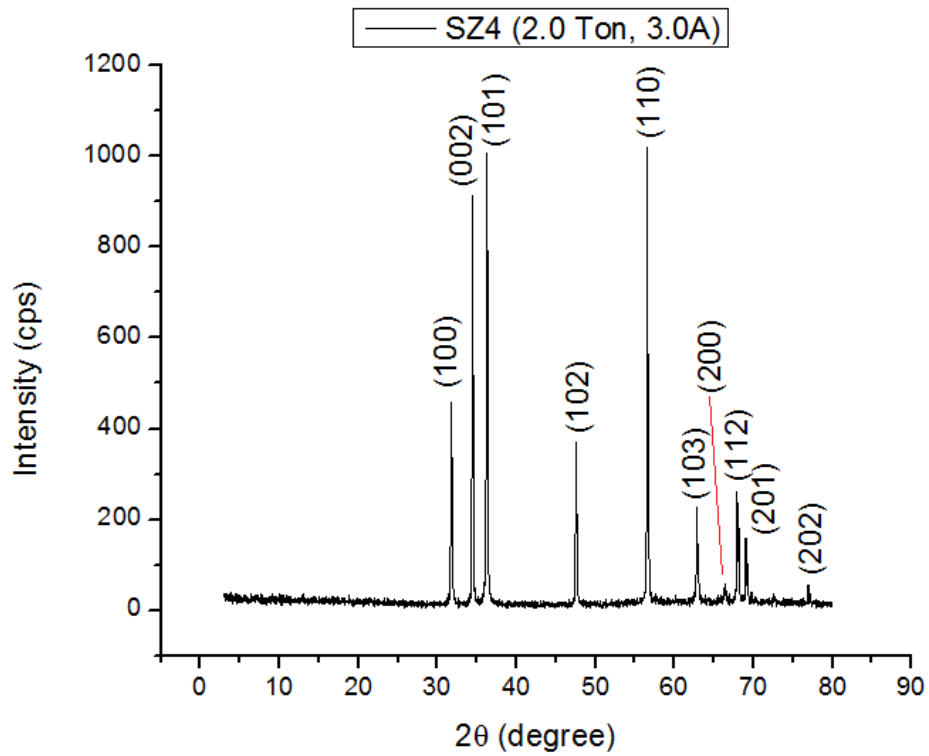


Figure 4.15. X-Ray Diffractogram of SZ4 (2.0 Ton, 3.0 Å).

Table 4.14

*(h k l) plane, d-spacing and crystalline size of SZ4 (2.0 Ton, 3.0 Å)*

<b>h</b>	<b>k</b>	<b>l</b>	<b>2<math>\theta</math></b> <b>(degree)</b>	<b><math>\beta</math></b> <b>(degree)</b>	<b>d-spacing</b> <b>(Å)</b>	<b>Crystalline</b> <b>size (Å)</b>	<b>Intensity</b> <b>(cps)</b>
0	0	2	34.4680	0.1260	2.5999	11.5216	904
1	0	0	31.7271	0.1290	2.8180	11.1739	425
1	0	1	36.2630	0.1370	2.4752	10.6495	1009
1	0	2	47.5190	0.0990	1.9118	15.3024	342
1	0	3	62.8610	0.1230	1.4771	13.2111	226
1	1	0	56.5560	0.0980	1.6259	16.0657	1014
1	1	2	67.9290	0.1180	1.3788	14.1676	248
2	0	0	66.4000	0.1800	1.4068	9.2057	29
2	0	1	69.0450	0.1010	1.3592	16.6623	137
2	0	2	76.952	0.1100	1.2380	16.1009	36

The XRD analysis for the first category with 2.0 Ton applied compact pressure would be ended by SZ2 (3.5 Å). Figure 4.16 showed the X-Ray Diffraction result of SZ2. The plane (1 01) had the highest intensity, that was 5633 cps, with d-spacing 2.4771 Å and crystalline structure 17.1833 Å. This peak might be given by rock crystal like structure grew in Figure 4.7 (d). Besides that, the plane (0 0 2) with high intensity 1538 cps might produced the coral like crystal in Figure 4.7 (a). This plane had d-spacing 2.6054 Å and crystalline structure 17.8527 Å.



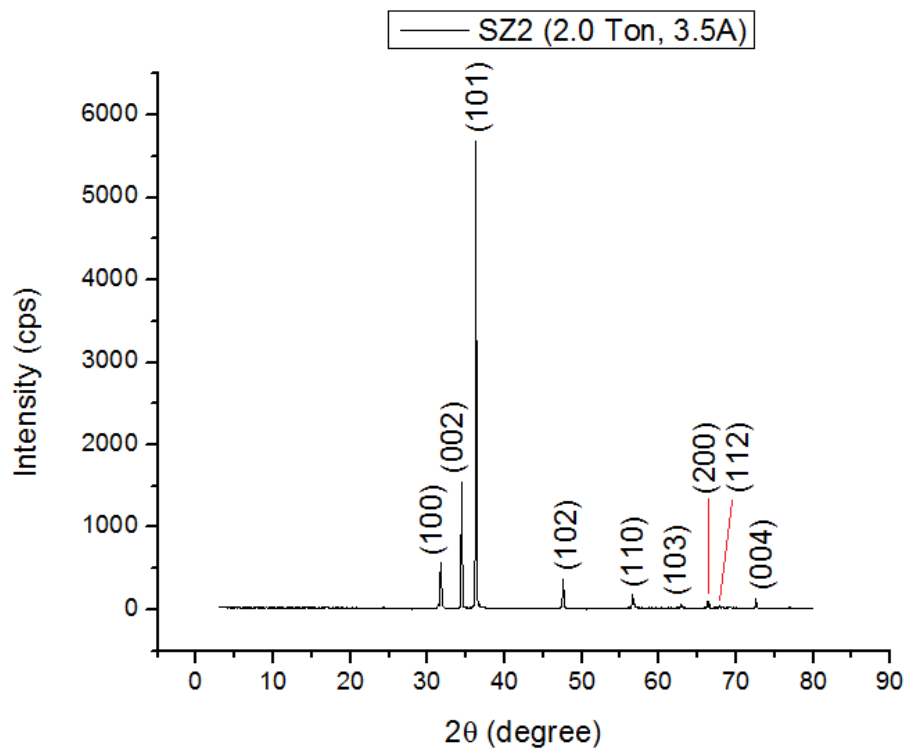


Figure 4.16.X-Ray Diffractogram of SZ2 (2.0 Ton, 3.5 A).

Table 4.15

(*h k l*) plane, *d*-spacing and crystalline size of SZ2 (2.0 Ton, 3.5 A).

<b>h</b>	<b>k</b>	<b>l</b>	<b>2θ</b> <b>(degree)</b>	<b>β</b> <b>(degree)</b>	<b>d-spacing</b> <b>(Å)</b>	<b>Crystalline</b> <b>size (Å)</b>	<b>Intensity</b> <b>(cps)</b>
0	0	2	34.3928	0.0813	2.6054	17.8527	1538
0	0	4	72.5070	0.0960	1.3026	17.9104	114
1	0	0	31.6770	0.1600	2.8223	9.0079	453
1	0	1	36.2337	0.0849	2.4771	17.1833	5633
1	0	2	47.5230	0.1090	1.9117	13.8987	351
1	0	3	62.8700	0.1500	1.4770	10.8336	42
1	1	0	56.5410	0.1270	1.6263	12.3962	143
1	1	2	67.8500	0.3100	1.3801	5.3903	14
2	0	0	66.3140	0.1000	1.4084	16.5621	97

The X-Ray analysis was continued with second category, which was 3.0 Ton applied compact pressure. Figure 4.17 showed the X-Ray Diffraction result of SZ15 (2.5 Å). Most of the crystals in SZ15 grew in the corn and rock crystal like structures as shown in Figure 4.8 (c). A conjecture had made about the crystal had the plane (1 0 1) had the highest intensity, that was 2204 cps, with d-spacing 2.4778 and crystalline structure 15.8389 Å. Besides that, the plane (1 0 0) with the intensity 1226 cps, d-spacing 2.8214 and crystalline structure 13.7266 Å might be contributed by the fiber glass like crystals in Figure 4.8 (b).

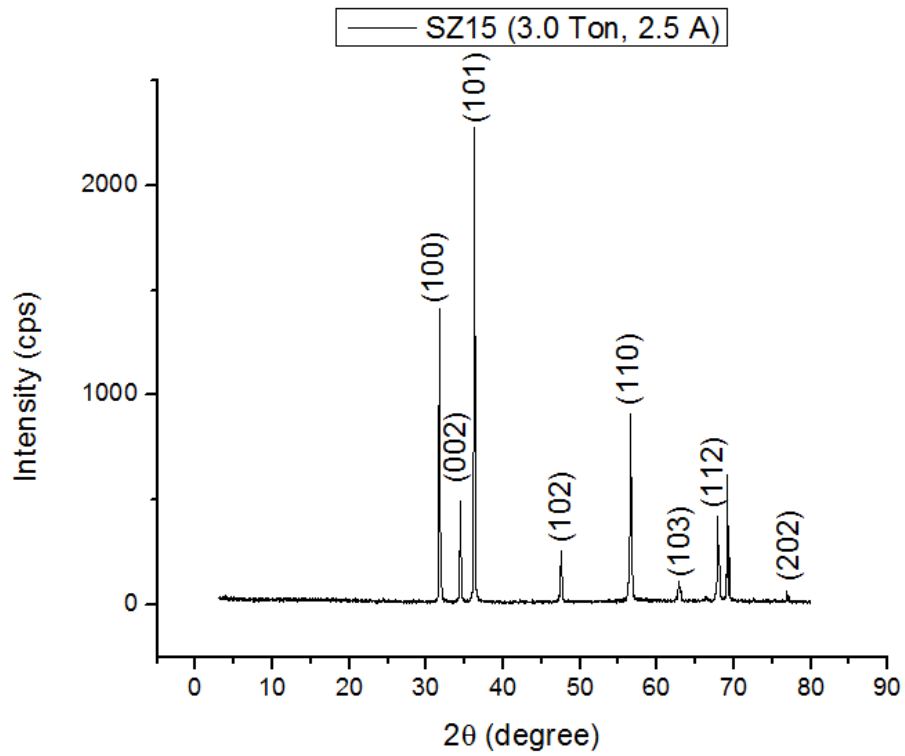


Figure 4.17. X-Ray Diffractogram of SZ15 (3.0 Ton, 2.5 Å).

Table 4.16

*(h k l) plane, d-spacing and crystalline size of SZ15 (3.0 Ton, 2.5 A).*

<b>h</b>	<b>k</b>	<b>l</b>	<b>2<math>\theta</math></b> <b>(degree)</b>	<b><math>\beta</math></b> <b>(degree)</b>	<b>d-spacing</b> <b>(Å)</b>	<b>Crystalline</b> <b>size (Å)</b>	<b>Intensity</b> <b>(cps)</b>
0	0	2	34.3990	0.0990	2.6050	14.6611	428
1	0	0	31.6880	0.1050	2.8214	13.7266	1226
1	0	1	36.2087	0.0921	2.4788	15.8389	2204
1	0	2	47.4920	0.1310	1.9129	11.5632	217
1	0	3	62.8250	0.2110	1.4779	7.6998	75
1	1	0	56.5770	0.1150	1.6284	13.6921	867
1	1	2	67.8820	0.1490	1.3796	11.2168	371
2	0	2	76.9160	0.1170	1.2385	15.1338	47

The analysis was continued with SZ12 (3.0 Å) and the X-Ray Diffraction result were shown in Figure 4.18. The plane (1 1 0) had the highest intensity, that was 1125 cps, with d-spacing 2.4806 Å and crystalline structure 10.4939 Å. This peak might be given by rock like crystals grew in Figure 4.9 (g) whereas the flower crystal like structure grew in Figure 4.9 (g) might corresponded to the peak (1 0 0). The plane (1 0 0) had intensity of 920 cps, d-spacing 2.8129 Å and crystalline structure 18.7226 Å.

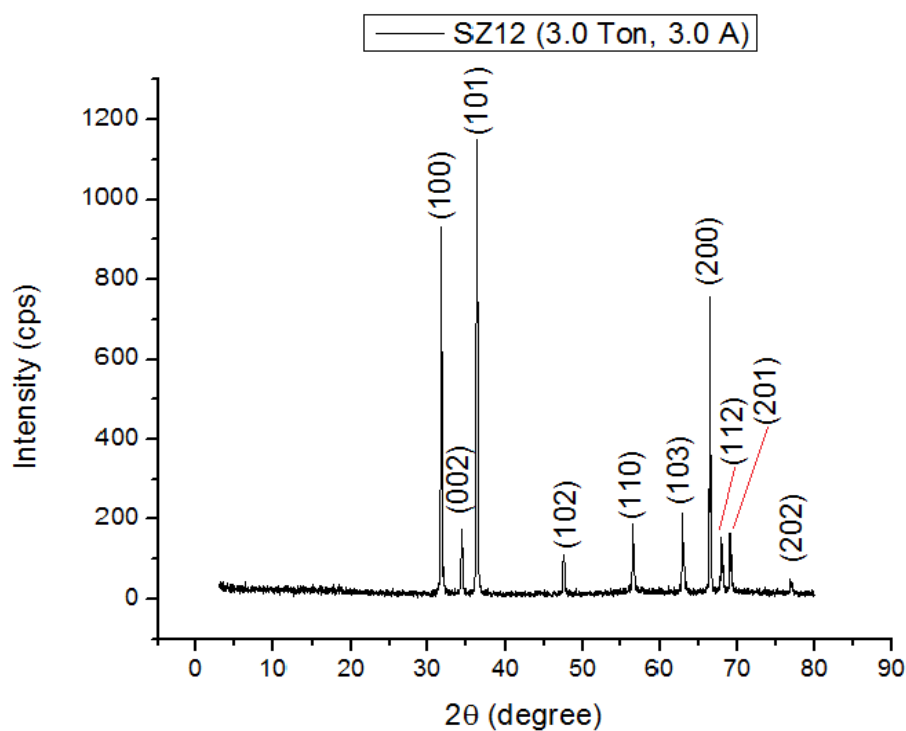


Figure 4.18. X-Ray Diffractogram of SZ12 (3.0 Ton, 3.0 Å).

Table 4.17

(*h k l*) plane, *d*-spacing and crystalline size of SZ12 (3.0 Ton, 3.0 Å).

<b>h</b>	<b>k</b>	<b>l</b>	<b>2θ</b> (degree)	<b>β</b> (degree)	<b>d-spacing</b> (Å)	<b>Crystalline</b> <b>size (Å)</b>	<b>Intensity</b> (cps)
0	0	2	34.4660	0.2220	2.6001	6.5392	180
1	0	0	31.7850	0.0770	2.8129	18.7226	920
1	0	1	36.1820	0.1390	2.4806	10.4939	1125
1	0	2	47.5150	0.1590	1.9120	9.5278	110
1	0	3	62.8460	0.1350	1.4775	12.0358	209
1	1	0	56.5580	0.1520	1.6259	10.3582	195
1	1	2	67.9430	0.1470	1.3785	11.3735	150
2	0	0	66.4190	0.1230	1.4064	13.4732	755
2	0	1	69.0530	0.1240	1.3590	13.5724	160
2	0	2	76.9480	0.1700	1.2381	10.4180	43

The XRD analysis for the second category with 3.0 Ton applied compact pressure would be ended by SZ13 (3.5 Å). Figure 4.10 showed the X-Ray Diffraction result of SZ13. The plane (1 00) had the highest intensity, that was 3125 cps, with d-spacing 2.8159 Å and crystalline structure 13.5993 Å. This peak might be given by crystals grew in Figure 4.10 (a).

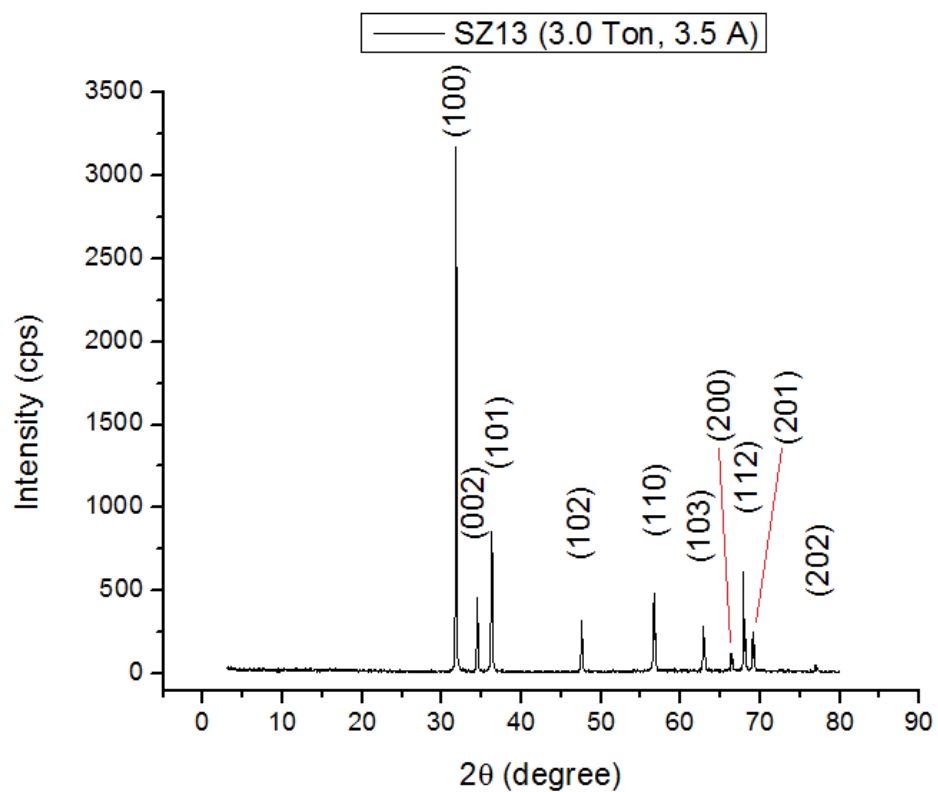


Figure 4.19. X-Ray Diffractogram of SZ13 (3.0 Ton, 3.5 Å).

Table 4.18

*(h k l) plane, d-spacing and crystalline size of SZ13 (3.0 Ton, 3.5 A).*

<b>h</b>	<b>k</b>	<b>l</b>	<b>2<math>\theta</math></b> <b>(degree)</b>	<b><math>\beta</math></b> <b>(degree)</b>	<b>d-spacing</b> <b>(Å)</b>	<b>Crystalline</b> <b>size (Å)</b>	<b>Intensity</b> <b>(cps)</b>
0	0	2	34.4410	0.1040	2.6019	13.9578	554
1	0	0	31.7510	0.1060	2.8159	13.5993	3125
1	0	1	36.2620	0.1540	2.4752	9.4739	875
1	0	2	47.5300	0.1560	1.9114	9.7116	290
1	0	3	62.8420	0.1220	1.4776	13.3180	273
1	1	0	56.6010	0.1120	1.6247	14.5072	563
1	1	2	67.9190	0.0570	1.3789	29.3276	519
2	0	0	66.3310	0.1140	1.4080	14.5296	103
2	0	1	69.0710	0.1050	1.3587	16.0300	238
2	0	2	76.9270	0.1400	1.2384	12.6485	35

The X-Ray analysis was continued with sample, SZ14. It was compacted with 3.0 Ton of pressure and the current applied was 3.5 A. The sample was added with copper powder during joule heating process. Figure 4.20 showed the X-Ray Diffraction result of SZ14. Figure 4.20 showed CuO corresponded to the peaks with higher intensity as compare to peaks corresponded to ZnO because the ZnO crystals were covered by copper powder. The peak (0 0 2) with highest intensity (287 cps) might contributed by crystal grew in Figure 4.11 (a). The crystalline size and d-spacing were 7.2441 Å and 2.5229 Å respectively. The peak (1 0 1) with intensity 89 cps, d-spacing, d= 2.4706 Å and crystalline size 6.9489 Å might be given out by crystals grew in Figure 4.12 (f). There were three peaks consisted characteristics of ZnO and CuO. Firstly, the peak had characteristic of ZnO (1 1 0) and CuO(1 1 2) with intensity 63 cps, d-spacing 1.6050 Å and crystalline size 0.1565 Å. Besides that the peak with intensity 77 cps, d-spacing 1.3780 Å and crystalline size 4.6449 Å had characteristics of ZnO (1 1 2) and CuO (1 1 3). Last but not least, the peak had characteristic of ZnO (2 0 0) and CuO (0 2 2) with intensity 63 cps, d-spacing 1.6050 Å and crystalline size 0.1565 Å.

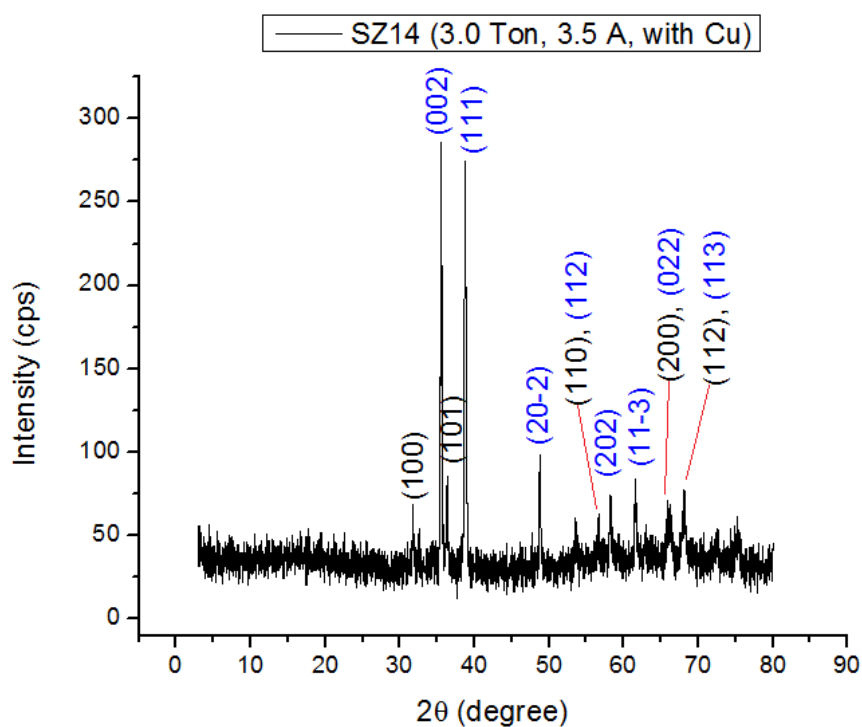


Figure 4.20. X-Ray Diffractogram of SZ14 (3.0 Ton, 3.5 A, with Cu).

Table 4.19

(*h k l*) plane, *d*-spacing and crystalline size of SZ14 (3.0 Ton, 3.5 A, with Cu).

<b>h</b>	<b>k</b>	<b>l</b>	<b>2θ</b> (degree)	<b>β</b> (degree)	<b>d-spacing</b> (Å)	<b>Crystalline</b> <b>size (Å)</b>	<b>Intensity</b> (cps)
1	0	0	31.7300	0.1200	2.8180	12.0121	70
1	0	1	36.3320	0.2100	2.4706	6.9489	89
0	0	2	35.5550	0.2010	2.5229	7.2441	287
1	1	1	38.6970	0.2230	2.3249	6.5899	263
1	1	3	61.5400	0.1900	1.5057	8.4932	84
2	0	2	58.1700	0.2200	1.5846	7.2119	75
2	0	2	48.6840	0.1900	1.8688	8.0096	99
1	1	0	57.4000	10.100	1.6050	0.1565	63
1	1	2					
1	1	2	67.9700	0.3600	1.3780	4.6449	77
1	1	3					
2	0	0	66.1500	0.6500	1.4114	2.5456	64
0	2	2					

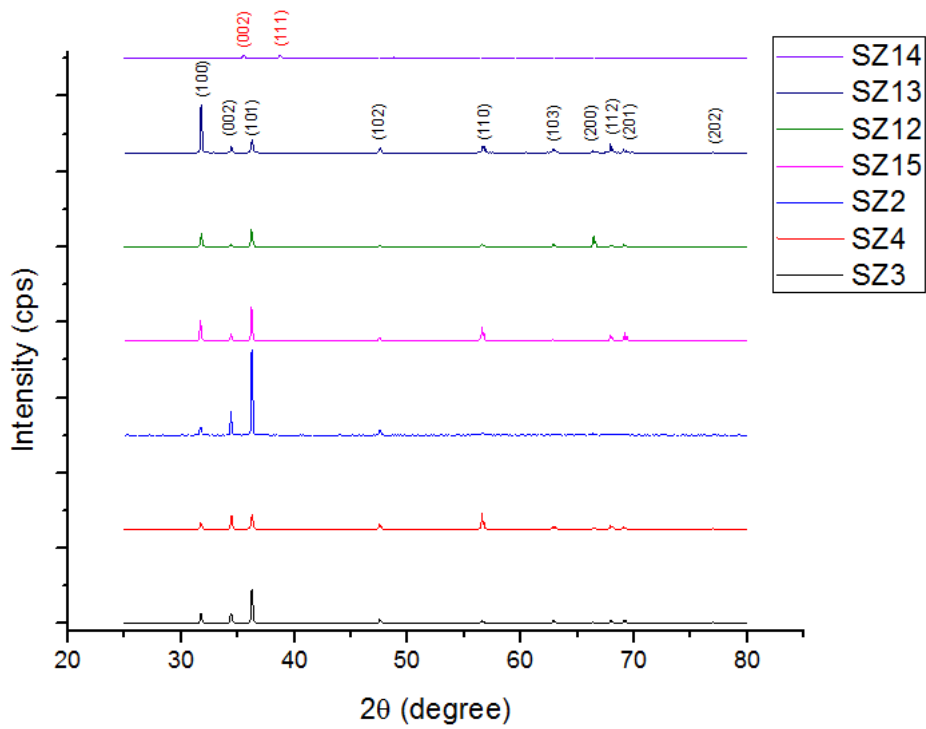


Figure 4.21. Combination of XRD results of all samples.

Figure 4.21 showed the comparison of XRD of all samples where red color of planes were corresponded to Cu powder and black color of planes were contributed by ZnO crystal. The XRD results showed most of the crystals grew on the plane (1 0 1). The crystal grew were in rock crystal like structure. This was proved by the plane (1 0 1) had the highest intensity in all the samples except SZ13 and SZ14. The highest intensity of crystal grew in SZ13 was plane (1 0 0). The highest intensity of crystal grew in SZ14 was contributed by Cu since large amount of Cu powder was placed on top of ZnO bar. This had affect the growth of ZnO crystal.



## **CHAPTER 5**

### **CONCLUSIONS AND RECOMMENDATION**

#### **5.1 CONCLUSIONS**

The preliminary objective of this research to grow various form of ZnO crystals using joule heating was achieved. The research had proved that 3.0 A and 15.0 V was the optimum current and voltage to form crystals among the range from 2.5 A to 3.5 A. The crystals grew vigorously by adopted 3.0 A current. From the analysis of result, it showed that, mostly crystals grew correspond to the planes (1 0 1) and (1 0 0). Rock crystal like structure and hexagonal crystal like structure were more easily to be formed as compared to others type of crystal. New form of crystals were formed in this research included sting fish crystal like structure with new borns structure surrounding it and orkid crystal like structure.

#### **5.2 RECOMMENDATIONS**

There are some limitation had to be improve in this project, therefore there are some recommendation to improve the research. Firstly, the dimension of ZnO bar must be cut into exactly same dimension by rubbing the surface of ZnO bar using sand paper to obtained more precise analysis result since the size of bar will affect the amount of current pass through it. Besides that, the sharp tip of crocodile clip should be flatten and try to increase the contact area between crocodile clip and ZnO bar to allow bigger amount of current pass though. Lastly, the XRD characterization should be done straight after SEM characterization to ensure obtain the correct location of crystals grew.

## REFERENCES

- A. M. Gsies, J. P. Goss, P. R. Briddon, Ramadan. M. Al-habashi, K. M. Etmimi, Khaled. A. S. Marghani., 2014. *World Academy of Science, Engineering and Technology International Journal of Mathematical, Computational, Physical, Electrical and Computer Engineering* Vol:8, No:1
- A. Manekkathodi, Y. J. Wu, L. W. Chu, S. Gwo, L. J. Chou, L. J. Chen., 2013. *Nanoscale*.
- A. Tsukazaki, M. Kubota, A. Ohtomo, T. Onuma, K. Ohtani, H. Ohno, S.F. Chichibu, M. Kawasaki., 2005. *Jpn. J. Appl. Phys.*, 44, L643.
- A.F.Kohan, G. Ceder, D. Morgan, C.G. Van de Wall., 2000. *Phys. Rev.B*, 61,15019.
- Amir Moezzi, Andrew M. McDonagh, Michael B. Cortie., 2007. *Zinc oxide particles: Synthesis, properties and applications*.
- B. D. Yao, Y. F. Chan, N. Wang., 2002. *Appl. Phys. Lett*:757
- B. J. Norris, J. Anderson, J. F. Wager, D. A. Keszler, J., 2003. *Phys. D: Appl. Phys.*, 36, L105.
- B. K. Meyer, H. Alves, D. M. Hofmann, W. Kriegseis, D. Forster, F. Bertram, J. Christen, A. Hoffmann, M. Straßburg, M. Dworzak, U. Haboeck, A. V. Rodina.m,2004.*Phys.StatusSolidiB*,241(2)231.
- Bagnall D. M., Chen Y. F., Zhu Z., Yao T., Koyama S., Shen M. Y., and Goto T., 1997. *Appl.Phys.Lett*:70
- Dai Nezaki, Masaaki Yasuda, Takanari Yasui, Masasuke Takata., 2004. *Selective area growth of ZnO crystals by electric current heating*.
- D.Nezaki,T.Okamoto,M.Takata.,2002.*KeyEng.Mater*:228.
- Dulub, L. A. Boatner, and U. Diebold., 2002. "STM study of the geometric and electronic structure of ZnO(0 0 0 1)-Zn, (0 0 0 1̄)-O, (1 0 1̄ 0), and (1 1 2̄ 0) surfaces,"*Surf.Sci.*,vol.519,no.3,pp.201–217.
- E. Fortunato, A. Goncalves, A. Marques, A. Viana, H. Aguas, L. Pereira, I. Ferreira, P. Vilarinho,R.Martins.,2004.*Surf. Coat. Technol.*, 180.
- G. K. Mani and J. B. B. Rayappan.,2014. "A simple and template free synthesis of branched ZnO nanoarchitectures for sensor applications," *RSC Adv*, vol. 4, no. 109,pp.64075–64084.

- Harish Kumar & Renu Rani., 2013. Structural and Optical Characterization of ZnO Nanoparticles Synthesized by Microemulsion Route. *International Letters of Chemistry, Physics, and Astronomy*.
- Hao Yamasaki, Ken-ichi Minato, Dai Nezaki, Tomoichiro Okamoto, Akira Kawamoto, Masasuke Takata., 2004. *Photoluminescence of zinc oxide crystals synthesized on zinc wire by electric current heating method*.
- Jagadish C and Pearton S J(ed)., 2006. *Zinc Oxide Bulk, Thin Films, and Nanostructures*.(New York:Elsevier)
- K. K. Kim, J. H. Song, H. J. Jung, W. K. Choi., 2000. *J. Appl. Phys*:3573
- M. Kawakami, A. B. Hartano, Y. Nakata, T. Okada., 2003. *Jpn J. Appl. Phys*:33
- M. Kawasaki, A. Ohtomo, I. Ohkubo, H. Koinuma, Z. K. Tang, P. Yu, G. K. L. Wong, B.P.Zhang, Y. Segawa., 1998. *Mater. Sci. Eng*:1354
- Maeda K., Sato M., Niikura I. and Fukuda T., 2005. *Semicond. Sci. Technol*:20F
- O. Dulub, L. A. Boatner, and U. Diebold., 2002. "STM study of the geometric and electronic structure of ZnO(0 0 0 1)-Zn, (0 0 0  $\bar{1}$ )-O, (1 0  $\bar{1}$  0), and (1 1  $\bar{2}$  0) surfaces," *Surf. Sci*.
- P. Bindu, Sabu Thomas., 2014. Estimation of Lattice Strain in ZnO nanoparticles: X-ray peak profile analysis, *Journal of Theoretical and Applied Physics*, Volume 8, Issue 4, pp 123-134.
- P. Yu, Z. K. Tang, G. K. L. Wong, M. Kawasaki, A. Ohtomo, H. Koinuma, Y. Segawa, J. Cryst. Growth, 184-185 (1998) 601.
- Rahaman. M. N., 2003. *Ceramic Processing and Sintering. 2<sup>nd</sup> Edition*, New York Marcel Dekker, Inc.
- Reynolds D. C., Look D. C., Jogai B., Litton C. W., Cantwell G. and Harsch W. C. 1999. *Phys. Rev. B*: 60.
- R. Sivakumar, T. Tsunoda, Y. Kuroki, T. Okamoto, M. Takata., 2012. *ZnO nanowire growth by electric current heating method: A study on effect of substrate temperature*.
- T. Asokan, G. N. K. Lyengar, G. R. Nagabhusgana., 1987. Studies on microstructure and density of sintered ZnO-based non-linear resistors, *Journal of Materials Science*, volume 22, Issue 6: 2229-2236.
- Thomas D G, 1960. *J. Phys. Chem. Solids*: 15.

- W. I. Park, D. H. Kim, S.W. Jung, G. C. Yi., 2002. *Appl. Phys. Lett* :4232
- W. J. Li, E. W. Shi, W. Z. Zhong, Z. W. Yin, J.,1999. *Cryst. Growth*: 186, 203.
- X.-M. Zhang, M.-Y. Lu, Y. Zhang, L.-J. Chen, Z.L. Wang, 2009. *Advance Material* 21(2009),2767-2770
- Xufei Wu, Jonghoon Lee, Vikas Varshney, Jennifer L. Wohlwend, Ajit K.Roy & Tengfei Luo, 2015.*Thermal Conductivity of Wurtzite Zinc-Oxide from First-Principles Lattice Dynamics – a Comparative Study with Gallium Nitride*
- Y. Sun, G. M. Fuge, N. A. Fox, D. J. Riley, M. N. R. Ashfold., 2005. *Adv. Mater*: 17, 2477.
- Z. L. Wang & J. Song., 2006. *Science*, 312(5771):242.